SHAPE-SELECTIVE CATALYSIS IN ZEOLITES

Sigmund M. Csicsery

Chevron Research Company, Richmond, California 94802

Introduction

Zeolites have four properties that make them especially interesting for heterogeneous catalysis: (1) they have exchangeable cations, allowing the introduction of cations with various catalytic properties; (2) if these cationic sites are exchanged to H^+, they can have a very high number of very strong acid sites; (3) their pore diameters are less than 10 Å; and (4) they have pores with one or more discreet sizes. These last two account for their molecular sieving properties. Zeolites have been applied as catalysts since 1960.

Pore diameters in molecular sieves depend on the number of tetrahedra in a ring (Figure 1). The actual pore size also depends on the type of cation present. Molecules like ammonia, hydrogen, oxygen, and argon can go through the pores of practically every type of molecular sieve. Type "A" sieves have cubic structure with pores just about big enough to allow normal paraffins through. Cations, however, occupy positions which block part of the pores. Monovalent cations (e.g., sodium, potassium) restrict the pore size to below ∿4 Å. None of the organic molecules (except methane) would be able to penetrate NaA, or LiA zeolites. Divalent cations, however, occupy only every other cationic position leaving enough space for normal paraffins to diffuse through. Isobutane is slightly wider than the pores of CaA so cannot enter. However, molecules with nominal dimensions of perhaps half an angstrom too large can make their ways through narrower pores than expected because molecular vibration allows them to wiggle through. In addition, bond cleavage, followed by reconstruction of the broken bond, could facilitate the diffusion of larger molecules through narrow pores (1).

If almost all of the catalytic sites are confined within this pore structure and if the pores are small, the fate of reactant molecules and the probability of forming product molecules are determined mostly by molecular dimensions and configurations. Only molecules whose dimensions are less than a critical size can enter the pores, have access to internal catalytic sites, and react there. Furthermore, only molecules that can leave appear in the final product.

Types of Shape Selectivities

We can distinguish various types of shape selectivities, depending on whether pore size limits the entrance of the reacting molecule, or the departure of the product molecule, or the formation of certain transition states.

> Reactant selectivity occurs when only part of the reactant molecules are small enough to diffuse through the catalyst pores (Figure 2).

Product selectivity occurs when some of the product formed within the pores are too bulky to diffuse out as observed products. They are either converted to less bulky molecules (e.g., by equilibration) or eventually deactivate the catalyst by blocking the pores (Figure 2).

Restricted transition state selectivity occurs when certain reactions are prevented because the corresponding transition state would require more space than available in the cavities. Neither reactant nor potential product molecules are prevented from diffusing through the pores. Reactions requiring smaller transition states proceed unhindered.

Molecular traffic control may occur in zeolites with more than one type of pore system. Reactant molecules here may preferentially enter the catalyst through one of the pore systems while products diffuse out by the other. Counterdiffusion is, thus, minimized here.

Examples will be discussed for each type of shape selectivity.

Diffusion

The importance of diffusion in shape-selective catalysis cannot be overemphasized. In general, one type of molecule will react preferentially and selectively in a shape-selective catalyst if its diffusivity is at least one or two orders of magnitude higher than that of competing molecular types (2-5). Too-large molecules will be absolutely unable to diffuse through the pores. Even those molecules which react preferentially have much smaller diffusivities in shape-selective catalysts than in large-pore catalysts.

Reactant- and Product-Type
Shape Selectivities

Shape selectivity was first described by Weisz and Frilette in 1960. P. B. Weisz, N. Y. Chen, V. J. Frilette, and J. N. Miale were not only the pioneers of shape-selective catalysis; but in their subsequent publications they demonstrated its many possible applications. They have described many examples of reactant- (and product-) type shape selectivity. Examples are selective hydrogenation of n-olefins over CaA-type (6-7) and Pt ZSM-5 (8) molecular sieves (Figure 4).

Most applications and manifestations of shape-selective catalysis involve acid-catalyzed reactions such as isomerization, cracking, dehydration, etc. Acid-catalyzed reactivities of primary, secondary, and tertiary carbon atoms differ. Tertiary carbon atoms react inherently much easier than secondary carbon atoms. Primary carbon atoms don't form carbonium ions under ordinary conditions and therefore do not react. Therefore, in most cases isoparaffins crack and isomerize much faster than normal paraffins. This order is reversed in most shape-selective acid catalysis; that is, normal paraffins react faster than branched ones which sometimes do not react at all.

117

Restricted Transition
State-Type Selectivity

In restricted transition state-type selectivity, certain reactions are prevented because the transition state is too large for the cavities of the molecular sieve. An example is acid-catalyzed transalkylation of dialkylbenzenes (9) (Figure 3). In this reaction one of the alkyl groups is transferred from one molecule to another. This is a bimolecular reaction involving a diphenylmethane transition state.

Meta-xylene in this reaction will yield 1,3,5-trialkylbenzene. Mordenite does not have enough space for the corresponding transition state. Thus, whereas the 1,2,4-isomer can form, the 1,3,5-isomer cannot (10,11). Symmetrical trialkylbenzenes are absent from the product, although they are the predominant components of the trialkylbenzene isomer mixtures at equilibrium (12-13). Figure 5 shows product distributions over Zeolon H-mordenite. Isomerization rates of the symmetrical mesitylene and the smaller hemimellitene over mordenite and HY are almost identical. This shows that symmetrical trialkylbenzenes are themselves not hindered within the pores of H-mordenite. In isomerization, the transition state involves only one molecule; so there is enough space to form the transition state in the internal cavity of the sieve.

Another example for transition state-type selectivity is isobutane isomerization over HZSM-5 (14-16).

One can distinguish experimentally between reactant and product-type selectivities and restricted transition state-type selectivities by studying particle size effects. Observed rates depend on the intrinsic, uninhibited rate constant and, if mass transfer is limiting, on the diffusivities of the reactant (or product) molecules and on the catalyst particle size. Reactant and product selectivities are mass transfer limited and, therefore, affected by crystallite size whereas restricted transition-state selectivity is not. Haag, Lago, and Weisz used this method to determine the causes of shape selectivity in the cracking of C_6 and C_9 paraffins and olefins over HZSM-5 (17).

The crystallite size effects observed allowed Haag, Lago, and Weisz to calculate effective diffusivities. This was the first known case for determination of molecular diffusivities in a zeolite at steady state and actual reaction conditions (Figure 6). Diffusivities decrease by four orders of magnitude from normal to gem-dimethyl paraffins. While branching has a large effect, the influence of the length of the molecule is small. Olefins have similar diffusivities to the corresponding paraffins. One surprising observation is that these diffusivities are about an order higher than the calculated Knudsen diffusivities.

An important consequence of the lack of space for the bulky transition state for transalkylation within HZSM-5 is that xylene isomerization proceeds without trimethylbenzene formation. This improves xylene yields and increases catalyst life.

The most important example of restricted transition state-type selectivity is the absence (or near absence) of coking in ZSM-5 type

molecular sieves. This has great significance because certain reactions can occur in the absence of metal hydrogenation components and high hydrogen pressure. Coking is less severe in ZSM-5 because the pores lack enough space for the polymerization of coke precursors. On ZSM-5 the coke is deposited on the outer surface of the crystallites, whereas in offretite and mordenite most of the coke forms within the pores (18) (Figure 7). Activity is barely affected in the first case, while it decreases rapidly in the second.

In large pore zeolites (e.g., HY, mordenite) the most significant step in coking is probably the alkylation of aromatics (19-22). These alkylaromatics cyclize or condense into fused-ring polycyclics, which eventually dehydrogenate to coke. Paraffins could also contribute to coking via conjunct polymerization, which leads to naphthenes.

Molecular Traffic Control

Molecular traffic control is a special type of shape selectivity. It could occur in zeolites with more than one type of intersecting pore systems. Reactant molecules here may preferentially enter the catalyst through one of the pore systems while the products diffuse out of the other. This may minimize counterdiffusion and, thus, increase reaction rate (23-24).

ZSM-5 has two types of channels, both of which have ten-membered ring openings. One channel system is sinusoidal and has nearly circular (5.4 Å x 5.6 Å) cross-section. The other channel system has elliptical openings (5.2 Å x 5.8 Å). These are straight and perpendicular to the first system (25-26). Whereas linear molecules can occupy both channel systems, 3-methylpentane and p-xylene occupy only the linear, elliptical pores. These suggest that normal aliphatics can diffuse freely in both systems; but aromatics and isoparaffins prefer the linear, elliptical channels. Examples might be benzene alkylation with ethylene, and toluene alkylation with methanol over ZSM-5 catalysts (27).

In "reverse molecular traffic control" small product molecules diffuse out through pores too narrow for larger reactants, thus avoiding counterdiffusion (28). Examples might be catalytic dewaxing or xylene isomerization (27).

Sequential adsorption measurements did not support the concept of molecular traffic control (29). However, it is questionable whether such kinetic phenomena can be proven or disproven by adsorption measurements (30).

Product selectivity, restricted transition state-type selectivity, and molecular traffic control may all contribute to several reactions in which p-xylene is formed above its equilibrium concentrations over ZSM-5 zeolite (2,4,5,31,32,33).

Control of Shape Selectivity

Shape selectivity can be improved by reducing the number of active sites on the external surface of zeolite crystallites. The external surface of a molecular sieve can be neutralized by poisoning with a

large molecule (34). The extent of shape selectivity can be also con-
trolled by cations (35-38). Decreasing the aluminum content in the
last stage of crystallization of ZSM-5 zeolites is another way to
reduce the number of active sites on the outside surface of crystal-
lites (39) and, thus, improve shape selectivity.

Erionite

Erionite (41-42) can selectively distinguish between normal and
isoparaffins. Over erionite the otherwise much-more-reactive
2-methylpentane reacts 50 times slower at 430°C than normal hexane at
320°C. The cavity of erionite has dimensions similar to the length of
n-octane. This coincidence is responsible for the so-called "cage" or
"window" effect (42-46).

Quantitative Measure of Shape Selectivity

A quantitative measure of shape selectivity (called "constraint index")
compares the cracking rates of normal-hexane and 3-methylpentane (46)
(Figure 37). Silica-alumina has a constraint index of 0.6. This ratio
represents the intrinsic cracking rates of normal paraffins and iso-
paraffins. Mordenite and rare earth Y are similarly unselective.
Erionite has a very high "constraint index," and so do various ZSM
catalysts.

Applications

We could remove undesirable impurities by cracking them to easily
removable molecules and distilling them away [such as in Selectoforming
(47, 48) and catalytic dewaxing (49-52)]. Impurities can also be
selectively burned inside molecular sieves and removed as CO_2 and CO.
Or impurities can be converted to harmless molecules.

One important class of applications of shape selectivity is to avoid
undesirable reactions. For instance, in xylene isomerization transi-
tion state-type selectivity limits transalkylation and coking over
ZSM-5 sieve (53). In toluene alkylation or disproportionation reac-
tions leading to the undesirable isomers (o- and m-xylenes) are avoided
(52-53). Most of these applications will be discussed in detail by
subsequent speakers of this Symposium.

References

1. Rabo, J. A., "Salt Occlusion in Zeolite Crystals," in Zeolite Chemistry and Catalysis, Jule A. Rabo, ed., A.C.S. Monograph No. 171, 332 (1976).

2. Chen, N. Y., Kaeding, W. W., and Dwyer, F. G., J. Amer. Chem. Soc., 101, 6783 (1979).

3. Védrine, J. C., Auroux, A., Dejaifve, P., Ducarme, V., Hoser, H., and Zhou, Sh., J. Catal., 73, 147 (1982).

4. Kaeding, W. W., Chu, C., Young, L. B., Weinstein, B., and Butter, S. A., J. Catal., 67, 159 (1981).

5. Kaeding, W. W., Chu, C., Young, L. B., and Butter, S. A., J. Catal., 69, 392 (1981).

6. Weisz, P. B. and Frilette, V. J., J. Phys. Chem. 64, 382 (1960).

7. Weisz, P. B., Frilette, V. J., Maatman, R. W., and Mower, E. B., J. Catal. 1, 307 (1962).

8. Dessau, R. M., J. Catal., 77, 304 (1982).

9. Csicsery, S. M., J. Org. Chem. 34, 3338 (1969).

10. Csicsery, S. M., J. Catal. 19, 394 (1970).

11. Csicsery, S. M., J. Catal. 23, 124 (1971).

12. Csicsery, S. M., J. Chem. Eng. Data 12, 118 (1967).

13. Venuto, P. B., private communication.

14. Hilaireau, P., Bearez, C., Chevalier, F., Perot, G., and Guisnet, M., Zeolites, 2, 69 (1982).

15. Valyon, J., Mihályfi, J., Beyer, H. K., and Jacobs, P. A., "Preprints of the Workshop on Adsorption of Hydrocarbons in Zeolites," Berlin (G.D.R.), 134 (1979).

16. Védrine, J. C., Auroux, A., Bolix, V., Dejaifve, P., Naccache, C., Wierzchowski, P., Derouane, E. G., Nagy, J. B., Gilson, J. P., Van Hoof, J. H. C., Van den Berg, J. P., and Wolthuizen, J., J. Catal., 59, 248 (1979).

17. Haag, W. O., Lago, R. M., and Weisz, P. B., Faraday General Discussion No. 72, p. 317 (1982). "Selectivity in Heterogeneous Catalysis," September 14-16, 1981, University of Nottingham, Nottingham, England.

18. Dejaifve, P., Auroux, A., Gravelle, P. C., Védrine, J. C., Gabelica, Z., and Derouane, E. G., J. Catal., 70, 123 (1981).

19. Walsh, D. E. and Rollmann, L. D., J. Catal., 56, 195 (1979).

20. Rollmann, L. D., J. Catal., 47, 113 (1977).

21. Walsh, D. E. and Rollmann, L. D., J. Catal., 49, 369 (1977).

22. Rollmann, L. D. and Walsh, D. E., J. Catal., 56, 139 (1979).

23. Derouane, E. G. and Gabelica, Z., J. Catal., 65, 486 (1980).

24. Derouane, E. G., "Catalysis by Zeolites," (B. Imelik et al., Editors), p. 5, Elsevier, Amsterdam, 1980.

25. Meier, W. M. and Olson, D. H., "Atlas of Zeolite Structure Types." Structure Commission of IZA, 1978 (distributor - Polycrystal Book Service, Pittsburgh, Pennsylvania).

26. Flanigen, E. M., Bennett, J. M., Grose, R. W., Cohen, J. P., Patton, R. L., Kirchner, R. M., and Smith, J. V., Nature 271, 512 (1978).

27. Derouane, E. G., Gabelica, Z., and Jacobs, P. A., J. Catal., 70, 238 (1981).

28. Lowe, B. M., Whan, D. A., and Spencer, M. S., J. Catal., 70, 237 (1981).

29. Pope, C. G., J. Catal., 72, 174 (1981).

30. Derouane, E. G., J. Catal., 72, 177 (1981).

31. Chen, N. Y. and Garwood, W. E., J. Catal. 52, 453 (1978).

32. Young, L. B., Butter, S. A., and Kaeding, W. W., J. Catal., 76, 418 (1982).

33. Wei, J., J. Catal., 76, 433 (1982).

34. Anderson, J. R., Foger, K., Mole, T., Rajadhyaksha, R. A., and Sanders, J. V., J. Catal., 58, 114 (1979).

35. Namba, S., Iwase, O., Takahashi, N., Yashima, T., and Hara, N., J. Catal., 56, 445 (1979).

36. Freeman, J. J. and Unland, M. L., J. Catal., 54, 183 (1978).

37. Unland, M. L., U.S. Patent No. 4,115,424 (1978).

38. Sefcik, M. D., J. AM. Chem. Soc., 101, 2164 (1969).

39. Rollmann, L. D., U.S. Patent No. 4,148,713 (April 10, 1979).

40. Fraenkel, D. and Gates, B. C., J. Amer. Chem. Soc., 102, 2478 (1980).

41. Gard, J. A. and Tait, J. M. Advan. Chem. Ser., 101, 230; (1971) Intern. Conf. Molecular Sieve Zeolites, 2nd, Worcester, Massachusetts, September 8-11, 1970.

42. Gorring, R. L., J. Catal., 31, 13 (1973).

43. Miale, J. N., Chen, N. Y., and Weisz, P. B., J. Catal., 6, 278 (1966).

44. Chen, N. Y., Lucki, S. J., and Mower, E. B., J. Catal., 13, 329 (1969).

45. Chen, N. Y. and Garwood, W. E., Advan. Chem. Ser. 121, 575; (1973) Intern. Conf. Molecular Sieves, 3rd, Zurich, Switzerland, September 3-7 (1973).

46. Young, L. B., U.S. Patent No. 3,962,364 (1976).

47. Chen, N. Y., Maziuk, J., Schwartz, A. B., and Weisz, P. B., Oil Gas J. 66, (47), 154 (1968).

48. Hydrocarbon Processing (September 1970) 192.

49. Chen, N. Y., Gorring, R. L., Ireland, H. R., and Stein, T. R., Oil, Gas J., 75, (23), 165 (1977).

50. Chen, N. Y., Garwood, W. E., U.S. Patent No. 3,700,585 (1972).

51. Chen, N. Y., and Garwood, W. E., Ind. Eng. Chem. Process Des. Dev., 17, 513 (1978).

52. Smith, K. W., Starr, W. C., and Chen, N. Y., Oil, Gas J. 78, (21), 75 (1980).

53. Weisz, P. B., Pure and Appl. Chem., 52, 2091 (1980).

FIGURE 1

PORE DIAMETERS IN ZEOLITES

No. of Tetrahedra in Ring	Maximum Free Dia., Å	Example
6	2.8	
8	4.3	Erionite, A
10	6.3	ZSM-5, Ferrierite
12	8.0	L, Y, Mordenite
18	15	Not Yet Observed

Typical Hydrocarbon Dimensions:

Benzene = 5.7 Å x 2.2 Å   n-Hexane = 3.5 x 4.2 Å
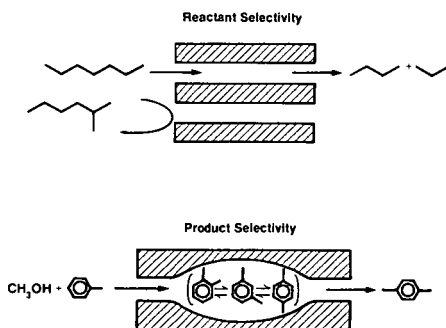
FIGURE 2

Reactant Selectivity

Product Selectivity

FIGURE 3

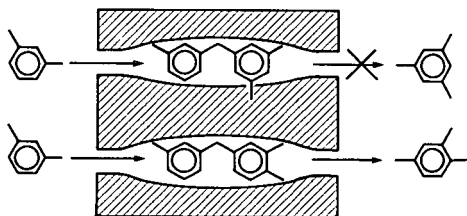RESTRICTED TRANSITION STATE SELECTIVITY
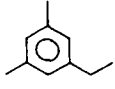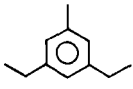
FIGURE 4

SHAPE SELECTIVE HYDROGENATION OVER Pt - ZSM-5

Catalyst	Temp., °C	Pt - Al_2O_3	Pt - ZSM-5
Hydrogenated, %			
Hexene	275	27	90
4,4-Dimethylhexene-1	275	35	<1
Styrene	400	57	50
2-Methylstyrene	400	58	<2

Dessau, J. Catal., 77, 304 (1982).

FIGURE 5

RESTRICTED TRANSITION STATE-TYPE SELECTIVITY IN THE
TRANSALKYLATED PRODUCT DISTRIBUTION OF
METHYLETHYLBENZENE
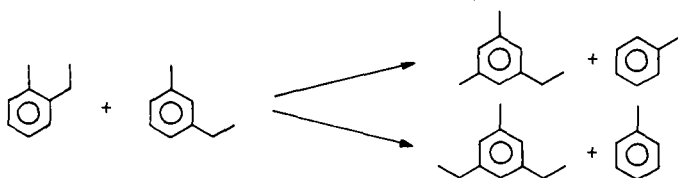
Catalyst	Reaction Temperature, °C	% of Total C_{10}	% of Total C_{11}
H-Mordenite	204	0.4	0.2
HY	204	31.3	16.1
Silica-Alumina	315	30.6	19.6
Thermodynamic Equilibrium	315	46.8	33.7

Csicsery, J. Catal. 19, 394 (1970).

FIGURE 7

COKE FORMATION IN ZEOLITES

A. Pentasil Zeolites

B. Mordenite (and Other Large Pore Zeolites)
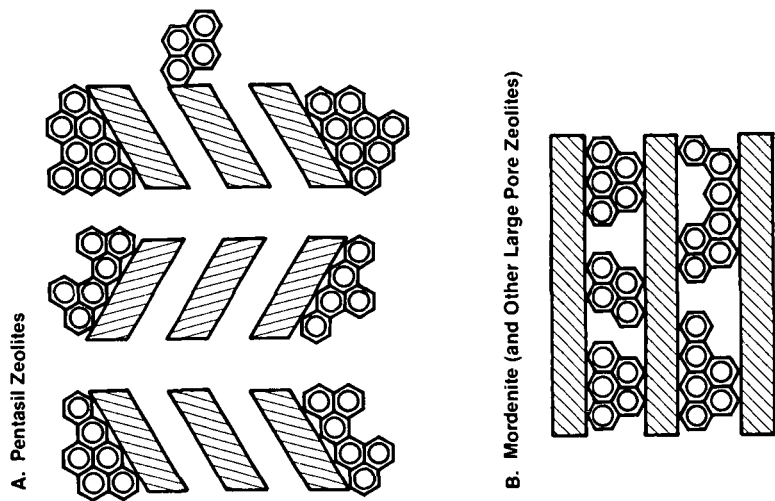
Dejaifve, et al., J. Catal., 70, 123 (1981).

FIGURE 6

DIFFUSIVITIES IN ZSM-5 538°C

Structure	D at 538°C, cm^2/S
C–C–C–C–C≡C	3×10^{-4}
C–C–C=C–C with C branch	4×10^{-5}
C–C(C)(C)–C	2×10^{-8}
C–C(C)(C)–C≡C	7×10^{-8}
C–C(C)(C)–C–C–C	3×10^{-8}

Haag, Lago, and Weisz, Faraday General Discussions, 72, 317 (1982).

CATALYTIC, PHYSICAL AND ACIDIC PROPERTIES OF PENTASIL ZEOLITES

Jacques C. Védrine
Institut de Recherches sur la Catalyse, C.N.R.S.,
2, av. Albert Einstein F 69626 Villeurbanne FRANCE

A large amount of efforts has been done in the recent years to under-
stand the fascinating shape selective properties of ZSM-5 or ZSM-11 zeolites[1-4].
It has appeared that the acid strength of the Brönsted sites varies in a wide
range for a same sample[5]. Moreover, depending on preparation conditions,
the morphology and size of the zeolitic crystallites and the Al concentration
within a crystallite and between crystallites may vary drastically[6-7]. It
follows that it is somewhat difficult to rationalize the effects of particle
size, of acid strength and of the nature of the zeolite (-5 or -11) on the
catalytic properties of the catalyst for acid-type reactions like methanol
conversion or alkylation of aromatics. The purpose of this presentation is to
sum up some of our recent works in that field.

Experimental part : ZSM-5 and ZSM-11 samples have been prepared in the labora-
tory following the procedures described in ref. 8 and 9 respectively. For
ZSM-5 samples the Al content of the samples was varied by using different Al
concentration in the preparation mixture. For ZSM-11 samples the temperature
and duration of the preparation were chosen to be 100°C, one month (sample 1)
and 170°C, one week (samples 2 and 3). Chemical compositions were determined
from atomic absorption measurements and are given in table 1. The samples were
calcined under N_2 flow at 500°C and then at 540°C under air flow. Acidifica-
tion was performed by exchanging Na cations by NH_4^+ in aqueous solution M/2
at 80°C, and by deammoniation at 540°C under air flow. One ZSM-5 sample was
treated by a trimethylphosphite solution in n-octane at 120°C as described
in ref. 10 resulting in a so called P-ZSM-5.

Table 1 : Physical characteristics of the different samples

Samples zeolite type modification	1 ZSM-11 no	2 ZSM-11 no	3 ZSM-11 no	4 ZSM-5 no	5 ZSM-5 no	6 P-ZSM-5 Phosphorus (1.1 wt%)
Chemical analysis						
atoms : Si : Al	37	31	43	23	9	10
Na : (Si+Al)x10²	0.3	0.5	0.1	0.2	0.7	0.7
XPS data						
atoms : Si : Al	24	30	70	26	10	9
TEM analysis						
Size of grains(μm)	0.6±0.2	1-2	6±2	0.5-2	0.5-2	0.5-2
shape	aggregate	core + needles	core + needles	parallelepipeds	parallelepipeds	parallelepipeds
	spheroidal	spherulitic	spherulitic			

Catalytic experiments were carried out in a flow microreactor (100 mg of catalyst) and analyses were performed on stream by gas chromatography.

Acidity characterization was performed using infra-red spectroscopy and micro-calorimetry of NH_3 adsorption at 150°C. The morphology of the zeolite grains was determined using a high resolution transmission electron micros-cope JEOL 100 CX and Al distribution within the grain was determined with a high resolution EDX-STEM from Vacuum Generators (HB 5). Surface composition of the grains was measured by XPS using a monochromatized HP 5950 A spectro-meter. X ray diffraction patterns were obtained using a conventionnal CuKα X ray source. At last the capacity of n-hexane absorption at room temperature was measured by volumetry.

Experimental results

The crystallinity of the samples prepared in the laboratory was deter-mined by X ray diffraction, infra-red spectroscopy of the vibrational modes (550 : 450 cm^{-1} ratios)[11], high resolution electron microdiffraction and absorption capacity for n-hexane (11-12 wt %). All samples were found to be well crystallized materials except sample 1 which probably contained approxi-mately 30 % of amorphous silica[10] and 70 % of aggregates of tiny crystalli-tes (5-10 nm in size) as evidenced from i.r. and n-hexane absorption data. The other two ZSM-11 samples (samples 2 ans 3) were formed of a core constituted by an aggregate of small 5-10 nm crystallites and of needles (500-1000 nm in size) emerging from the core with a spherulitic shape[7]. High resolution microdiffraction unambiguously showed that the tiny crystallites were well crystallized ZSM zeolite.ZSM-5 samples were formed of well crystallized paral-lelepipeds of 0.5 to 2 μm in size. Physical and chemical characteristics of the samples are given in table 1. Their catalytic properties for methanol conversion and alkylation of toluene by methanol are summarized in tables 2 and 3.

Table 2 : Catalytic properties of ZSM-5 and ZSM-11 samples in the reaction of methanol conversion at 370°C with N_2 as a carrier gas, flow rate = 5 l h^{-1}, WHSV = 11 h^{-1}

Samples	1	2	3	4	5	6
Conversion (%)	90	84	70	89	89	89
Hydrocarbons %						
aliphatics	80	84	75	78	70	84
aromatics	20	16	25	22	30	16
Aromatics (%)						
xylenes	26	27	29	46	50	64
$A_6 + A_7$	6	7	5	9	6	8
Others	68	66	66	45	44	28
(m + p) : 0 xylenes	3	3	5	13	11	35

Table 3 : Catalytic properties of ZSM-5 and ZSM-11 samples in the reaction of alkylation of toluene by methanol at 400°C, with N_2 as a gas carrier and a total flow rate equal to 1.85 l h^{-1}, WHSV = 4.5/5 h^{-1}

Samples Zeolite	2 ZSM-11	4 ZSM-5	5 P-ZSM-5
Conversion (%)			
methanol	100	98	100
toluene	18	16	10
Hydrocarbons (%)			
aliphatics	1.3	4.1	11.6
xylenes	81.0	88.0	84.5
trimethylbenzenes	12.9	4.1	1.0
others	4.8	3.8	4.9
Selectivities (%)			
p-xylene	29.1	52.1	94.6
m-xylene	49.8	36.5	3.8
o-xylene	21.1	11.4	1.4
TMB 135	2.3	-	-
TMB 124	94.6	100	100
TMB 123	2.3	-	-

The main features of catalytic properties are that ZSM-5 samples present more shape selective properties than ZSM-11 whatever the particle size, presumably because ZSM-11 has more free space (+ 30 %) at the channel intersections. Detailed analysis of the methanol conversion reaction[7] shows that when the grain size of ZSM-11 samples increases more light hydrocarbons ($C_1 + C_2$) and less heavier hydrocarbons (C_6^+ and A_9^+) are formed. This very probably arises from the longer length path for the reactants when the particle size increases.

The i.r. OH bands at 3720-3740 and 3600-3605 cm^{-1} were observed for all samples. The 3600 cm^{-1} band was shown by NH_3 adsorption to be acidic while the 3720-3740 cm^{-1} band was shown to have its relative intensity decreasing when the particle size increased due to a decrease in the number of terminal silanols. Modification by phosphorus was shown to decrease the number of OH groups by about one half but their strength remained comparable[10]. The EDX-STEM characterization showed that Al was not homogeneously localized in the zeolite framework. For spherulitic ZSM-11 grains the needles were shown to present in average about twice less Al than the core and evenmore an heterogeneous distribution of Al from the inner to the outer layers. For ZSM-5 samples heterogeneity in Al concentration within a same zeolitic grain or between grains was observed which precluded any rationalized law[7].

Acidity strength and acid site concentration were determined by mesuring microcalorimetrically the differential heat of ammonia adsorption at 150°C. It was observed that the strongest acid sites were obtained for relatively low Al content but obviously the number of strong acid sites decreased with the Al content decreasing. Acidity strength was observed to be heterogeneous which is in agreement with the heterogeneity in Al distribution. The number of strong acid sites was found to equal 1.6, 1.8, 1.8, 2.4, 2.3, 1.3 per u.c respectively for samples 1 to 6, after outgassing at 400°C.

Conclusions : _These characterizationslead to   the following conclusions :_

. _Crystal growth of ZSM-11 particles seems to be particularly difficult_
  leading to aggregates or core of tiny cristallites, 5-10 nm in size with
  a relatively high Al content (Si : Al ≃ 30 against 50 in the preparation
  mixture). When Al content is low the crystal growth is then sharply enhanced

. _ZSM-5 presents much more shape selectivity for less bulky aromatics than_
  ZSM-11 in methanol conversion and toluene alkylation reactions. This is
  presumably due to larger free space at the channel intersections of ZSM-11
  sample.

. _Acid strength and site distributionsdo not seem to play an important role_
  in selectivity for the previous reactions as far as acid sites of suffi-
  cient strength are present.

. _The particle size which modifies the channel length plays only a secondary_
  role in the selectivity for aliphatics and aromatics.

. _The preparation conditions particularly Al concentration and stirring during_
  synthesis seem to play a great role in the crystal growth and in the morpho-
  logy of the zeolitic grains.

References :

1. _C.C. CHANG and A.J. SILVESTRI, J. Catal. 47, 249 (1977)._

2. _P.B. WEISZ in Proceed, 7th Intern. Cong. on Catalysis, Tokyo, Edit. by_
   T. SEIYAMA and K. TANABE, Elsevier, Amsterdam 1981, p. 3.

3. _E.G. DEROUANE, J.B. NAGY, P. DEJAIFVE, J.H.C. Van HOOF, B.P. SPEKMAN,_
   C. NACCACHE and J.C. VEDRINE, C.R. Acad. Sci., Paris, Ser C 284, 945,
   (1977)and J. Catal 53, 40 (1978).

4. _E.G. DEROUANE and J.C. VEDRINE, J. Molec. Catalysis 8, 479 (1980)._

5. _A. AUROUX, V. BOLIS, P. WIERZCHOWSKI, P.C. GRAVELLE and J.C. VEDRINE,_
   JCS Faraday Trans II, 75, 2544 (1979).

6. _E.G. DEROUANE, S. DETREMMERIE, Z. GABELICA and N. BLOM, Appl. Catal. 1,_
   201 (1981), R. von BALLMOOS AND W.N. MEIER,Nature 289, 782 (1981).

7. _A. AUROUX, H. DEXPERT, C. LECLERCQ and J.C. VEDRINE, Submitted to Appl._
   Catal. october 1982.

8. _R.J. ARGAUER and G.R. LANDOLT, US Patent, 3702 886 (1972)._

9. _P. CHU, US Patent 3709 979 (1972)._

10. _J.C. VEDRINE, A. AUROUX, P. DEJAIFVE, V. DUCARME, H. HOSER and S. ZHOU,_
    J. Catal. 73, 147 (1982).

11. _G. COUDURIER, C. NACCACHE and J.C. VEDRINE, JCS Chem. Commun. 1982 in press._

    P.A. JACOBS, E.G. DEROUANE and J. WEITKAMP, JCS Chem. Commun. 1981, 591

The bifunctional conversion of cyclooctane. A suitable
reaction to test shape-selective effects in high-silica
zeolites.

by : P.A. Jacobs, M. Tielen and R. Sosa Hernandez

INTRODUCTION

It was reported earlier [1] that the bifunctional
conversion of n-paraffines into feed isomers or hydro-
cracked products was distinctly different over wide pore
zeolites of the faujasite-type compared to those of the
Pentasil-type. It was also established [1] that the rate
of conversion of n-decane into its monomethyl branched
feed isomers was determined by the pore structure in case
of the Pentasil-zeolites. Branching at the paraffin-end
was found to be favored in MFI-zeolites (ZSM-5) while in
MEL-structures (ZSM-11) the pore intersections allowed
also methyl-branching in the 3-position. This clearly
indicates that the structure of the pores in medium or
small pore zeolites can determine the product selectivity.
Vice versa a well-choosen catalytic test reaction may give
useful information on the dimensions and geometry of the
zeolite pores.

It was therefore the aim of the present work to select
a suitable probe molecule, the catalytic conversion of
which will given useful information on the dimensions and
geometry of zeolite pores in general and on the occurence
of transition state shape selectivity. More particularly,
in the present work it is reported how cyclooctane is
converted on Pt-loaded acid zeolites. Small amounts of

Pt are added in order to ensure constant activity in
time and to avoid perturbance of the measurements by
differences in rate of deactivation. Three zeolite
structures (FAU, MFI and MEL) with identical chemical
composition are compared.

EXPERIMENTAL

The acid forms of HZSM-5 and HZSM-11 had a Si/Al
ratio of 60. Ultrastable Y-zeolite was treated with
$SiCl_4$ and had the same chemical composition (FAU^*).
These samples were impregnated with $Pt(NH_3)_4Cl_2$ so as
to obtain 1 % by weight loading with the metal.

The reaction with cyclooctane was carried out at
atmospheric pressure in a continuous flow-reactor at a
WHSV of 0.5 h^{-1}. Analysis of the reaction products
was done on-line with high-resolution capillary gas-
chromatography.


RESULTS AND DISCUSSION

The activity sequence MEL > MFI > FAU^* for cyclo-
octane conversion (Fig. 1) is different from the one
obtained for n-decane on the same samples : MFI >
MEL > FAU^*. Comparison with the acid strength
distribution measurements [1] shows that for the present
reaction only acid sites of intermediate strength are
needed. The same figure indicates that the catalysts
show stable behavior in the temperature range investi-
gated. Just as for the case of n-paraffin conversion,
feed isomerization and cracking (Fig. 2) are consecutive
phenomena.

When the individual product yield is plotted against cyclooctane conversion (Figs. 3 - 5), it was found that ethylcyclohexane, methylcycloheptane and bis[330]cyclo-octane are primary products. Methylcycloheptane may be formed via protonated cyclopropane intermediates, just as in the case of the ethylcyclohexane conversion [2]:

It is stabilized in the pentasil-type structures, more particularly in MEL.

The rate formation of bis[330]cyclooctanes (c + t) parallels the rate of isomerization to methylcyclo-heptane. The formation of a bicyclic molecule out of the cyclooctyl carbenium ion, requires that the ring is deformed to a chair-type form :
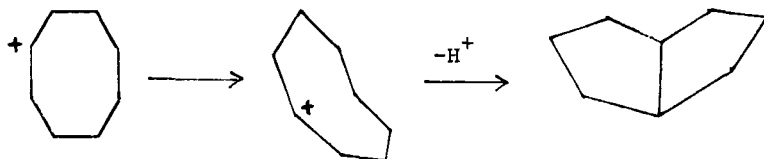
The direct formation of ethycyclohexane without the formation of a primary carbenium ion, can only occur via the formation of a protonated cyclobutyl-structure :
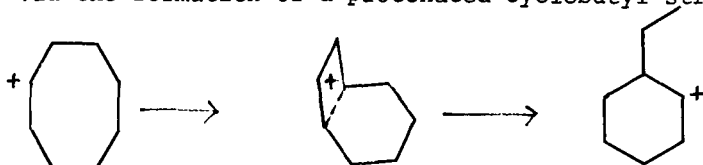
The precursors of ethylcyclohexane and bis[330]cyclo-
octane from cyclooctane are therefore cyclooctyl
cations deformed in a totally different manner, most
probably under influence of the geometry of the zeolite
pores. It is therefore straightforward that the
transformation of cyclooctane will depend mainly upon
the dimensions and structure of the zeolite pores.

REFERENCES

1. P.A. Jacobs, J. Martens, J. Weitkamp and H.K. Beyer,
   Disc. Faraday Soc., 1982, 353.
2. M. Nitta and P.A. Jacobs, Studies on Surface Science
   and Catalysis, 5, 1980, 251.
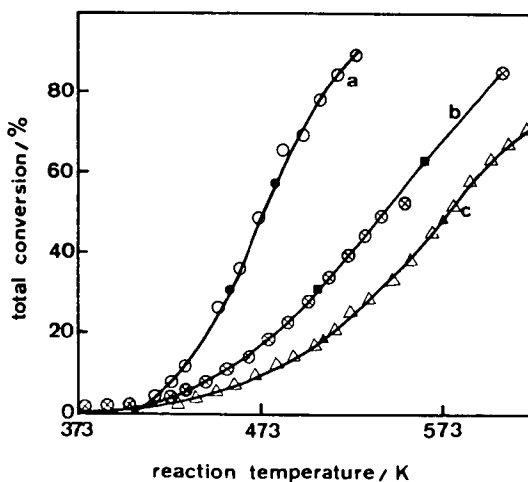
Figure 1

Total cyclooctane conversion in hydrogen over Pt-loaded
acid a) MEL, b) MFI and c) FAU⁓. Full points were
obtained during a second cycle of temperature rise.

<u>Figure 2</u>

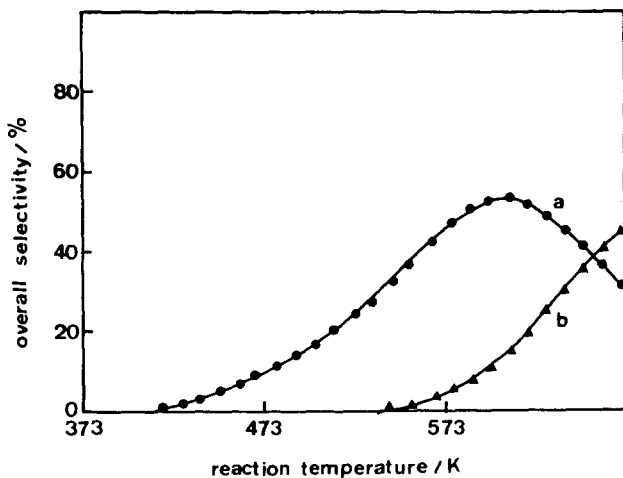Overall selectivity of cyclooctane conversion over 1 Pt/
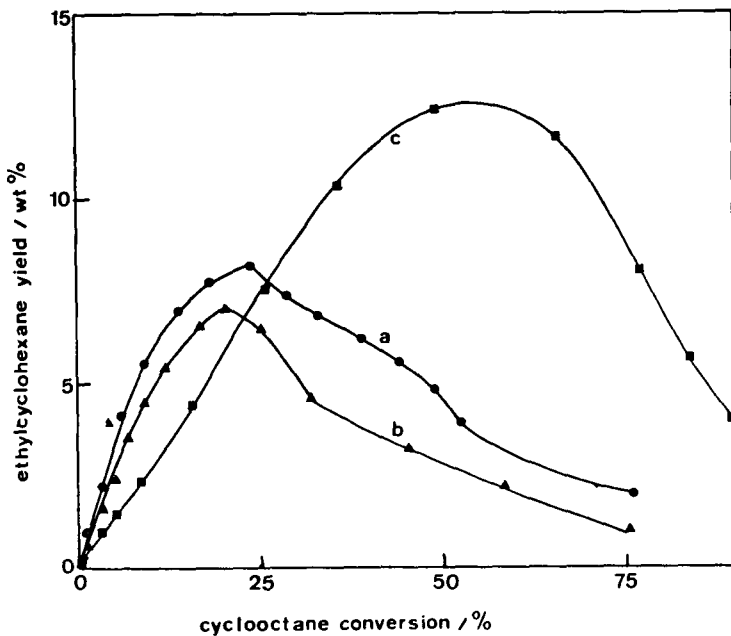H/MEL : a) feed isomers, and b) cracked products.

<u>Figure 3</u>

Yield of ethylcyclohexane from cyclooctane over FAU" (a),
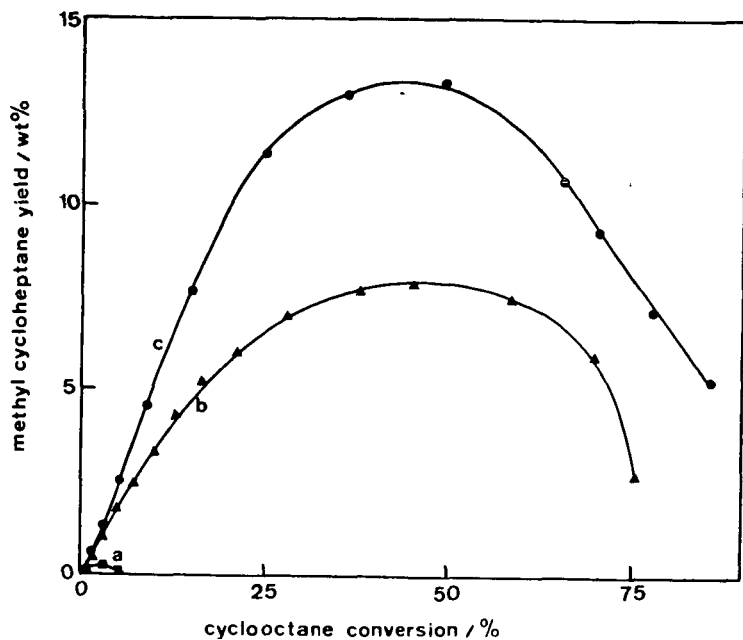MFI (b), and MEL(c).

Figure 4

Yield of methylcycloheptane from cyclooctane on a) FAU",
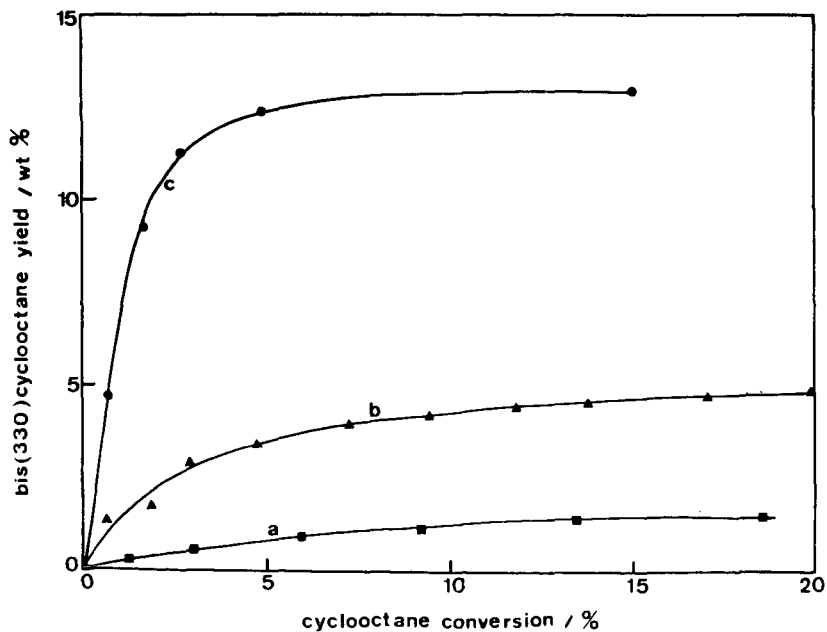b) MFI, and c) MEL - zeolites.

Figure 5

Yield of bis[330]cyclooctane from cyclooctane over a)
FAU", b) MFI, and c) MEL - zeolites.

Shape Selective Catalysis and Reaction Mechanisms

M. GUISNET and G. PEROT

ERA CNRS Catalyse Organique, Université de Poitiers
40, Avenue du Recteur Pineau, 86022 Poitiers Cedex, France

Thanks to the progress recently accomplished in the field of the synthesis and the modifications of zeolitic materials, the chemist now disposes of a large choice of acid catalysts. The problem lies in the selection, through a reliable method, of the one best suited for obtaining selectively a given reaction. The aim of this paper is to show that, by using model reactions, catalysts can be chosen on the basis of their shape selective properties. For this however the reaction mechanisms as well as the reasons for possible modifications in rate and orientation must be perfectly known.

1. Main factors governing reaction selectivity over acid zeolites

    1.1. Isomerization and disproportionation of aromatic hydrocarbons over zeolites.

        1.1.1. Xylene isomerization

Over amorphous catalysts (1-3) xylene isomerization involves methyl shift in benzenium ion intermediates as the rate limiting step (scheme 1).
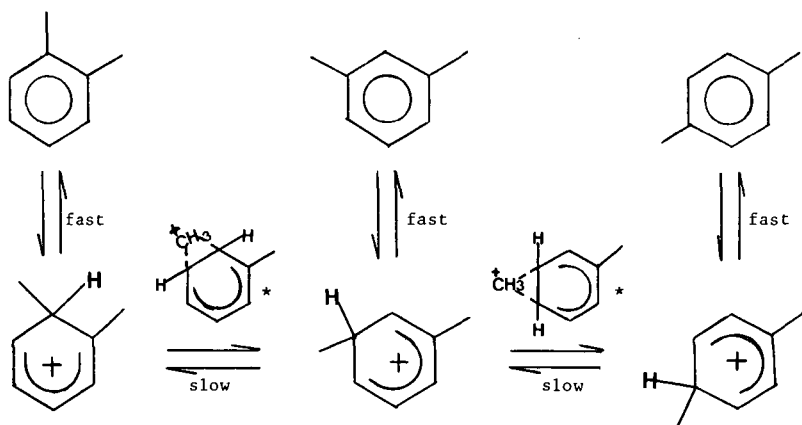
Scheme 1 : Isomerization of xylenes on acid catalysts * Transition state according to (4).

With m-xylene as the reactant and over amorphous catalysts and Y zeolite, two parallel reactions leading to o-xylene and p-xylene can take place at similar rates. However over mordenite, offretite and ZSM5, the p-xylene formation is faster (5). This is mainly a matter of diffusion rate (6). The p-xylene molecule being smaller in size diffuses out of the porous structure more readily than o-xylene. It must be noticed that the intermediates and the transition states involved in the two reactions differ slightly in size and structure. Thus the possibility of steric effects cannot be excluded.

The isomerization of o-xylene into p-xylene involves two consecutive steps. At 350°C, the reaction is negligible over amorphous catalysts and Y zeolite but quite important over mordenite and very important over ZSM5 (5). Three factors converge to increase p-xylene selectivity from Y zeolite to mordenite and ZSM5 : i) the decrease in average pore dimension which increases residence time in the structure ; ii) the increase in acid strength which increases the rates of the two consecutive steps leading from o-xylene to p-xylene ; iii) the smaller size of p-xylene, favoring its desorption.

1.1.2. Xylene disproportionation

Xylenes can undergo simultaneously isomerization as well as disproportionation into toluene and trimethylbenzenes. The disproportionation mechanism involves bimolecular intermediates (1,7) much more bulky than the benzenium intermediates involved in isomerization. This is probably why the disproportionation/isomerization rate ratio (r_D/r_I) increases as more space becomes available in the porous structure of the zeolite.

However r_D/r_I also seems to depend on the acidity of the zeolite. It decreases as the degree of exchange of protons for sodium cations in H-mordenite increases (8,9). This is more a matter of site density than acid strength. Indeed poisoning experiments with pyridine show that the acid strength required for both reactions is practically the same. But disproportionation requires probably two adjacent acid sites (1,7,10) while isomerization requires only one acid site. Hence the decrease in r_D/r_I from Y zeolite to ZSM5 may partly be explained by the site density decrease.

1.2. Alkane transformation

Over acid and bifunctional catalysts, alkanes undergo three main reactions : isomerization, cracking and disproportionation. All three of them involve carbocations as intermediates and their relative importance depends both on the characteristics of the alkane (size, degree of branching) and of the catalyst (acidity, porous structure, hydrogenation activity).

Scheme 2 shows the different chemical steps involved in the isomerization and the cracking of alkanes.
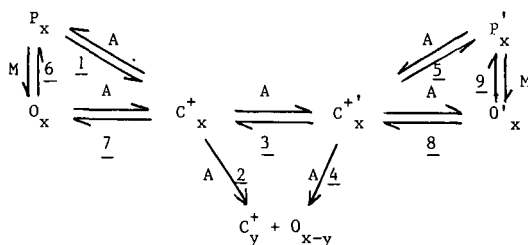
Scheme 2 : Isomerization and cracking of alkanes on acid and on bifunctional catalysts.
P:paraffin , O:olefin , C^+:carbocation , x,y:number of carbon atoms, A:acid step , M:metallic step.

1.2.1. Alkane transformation on pure zeolite catalysts

Alkane cracking on pure acid catalysts occurs through steps 1,2,3 and 4 of scheme 2. The carbenium ion formation certainly results from intermolecular hydride transfer between a reactant molecule and a preadsorbed cation while steps 2, 3 and 4 are considered as monomolecular reactions.

In the absence of steric constraints or of diffusional limitations, the cracking rate is related to the stability of the intermediate carbenium ions (C_x^+ and C_y^+). Thus over Y zeolite at 400°C isooctane cracking is 25 to 40 times faster than n-hexane cracking and 150 to 300 times faster than n-pentane cracking. The difference in reactivity of alkanes depends on the active sites : the greater their acid strength, the smaller the difference (12).

The intracrystalline structure has also a considerable influence on the relative reactivities of alkanes. Frilette et al (11) consider as shape selective the zeolites for which the "constraint index" CI (ratio of the apparent cracking rate constants of n-hexane and 3-methylpentane) is greater than 1. Due to the higher reactivity of 3-methylpentane towards carbenium ion formation, the CI of non-shape selective materials is smaller than 1. In the case of intermediate pore size zeolites the CI value (1 < CI < 12) is determined by steric constraints in the bimolecular formation of the carbenium ion (step 1, scheme 2) (13,14). On the contrary for erionite which has small pore openings and large cavities the high value of CI is due only to differences in diffusional limitations for n-hexane on the one hand and 3-methylpentane on the other.

The acidity and the structure of zeolites also influence considerably the product distribution of alkane cracking (12). In the case of isooctane about 75 % of the cracking products can be considered as resulting from the successive steps 1 and 2 of scheme 2, the remaining 25 % result from one isomerization step followed by cracking of the rearranged carbocation (sequence 1,3,4). Over mordenite and ZSM5, direct cracking (sequence 1,2) is responsible respectively for 50 and 10 % of the products only, the remainder results from multiple transformations of isooctane. The differences between the three zeolites can be attributed to diffusional limitations.

In the case of pentanes and hexanes, the cracking steps (2,4) become so slow that the formation of isomers (step 5) is observed. The isomerization/cracking rate ratio depends on the zeolite. For n-pentane transformation at 400°C, it increases from almost zero over ZSM5 to about 0.7 over mordenite and 3.5 over Y zeolite (12). This may be due to the intrinsic selectivity of the catalytic sites but steric constraints to the bimolecular transition state of step 5 may also play an important role on ZSM5.

Over mordenite pentane cracking and isomerization are accompanied by some disproportionation into C_4 and C_6 products. With butanes this reaction is the only one that can be observed at low conversion (15). This is easily understandable since butane disproportionation involves secondary carbenium ions while its cracking or intramolecular isomerization necessarily involves primary cation (16). Disproportionation needing very strong acid sites (17), Y zeolite is less active than mordenite. Another explanation must be found for the inactivity of ZSM5. Probably the bimolecular C_8 intermediate cannot be formed inside the porous structure of ZSM5. On the other hand, disproportionation is certainly a "demanding reaction" (requiring several sites) so that the low density of acid sites in ZSM5 could explain its inactivity.

1.2.2. Isomerization and cracking of n-heptane over mechanical mixtures of platinum-alumina and zeolites (Y, mordenite, ZSM5).

The presence of the metallic component increases the carbocation formation ($P_x \rightarrow C_x^+$) and isomer desorption ($C_x^{+'} \rightarrow P_x'$) rates. On bifunctional catalysts, C_x^+ formation involves successively i) the alcane dehydrogenation on the metallic sites (reaction 6) ii) the migration of the intermediate olefins from the metallic to the acid sites and iii) the adsorption of olefins on Brönsted acid sites (step 7). The isomer desorption involves the reverse sequence.

As has been mentionned by other authors (18-20) in the case of heavier n-alkanes, cracking always follows isomerization : the cracking of linear carbocations (step 2) compared to their isomerization (step 3) and to the cracking of branched cations (step 4) is very slow. In accordance with this step-by-step pathway, it can be observed that the isomerization/cracking rate ratio (r_I/r_c) depends on the amount of platinum-alumina in the catalyst (i.e. on the residence time of the intermediate olefins on the zeolite). At low platinum-alumina contents the products result from a multistep

139

acid catalyzed reaction. This reaction leads to a total cracking of each individual molecule of dehydrogenated n-heptane : therefore, light products are largely predominant, r_c increases faster than r_I. At high platinum-alumina contents, the isocation cracking (step 4) now competes with its desorption to isoheptanes ($C_x^{+'} \rightarrow P_x'$) and r_I increases at the expense of r_c. r_I/r_c should in fact increase to a limit which would depend on the characteristics of the zeolite particles (size ; pore dimensions ; nature, strength and density of the acid sites).

Taking into consideration the above examples it can be concluded that the selectivity of the reactions on shape-selective materials depends on the frequently simultaneous influence of three well-known factors :

a) own characteristics of the catalytic centers ;

b) limitations to the diffusion of reactants and products ;

c) steric constraints to the formation of transition states.

However, no evidence is found that diffusional limitations or steric constraints may lead to the formation of new intermediates.

2. Characterization of zeolites using model reactions.

The relationship between the structure of zeolites and their selectivity in a given reaction may be used to screen the best catalysts to characterize the porosity of synthetic or modified materials. The information that will be obtained will depend on the above factors. The ideal conditions for a good characterization of the porous structure are the following : i) factor a is known ; ii) the collected information concerns only one or other of factors b and c. Moreover in every case it is important that the influence of the external surface on the activity be known and if possible suppressed (21).

2.1. Diffusional limitations (factor b)

In order to limit the influence of steric constraints (factor c), reactions involving only monomolecular intermediates are recommended.

The relative reactivities of a series of organic compounds may be used. In this case the reactivity may vary according to the size of both the reactant and the products. Moreover as the reactants in one given series (alkanes, alcohols...) differ slightly, the reactivity can depend on the characteristics of the catalytic centers (factor a) which may change from one zeolite to the other.

One reactant undergoing competitive reactions can also be used. In this case, the selectivity depends only on the size of the products and a more precise determination of pore aperture can thus be obtained. Moreover, if the competitive reactions involved proceed through the same mechanism (as is the case for m-xylene isomerization) the influence of factor a can be considered as negligible.

Reactions involving consecutive steps (e.g. o-xylene isomerization) are not well adapted to the characterization of the porous structure of zeolites because their selectivity depends not only on pore size but also on the density and activity of acid centers.

2.2. Steric constraints in the neighbourhood of the active centers (factor c)

Reactions for which diffusional limitations (factor b) can be neglected must be chosen. Those involving bimolecular transition states are particularly well suited since the molecules of both the reactants and the products are generally much smaller than the transition states. However, even in this case the effect of factor b cannot always be excluded (see 1.2.1. constraint index).

In practice the inhibition to the transition state formation can be measured by comparing the rates of the bimolecular reaction and of another reaction without steric constraints.

To be free of the influence of factor a, it is convenient to choose a reactant offering the possibility of several competitive transformations through the same mechanism (e.g. formation of isomers) with one acting as the "shape sensitive" reaction and the other as reference. The disproportionation of m-xylene into 1,2,3- , 1,2,4- and 1,3,5-trimethylbenzenes offers such a possibility inasmuch as the formation of 1,3,5-trimethylbenzene suffers the intervention of a bulkier intermediate than that of 1,2,3- and 1,2,4-trimethylbenzenes (22).

However, if the mechanisms of the "shape sensitive" reaction and of the reaction taken as reference are different (e.g. disproportionation and isomerization of aromatics), factor a becomes decisively important since the relative rates of transformation in the two directions may depend on the density and on the strength of the acid sites.

The differences in reactivities of reactants belonging to the same class of compounds can also be used (e.g. constraint index measurement). Again attention must be drawn to the fact that different reactants entail differences in reactivity which could be dependent on the acid strength of the zeolite.

It can be noticed finally that it is possible to characterize in one experiment factors b and c if the reactant undergoes several reactions whose selectivities depend for some only on factor b, for others only on factor c. Such is the case for m-xylene transformation (5) : the isomerization selectivity supplies information on pore size while the disproportionation/isomerization rate ratio as well as the distribution of the trimethylbenzenes supplies information on the space disposable in the neighbourhood of the active sites.

LITERATURE CITED

(1) Poutsma, M.L., in Zeolite Chemistry and Catalysis, J.A. Rabo Ed., p. 437, ACS Monograph 171, American Chemical Society, Washington 1976.
(2) Hanson, K.L. and Engel, A.J., A.I. ChE Journal 13, 260 (1967).
(3) Cortes, A. and Corma, A., J. Catal. 51, 338 (1978).
(4) Matsumoto, H., Take J.I. and YONEDA, Y., J. Catal. 11, 211 (1968), J. Catal. 19, 113 (1970).
(5) Gnep, N.S., Tejada, J., Guisnet, M., Bull. Soc. Chim. 5 (1982).
(6) Young, L.B., Butter, S.A. and Kaeding, W.W., J. Catal. 76, 418 (1982).
(7) Gnep, N.S. and Guisnet, M., Appl. Catal. 1, 329 (1981).
(8) Ratnasamy, P., Sivasankar, S. and Vishnoi, S., J. Catal. 69, 428 (1981).
(9) Tejada, J., Gnep, N.S., Guisnet, M., to be published.
(10) Pukanic, G.W. and Massoth, F.E., J. Catal. 28, 304 (1973).
(11) Frilette, V.J., Haag, W.O., Lago, R.M., J. Catal. 67, 218 (1981).
(12) Hilaireau, P., Bourdillon, G., Perot, G., Guisnet, M., to be published.
(13) Weisz, P.B., in Proc. 7th Intern. Congr. Catalysis, Tokyo (1980) ; Plenary Lectures, Preprint P1.
(14) Haag, W.O., Lago, R.M. and Weisz, P.B., Faraday Discussions of the Chemical Society 72, 317 (1981).
(15) Guisnet, M., Gnep, N.S., Bearez, C. and Chevalier, F., in "Catalysis by Zeolites" (B. Imelik et al Eds) Elsevier Scientific Publishing Company, Amsterdam 77 (1980).
(16) Hilaireau, P., Bearez, C., Chevalier, F., Perot, G. and Guisnet, M., Zeolites 2, 69 (1982).
(17) Bearez, C., Chevalier, F., Guisnet, M., to be published.
(18) Steinjs, M., Froment, G.F., Jacobs, P.A., Uytterhoeven, J.B., Weitkamp, J., Erdöl, Kohle, Erdgas, Petrochem. 31, 581 (1978).
(19) Steinjs, M. and Froment, G.F., Jacobs, P. and Uytterhoeven, J.B., Weitkamp, J., Ind. Eng. Chem. Prod. Res. Dev. 20, 654 (1981).
(20) Steinjs, M. and Froment, G.F., Ind. Eng. Chem. Prod. Res. Dev. 20, 660 (1981).
(21) Kibby, C.L., Perrotta, A.J. and Massoth, F.E., J. Catal. 35, 256 (1974).
(22) Csicsery, S.M., in Zeolite Chemistry and Catalysis, J.A. Rabo Ed., p. 680, ACS Monograph 171, American Chemical Society, Washington 1976.

ON THE MECHANISM OF METHANOL CONVERSION OVER ZEOLITE

Yoshio Ono

Department of Chemical Engineering, Tokyo Institute of
Technology, Meguro-ku, Tokyo, 152, Japan

INTRODUCTION

Zeolites convert methanol into hydrocarbons. The most intriguing
problem concerning the mechanism of the conversion is the way of
forming carbon-carbon bonds from methanol. Chang and Silvestri(1)
proposed the participation of carbenoid species, which is assumed
to be produced by a concerted α-elimination mechanism, involving both
acidic and basic sites. Kaeding and Butter(2) proposed a mechanism
involving the reaction of an incipient methyl carbenium ion from
protonated dimethyl ether (or methanol) and the methyl group of di-
methyl ether, at which a negative center is created by the aid of an
anionic site on the catalyst. The attack of methyl carbenium ion
on the C-H bond of methyl group is more stressed in the mechanism
involving a pentacoordinated carbon center(3,4), as originally pro-
posed in the polymerization or alkylation of methane in superacid
chemistry(5,6). van der Berg et al.(7) suggested that the Stevens-
type rearrangement of trimethyl oxonium ion could be the first step
of the C-C bond formation. The intermediacy of methyl radical was
proposed by Zatorski and Krzyzanowsky(8). Apart from the detailed
mechanism of the C-C bond formation, the reaction is suggested to
have an autocatalytic character(4,9,10). Here, the origin of the
autocatalytic phenomena and its implication for the mechanism is
discussed, and then the scheme of the first C-C bond formation is
discussed to conclude that "methyl carbenium ion" species is the
most plausible intermediate.

RESULTS AND DISCUSSION

Autocatalytic Phenomena

The autocatalytic behavior of the conversion was first pointed
out by Chen and Reagan(9), who noticed that the rate of conversion
of methanol was very slow at low conversion levels, but it accele-
rated rapidly as the concentration of hydrocarbons increased.
Another feature of the autocatalysis is observed in the dependence
of the hydrocarbon yield on the reaction temperature(10). Thus,
the abrupt increase of the hydrocarbon yield is observed in a small
temperature range, and the temperature of the jump depends on the
acidity of ZSM-5 zeolite. The jump of the hydrocarbon yield with
temperature is observed also for the conversion over ferrierite.
The autocatalysis was more clearly visualized in the reaction
under low-pressure and low-temperature conditions(4). The reaction
was carried out in a gas-recirculation system. At 492 K, only a
small amount of hydrocarbons was formed for the first 8 h, though
most of methanol was converted into dimethyl ether. After 12 h,
the hydrocarbon yield increased aburptly, reaching 80 % at 18 h.
At higher temperatures, the reaction proceeded in a similar fashion,
but faster. The induction period lasted for 4-5 and 1.5-2 h at
512 and 531 K, respectively. These kinetic features indicate
clearly the autocatalytic nature of the conversion.

In order to confirm that the reaction is autocatalytic, some of the reaction products were added to the starting methanol. The addition of ethylene or cis-2-butene (5 % of methanol in moles) decreased the "induction period" to 2 h at 512 K. This is about half of the period in the reaction with pure methanol. On the other hand, the addition of paraffins had no effect on the induction period. Therefore, it is concluded that the autocatalysis is caused by the reaction of methanol and olefins, which is much faster than the reaction to produce incipient olefins. Thus, as proposed by Chen and Reagen(9), the reaction can be divided into the following two steps.

$$CH_3OH \xrightarrow{\ k_1\ } \text{olefins (ethylene)}$$

$$\text{olefins} + CH_3OH \xrightarrow{\ k_2\ } \text{olefins (+ paraffins)}$$
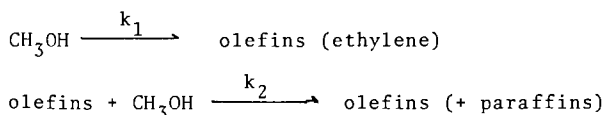
The ratio of the rate constants (k_1/k_2) for the two reactions was estimated as 7×10^{-4} and 1.1×10^{-3}, respectively(4). The abrupt change of the conversion with temperature, as observed in a flow system, may be caused at the temperature, at which the certain amount of olefins is accumulated in a reactor. As for the mechanism, one must consider the two steps separately. The second step, the propagation of the carbon-chain, plausibly involves the electrophilic methylation of olefins, for which Bronsted acid sites are responsible, as first pointed by Anderson et al.(11). The scheme of the first step will be discussed below.

Conversion of Methanol over Nafion-H and Heteropolyacids

To obtain information on the sites responsible for the conversion, the reaction was carried out in a gas-recirculation system over the catalyst with preadsorbed pyridine. Prior to the reaction, the catalyst was exposed to pyridine vapor for 2 h at 473 K, and then evacuated at 512 K for 1 h. The only product observed was dimethyl ether and no hydrocarbons were produced in 47 h. The reaction over Na-ZSM-5 give a similar result. These facts indicates that the acid sites plays a decisive role in the formation of hydrocarbons. This implies that the reaction should proceed also over strongly acidic solid other than zeolites.

Nafion-H, a perflorinated resin sulfonic acid, is known to have high catalytic activities for the alkylation of benzene with alcohols and the methylation of phenol with methanol, and is reported to be a solid superacid. The conversion of methanol over Nafion-H was examined with a closed-recirculation system(4). Methanol of 7.7×10^3 Pa was introduced over 1 g of Nafion-H at 512 K, and the gas-phase composition was analyzed at appropriate intervals. Dimethyl ether is the only product for the first 2 h, and after 2 h, the rate of hydrocarbon formation was accelerated with time, which is characteristic of an autocatalytic reaction. The fact that the features of the conversion over Nafion-H resembles those over ZSM-5 strongly indicates that Bronsted acid sites are active centers for the conversion.

It was found that dodecatungstophosphoric acid ($H_3PW_{12}O_{40}$), a highly acidic solid, also had high activities for methanol conversion(12).
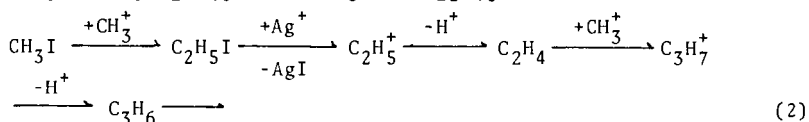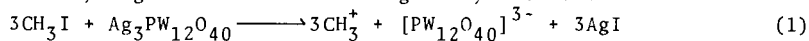
Interaction of Methanol with ZSM-5, Infrared Study

Infrared spectroscopic study revealed that methanol (CD_3OH) reacts with the acidic hydroxyl group of ZSM-5 to form methoxyl group (CD_3O-) at 423 K. When the zeolite which beared CD_3O- groups was heated at 512 K, the CD_3 bands completely disappeared and bands due to O-D stretching appeared, indicating that the desorption of methoxyl groups is accompanied with the cleavage of C-D bonds. The analysis of molecules desorbed from the surface revealed that the decomposition of the methoxyl groups leads to the formation of hydrocarbons.
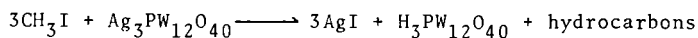
The reaction of the methoxyl group with benzene gave toluene, indicating that the surface methoxyl groups can be a source of "methyl carbenium ions". In other words, the "methoxyl groups" in ZSM-5 could be more properly comprehended as part of a methyl ester of the zeolitic acid than as part of a metal alkoxide, just as a methyl group in dimethyl sulfate, a good methylating agent.

Selfcondensation of Methyl Iodide over $Ag_3PW_{12}O_{40}$

In order to ascertain the role of methyl carbenium ions in the formation of carbon-carbon bonds, the attempt to generate them was made; methyl iodide was reacted with $Ag_3PW_{12}O_{40}$. Methyl carbenium ions were supposed to be generated according to Eq.(1) because of the high tendency of forming silver iodide, and then to attack the carbon-hydrogen bonds of remaining methyl iodide.

$$3CH_3I + Ag_3PW_{12}O_{40} \longrightarrow 3CH_3^+ + [PW_{12}O_{40}]^{3-} + 3AgI \qquad (1)$$

$$CH_3I \xrightarrow{+CH_3^+} C_2H_5I \xrightarrow[-AgI]{+Ag^+} C_2H_5^+ \xrightarrow{-H^+} C_2H_4 \xrightarrow{+CH_3^+} C_3H_7^+$$

$$\xrightarrow{-H^+} C_3H_6 \longrightarrow \qquad (2)$$

The expected overall reaction is summarized as

$$3CH_3I + Ag_3PW_{12}O_{40} \longrightarrow 3AgI + H_3PW_{12}O_{40} + \text{hydrocarbons}$$

Experiments were carried out as follows. The powder of $Ag_3PW_{12}O_{40}$ (0.28 mmol) was reacted with methyl iodide vapor (1.80 mmol) at 423 or 573 K in a closed-recirculation system. The results are given in Table 1. The reaction was almost finished by the time when the first analyses were made, 15 and 5 min for the reaction at 423 and 573 K, respectively, the only minor change in the gas-phase composition being observed thereafter. About 3 moles of methyl iodide disappeared from the gas phase, and, at the same time, most of carbon atoms from consumed methyl iodide appeared as hydrocarbons, as was expected from Eq.(2). It should be noted that methyl iodide does not convert into hydrocarbons over $H_3PW_{12}O_{40}$ or ZSM-5 even at 573 K. At 573 K, the distribution of the hydrocarbon products of the stoichiometric reaction of CH_3I and $Ag_3PW_{12}O_{40}$ are very similar to that of the products in the catalytic conversion of methanol over $Ag_3PW_{12}O_{40}$ supported on active carbon, indicating that the mechanism of the propagation of the carbon-carbon chain is the same in the two systems.

The results clearly shows that methyl carbenium ions play an essential role in the formation of carbon-carbon bonds. It is worthy of note that hydrocarbon formation is fast in the CH_3I-$Ag_3PW_{12}O_{40}$ system even at 423 K. At the same temperature, methanol gives methoxyl group over ZSM-5 and yields dimethyl ether, but not

Table 1   Reaction Products of Reaction of CH_3I and $Ag_3PW_{12}O_{40}$

Temperature/K	423		573		573[**]
Reaction time/min	15	30	5	40	
$Ag_3PW_{12}O_{40}$ used/mmol(A)	0.28		0.28		
CH_3I consumed/mmol(B)	0.95	1.04	0.80	1.22	
B/A	3.4	3.7	2.9	4.4	
Carbon atoms in hydrocarbons/mmol(C)	0.83	0.75	0.82	0.81	
C/A	3.0	2.7	2.9	2.9	
Distribution of Hydrocarbons[*]					
CH_4	0	0.2	6.3	5.9	6.8
C_2H_4	0.1	0	10.5	7.9	16.6
C_2H_6	—	—	—	—	0.6
C_3H_6	0.3	0.7	21.2	10.8	18.7
C_3H_8	0	0	8.4	28.3	5.6
C_4H_8	11.9	17.3	21.2	15.9	33.9
C_4H_{10}	33.7	34.1	12.5	17.8	
C_5	23.2	23.0	13.5	10.0	10.6
C_6	8.2	9.9	6.3	3.3	
C_7	18.2	13.9	0.1	0.1	7.2
C_8	4.3	0.9	0	—	

[*] Distributions were calculated on carbon-number basis exclusive of ethane used as an internal standard. Separate experiments revealed that ethane yield was negligible at 423 K and 1.0 % at 573 K.
[**] Hydrocarbon distribution in methanol conversion over $Ag_3PW_{12}O_{40}$ supported on active-carbon under the conditions of W/F = 50 g h mol^{-1} and methanol pressure of 10 x 1.3 kPa.

hydrocarbons. Difference in the temperature required for C-C bond formation in the two systems indicates that the reactivity of CH_3 moiety depends on the chemical environment, where CH_3 moiety is located. The less reactive CH_3 in methoxyl groups in ZSM-5 need higher temperature to be reactive enough to attack on C-H bonds, in comparison with incipient CH_3^+ from by the stoichiometric reaction.

REFERENCES

(1) Chang, C. D., and Silvestri, A. J., J. Catal., 47, 249 (1977)
(2) Kaeding, W. W., and Butter, S. A., J. Catal., 61, 155 (1980)
(3) Kagi, D., J. Catal., 69, 242 (1981)
(4) Ono, Y., and Mori, T., J. Chem. Soc., Faraday Trans. I, 77, 2209 (1981)
(5) Olah, G. A., Klopman, G., and Schlosberg, R. H., J. Am. Chem. Soc., 91, 3261 (1969)
(6) Olah, G. A., DeMember, J. R., and Shen, J., J. Am. Chem. Soc., 95, 4952 (1973)
(7) van den Berg, J. P., Wolthuizen, J. P., and van Hooff, J. H. C., "Proceedings 5th Internat. Conf. on Zeolites, Naples, 1980" (L. V. Ree, Ed.) p.649, Hayden, New York, 1980
(8) Zatorski, W., and Kryzanowski, S., Acta Phys. Chem., 24, 347 (1978)
(9) Chen, N. Y., and Reagan, W. J., J. Catal., 59, 123 (1979)
(10) Ono, Y., Imai, E., and Mori, T., Z. Phys. Chem., N.F., 115, 99 (1979)
(11) Anderson, J. R., Mole, T., and Christov, V., J. Catal., 61, 477 (1980)
(12) Baba, T., Sakai, J., and Ono, Y., Bull. Chem. Soc. Jpn., 55, 2657 (1982)

Synergism in Acetic Acid/Methanol Reactions Over ZSM-5 Zeolites

Clarence D. Chang, Nai-Yuen Chen,
L. R. Koenig and Dennis E. Walsh

Mobil Research and Development Corporation
Central Research Division
P. O. Box 1025
Princeton, New Jersey 08540

INTRODUCTION

Carboxylic acids are readily converted to aromatic hydrocarbons over ZSM-5 zeolites (1). The initial step of the reaction sequence involves oxygen elimination by decarboxylation, decarbonylation and/or dehydration. The residual hydrocarbon moiety is then aromatized, we believe, via classical carbenium ion pathways (2).

The reaction causes rapid catalyst deactivation, which can be alleviated by adding methanol to the feed (3). The synergistic effect of methanol on acetic acid aromatization is the subject of this study.

EXPERIMENTAL DATA

A. FIXED BED RESULTS

Acetic Acid

Acetic acid was reacted over HZSM-5 at 316°C and 370°C, 1 atm., 1 LHSV. Results are shown in Table 1. At 316°C, activity is low (8% conversion). Decarboxylation is the principal mode of oxygen elimination, resulting in acetone and hydrocarbons, mainly isobutylenes and aromatics. At 370°C, both decarboxylation and dehydration are important, however, catalyst deactivation is rapid, with conversions dropping from 100% to 71.4% in 1.3 hr.

Again the main products are acetone, isobutylene and aromatics. Decarbonylation is a relatively minor reaction.

Acetic Acid/Methanol Mixture

A 4/1 molar mixture of methanol/acetic acid was reacted over HZSM-5 at 370°C, 1 atm., 1 As seen in Table 1, the conversion remains quantitative after 3 hr. No evidence of catalyst deactivation was seen during this period. The addition of methanol suppresses CO_2 formation, and dehydration becomes the main oxygen-elimination reaction. The hydrocarbons are mostly aromatic (79%).

B. FLUID-BED RESULTS

Experimental data are presented in Table 2. Two conversions are presented for each run. "Total conversion" represents the conversion to all products, while "conversion to non-oxygenates" represents conversion to all hydrocarbon, COx and H_2O products. The overall yields from the methanol experiment are in reasonable agreement with data obtained in the fluid bed MTG process (5). The hydrocarbon gas products, however, are higher in propene and lower in isobutane probably due to the lower reaction pressure used in this study.

Acetic Acid and Methylacetate

The data obtained for acetic acid illustrate several interesting points which can be contrasted with the earlier continuous operation in a fixed bed. First, total conversions >90% may be maintained indefinitely provided periodic catalyst regeneration is employed. The experimental data show that decarboxylation takes place to a large extent.

On a weight basis, acetic acid yields less than 40% as much hydrocarbon as methanol. The lower yield is primarily due to carbon loss by decarboxylation, and to a small extent, to coke and CO production.

Methyl acetate has a higher carbon content (48.6% C) than acetic acid and methanol and despite decarboxylation and coke, the observed hydrocarbon yield remains comparable to that of methanol. Moreover, selectivity for direct conversion to C_5^+ hydrocarbons is higher than that of acetic acid or methanol (79.5%). Thus, the direct yield of C_5^+ liquid hydrocarbons is 32.1% on charge vs 23.3% for methanol.

Acetic Acid/Methanol Mixtures

Processing a 1.9/1 or a 3.8/1 molar mixture of CH_3OH and acetic acid provided observations similar to fixed-bed results, i.e. an enhancement in C_5^+ liquid yield at the expense of C_4^- vs what might be expected if the mixture behaved as the average of its two components, the calculated values for which are shown in parentheses in Table 2. The selectivities of the hydrocarbon products amplify the observed synergism with respect to C_5^+ liquids. Furthermore, there is an enhancement in total hydrocarbon yield vs linear combination expectations.

This is illustrated in Figure 1 which shows the effect of increasing mole percent methanol in the MeOH/acetic acid charge and attendant decrease in oxygen rejection as CO_2 and increase in oxygen removal as H_2O. Thus, more carbon remains available to form hydrocarbon products, much of it becoming C_5^+ liquids.
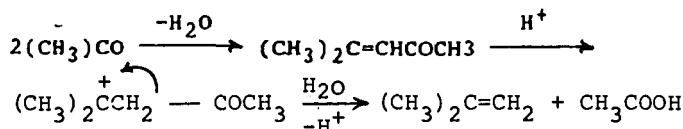
147

DISCUSSION

A. AROMATIZATION PATHWAY FOR ACETIC ACID

As shown previously, the major initial products of acetic acid reaction over HZSM-5 are acetone, isobutylene and CO_2.

Acetone formation from acetic acid is a known reaction and is often referred to as "ketonization" (6,7). The reaction was originally observed on 3d-oxides, but has been reported for SiO_2/Al_2O_3 and mordenite (8,9) catalysts. The mechanism of ketonization via decarboxylation is discussed later.

Isobutylene formation from acetone decomposition over silica gel and SiO_2-Al_2O_3 (8,9,10) and zeolites (1,12) has also been reported. The reaction mechanism over acid zeolites is believed to involve an aldol condensation followed by β-scission (12):

$$2(CH_3)CO \xrightarrow{-H_2O} (CH_3)_2C=CHCOCH3 \xrightarrow{H^+}$$

$$(CH_3)_2\overset{+}{C}CH_2 - COCH_3 \xrightarrow[-H^+]{H_2O} (CH_3)_2C=CH_2 + CH_3COOH$$

In the present case, the isobutylene is converted by HZSM-5 to aromatics and paraffins, while the acetic acid re-enters the catalytic cycle.

Neglecting catalyst deactivation for the moment, the main reactions of hydrocarbon formation from acetic acid over HZSM-5 are summarized in the following scheme:

Scheme A

$$CH_3COOH \quad \rightthreetimes \quad CH_3COOH \quad \rightthreetimes \quad (CH_3)_2C=CH_2 \longrightarrow [CH_2]_x$$

$$CO_2 + H_2O \qquad 2(CH_3)_2CO$$

$[CH_2]_x$ = aromatics + paraffins
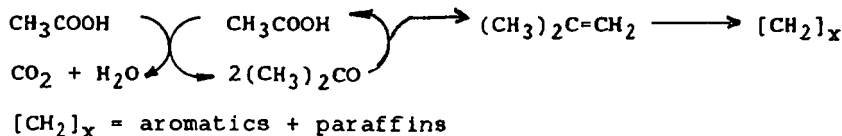
B. MECHANISM OF CATALYST DEACTIVATION AND THE ROLE OF METHANOL

The ketonization of acetic acid over 3d-oxides such as chromia and TiO_2 at 350°-460°C has been shown to involve the bimolecular nucleophilic attack of an acylium ion by an acetate species with CO_2 elimination (7,13):

$$CH_3\overset{+}{C}O + CH_3\overset{O}{\underset{|}{C}}-O^- \longrightarrow (CH_3)_2CO + CO_2$$

Over the TiO_2, the acylium ion precursor was ketene, detected by IR (7).

It seems reasonable to assume a similar mechanism for strongly acidic zeolites, except that in this case, the acylium ion may be directly generated:

$$CH_3COOH + HO\text{-zeol} \longrightarrow CH_3\overset{+}{C}O \quad \overset{-}{O}\text{-zeol} + H_2O$$

At sufficiently high temperature, an acetate species results, as has been reported for NaHY (14):
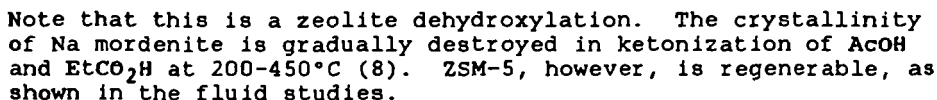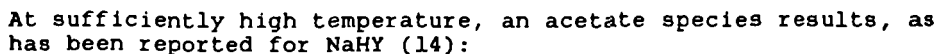
$$RCOOH + HO\text{-zeol} \xrightarrow{350°C} R\overset{-}{C}OO + \overset{+}{zeol} + H_2O$$

Note that this is a zeolite dehydroxylation. The crystallinity of Na mordenite is gradually destroyed in ketonization of AcOH and $EtCO_2H$ at 200-450°C (8). ZSM-5, however, is regenerable, as shown in the fluid studies.

We assume that dehydroxylation is the primary mechanism of zeolite deactivation by carboxylic acids. We propose that the acylium ion is the precursor to acetate

$$CH_3\overset{+}{C}O \quad \overset{-}{O}\text{-zeol} \xrightarrow{\Delta} CH_3\overset{-}{C}OO + \overset{+}{zeol}$$

and that methanol "traps" the acylium ion

$$CH_3OH \longrightarrow [:CH_2] + H_2O$$
$$CH_3\overset{+}{C}O + :CH_2 \longrightarrow CH_3CO\overset{+}{C}H_2$$

The resulting α-ketocarbenium ion is converted to acetone by hydride abstraction from a suitable source, e.g. isoalkane.

$$CH_3CO\overset{+}{C}H_2 + RH \longrightarrow (CH_3)_2CO + R^+$$

As support for this step we cite the $AlCl_3$-catalyzed conversion of pivaloyl chloride to methylisopropyl ketone in the presence of isopentane as hydride source (15):

This intervention by methanol, therefore, competes with acetate formation, CO_2 formation and attendant zeolite

dehydroxylation/deactivation. The proposed mechanism is
summarized as Scheme B.

Scheme B

H_2O

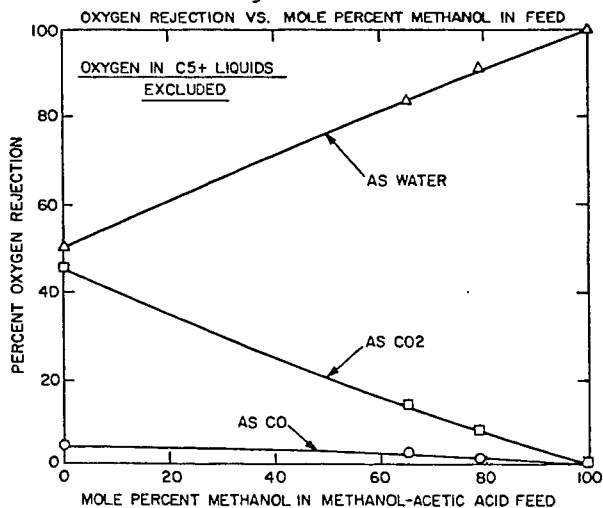This scheme can obviously be adapted to methyl acetate conversion
by including the equilibrium between methyl acetate, methanol and
acetic acid.

Figure 1.

OXYGEN REJECTION VS. MOLE PERCENT METHANOL IN FEED

OXYGEN IN C5+ LIQUIDS EXCLUDED

AS WATER

AS CO2

AS CO

PERCENT OXYGEN REJECTION

MOLE PERCENT METHANOL IN METHANOL-ACETIC ACID FEED

150

References

1. Chang, C. D. and Silvestri, A. J., J. Catal. $\underline{47}$, 249, (1977).

2. Poutsma, M. L., in "Zeolite Chemistry and Catalysis", (Ed. J. A. Rabo), ACS Monograph 171, 1976, Ch.8.

3. Chang, C. D., Lang, W. H. and Silvestri, A. J., U.S. Patent 3,998,898.

4. (a) Argauer, R. J. and Landolt, G. R., U.S. Patent 3,702,886;
   (b) Olson, D. H., Kokotailo, G. T., Lawton, S. L. and Meier, W. M., J. Phys. Chem. $\underline{85}$, 2238 (1981).

5. Liederman, D., Jacob, S. M., Voltz, S. E. and Wise, J. J., 2nd. Eng. Chem. Process Des. Dev. $\underline{17}$(3), 340 (1978).

6. Kuriacose, J. C. and Jewur, S. S., J. Catal. $\underline{50}$, 330 (1977), and references therein.

7. Gonzalez, F., Munuera, G. and Prieto, J. A., J. Chem. Soc., Faraday Trans. 1, $\underline{74}$(6), 1517 (1978).

8. Sosnina, I. E. and Lysenko, S. V., Vestn. Mosk. Univ., Khim. $\underline{14}$(3), 354 (1973).

9. Sosnina, I. E., Zh. Fix. Khim. $\underline{51}$, 2001 (1977).

10. Fujii, R., J. Chem. Soc. Japan $\underline{65}$, 181 (1944).

11. Kurganova, S.Ya., Rudenko, A. P. and Balandin, A. A., Zh. Org. Khim. $\underline{2}$(5), 804 (1966).

12. Chang, C. D., Lang, W. H. and Bell, W. K., in "Catalysis in Organic Synthesis, 1981", (Ed. W. E. Moser), in press.

13. Swaminathan, R. and Kuriacose, J. C., J. Catal. $\underline{16}$, 357 (1969).

14. Bielanski, A. and Datka, J., J. Catal. $\underline{32}$, 183 (1974).

15. Balaban, A. T. and Nenitzescu, C. D., Annalen $\underline{625}$, 66 (1959).

16. Dimethyl phenols are most likely formed according to the following mechanism:

$$3(CH_3)_2CO \xrightarrow{-2H_2O} \text{(cyclohexenone)} \xrightarrow[-CH_3]{-H_2} \text{(phenol)} \rightleftharpoons \text{isomers}$$
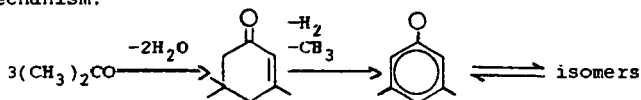
   Step A is well known (17,18). The dimethyl analogue of Step B has been described by Horning (19). Demethylation from a quaternary carbon upon dehydrogenation is a known reaction (20).

17. Whitmore, F. C., "Organic Chemistry", Van Nostrand, N.Y., 1937, p.253.

18. Szabo, D., Acta Chim. Acad. Sci. Hung. $\underline{33}$, 425, (1962).

19. Horning, E. C., J. Amer. Chem. Soc. $\underline{67}$, 1421 (1945).

20. Linstead, R. P., and Thomas, S. L. S., J. Chem. Soc., 1127 (1940).

TABLE 1

Conversion of AcOH and AcOH/MeOH over HZSM-5

Fixed Bed Data

Feed	AcOH	AcOH	AcOH	AcOH(1 mol) + MeOH(4 mol)
T, °C	316	370	370	370
P, psig	0	0	0	0
LHSV, hr^{-1}	1	1	1	1
TOS, hr	1.5	1.3	3.0	3.0
Conversion, wt.%	8.0	71.4(a)	60.7	100
Products, wt.%				
H_2	0.1	--	--	--
CO	1.7	1.6	1.5	1.3
CO_2	32.9	15.7	22.8	3.2
H_2O	tr	56.1	24.3	55.7
Acetone	33.4	6.0	32.8	--
Other O-cpds	2.7	0.7(b)	3.8(b)	--
Hydrocarbons	29.2	19.9	14.8	39.8
Hydrocarbons, wt.%				
C_1	--	--	0.1	1.2
C_2	--	--	0.2	0.5
$C_2^=$	0.6	1.7	1.3	1.2
C_3	--	2.7	0.1	5.6
$C_3^=$	1.8	2.7	3.3	0.8
C_4	--	0.4	0.2	3.4
$C_4^=$	17.1(c)	7.1(c)	26.2(c)	1.3
C_5	--	0.1	--	2.7
$C_5^=$	--	0.3	0.3	0.3
C_6^+ aliphatic	--	--	0.1	4.0
Aromatics	80.5	84.6	68.1	79.0

(a) 100% conversion at 0.3 hr.
(b) >70% dimethylphenols (16).
(c) >75% isobutylene.
(d) 81% conversion at 1.5 hr.

TABLE 2

Conversion of AcOH, MeOAc and AcOH/MeOH over HZSM-5

Fluid Bed Data

410°C, 1 atm, 1.0-1.1 WHSV, 20 min Reaction Intervals

	Methanol CH_3OH	Acetic Acid CH_3COOH	Methyl Acetate $CH_3CO_2CH_3$	1.9/1 (molar) MeOH/ Acetic Acid	3.8/1 (molar) MeOH/ Acetic Acid
Total Conversion	98.6	91.2	89.4	>91 (94.9)	95
Conversion to Non-Oxygenates	98.6	79.8	86.1	90.4 (89.2)	--
Products (Wt.% of Charge)					
CO	0.0	3.7	6.2	2.1 (1.8)	1.1 (1.2)
CO_2	0.2	31.4	17.6	9.4 (15.8)	5.2 (10.6)
H_2O	55.8	28.4	21.5	45.3 (42.1)	48.8 (46.7)
Oxygenates	1.4	20.2	13.9	9.6 (10.8)	5.2 (7.7)
C_4^- Hydro-carbon gas	19.0	3.8	6.0	7.9 (11.4)	9.9 (13.9)
C_5^+ liquid Hydrocarbon	23.3	10.6	32.1	24.9 (17.0)	28.7 (19.1)
Total Hydro-carbons	42.3	14.4	38.1	32.8 (28.4)	38.6 (33.0)
Coke	0.3	1.9	2.7	0.8 (1.1)	1.1 (0.8)
Wt.%'s of Hydrocarbon					
$C_1 + C_2$	5.4	1.5	5.6	7.2	7.6
$C_3^=$	1.6	0.1	0.7	0.4	0.6
C_3	25.9	5.2	6.7	13.8	14.2
$iC_4^=$	5.5	0.5	0.3	0.4	0.5
$nC_4^=$	0.4	0.3	0.0	0.1	0.1
C_4	5.8	15.7	1.4	1.6	1.9
Total C_4^-	44.6	23.3	14.7	23.5 (34.0)	24.9 (37.5)
C_5^+ liquid	54.7	65.0	78.7	74.1 (59.8)	72.3 (58.1)
Coke	0.7	11.7	6.6	2.4 (6.2)	2.8 (4.4)

Hydroconversion of Long-Chain n-Alkanes on Pt/HZSM-5
Zeolite

by Jens Weitkamp [a] and Peter A. Jacobs [b]

a) Engler-Bunte-Institute
   Division of Gas, Oil, and Coal
   University of Karlsruhe
   Richard-Willstätter-Allee 5
   D-7500 Karlsruhe, West-Germany

b) Centrum voor Oppervlaktescheikunde
   en Colloïdale Scheikunde
   Katholieke Universiteit Leuven
   De Croylaan 42
   B-3030 Leuven, Belgium

Zeolite catalysts of medium-pore size are getting increasing
acceptance in commercial processes, e.g., in hydrodewaxing
of middle distillates. In this process n-paraffins and part
of the isomers with one methyl branching are selectively
hydrocracked in order to improve the low temperature pro-
perties, especially the pour point. Nonetheless, relatively
little is known on the shape-selectivity effects occuring
during hydroconversion of long-chain alkanes on medium-pore
zeolites. Recently, the authors reported (1) on the shape-
selective isomerization and hydrocracking of n-decane on
Pentasil zeolites. The present paper extends these data to
the homologous series of n-alkanes with 9 to 16 carbon atoms.

A Pt/HZSM-5 zeolite catalyst was employed throughout this
study. The zeolite with a Si/Al ratio of 60 was prepared
according to published methods (2). It was loaded with 0.5
wt.-% of platinum by contact with an aqueous solution of
$[Pt(NH_3)_4]Cl_2$. The catalytic experiments were conducted with
the pure n-alkanes in a hydrogen atmosphere at a total pressure
of 2 MPa and a hydrocarbon partial pressure of 20 kPa except
for n-hexadecane where the latter was 10 kPa to avoid conden-
sation at low reaction temperatures. A fixed bed reactor was
used. $W/F_{n-alkane}$ was in the order of 100 g·h/mol. With each
feed the reaction temperature was varied between 200 and
300 $^{\circ}$C so that a wide range of conversion could be covered.
Product analysis was achieved by capillary GLC techniques.

Two types of reaction occur during hydroconversion of n-
alkanes on Pt/HZSM-5, viz. isomerization and hydrocracking.
In Fig. 1 the yields of branched isomers and of hydrocracked
products are plotted versus temperature for the experiments
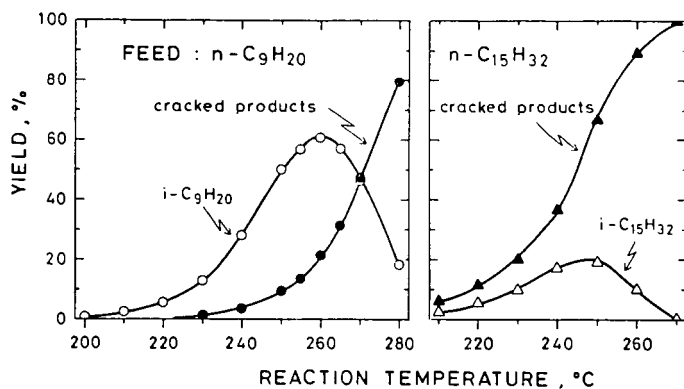with n-nonane and n-pentadecane.

Fig. 1: Hydroconversion of n-Nonane and n-Petadecane
on Pt/HZSM-5

While n-nonane can be isomerized under mild conditions with-
out significant hydrocracking the yield of i-pentadecanes
from n-pentadecane is low throughout the whole range of
temperature and, hence, of conversion. The quantitative eva-
luation of the influence of reaction temperature on conver-
sion shows that the apparent energy of activation decreases
with increasing chain length. This could indicate increasing
diffusional resistances.

The distributions of i-alkanes formed by isomerization of the
n-alkanes differ substantially from those observed over
faujasite zeolites (3). In particular, methyl isomers strongly
predominate on Pt/HZSM-5 up to 90 % conversion. Small amounts
of dimethyl isomers with one branching in the 2-position are
also formed while ethyl isomers are absent. These results
are best interpreted in terms of product shape-selectivity.

Distributions of individual methyl isomers formed from three
selected n-alkanes at moderate conversions around 10 % are
given in Table 1. The main product from n-nonane is 2-methyl-
octane. This is in principal agreement with our earlier
results (1) of n-decane conversion on Pt/HZSM-5 and might
reflect a restricted transition state shape-selectivity.
On the other hand, roughly equal amounts of individual
methyl isomers are formed from n-tridecane and n-pentade-
cane (Table 1). These distributions are problably close
to equilibrium.

Table 1: Distributions of Methyl Isomers Formed from
         Various n-Alkanes (Values in mol-% of total
         methyl isomers)

Feed	$n - C_9H_{20}$	$n - C_{13}H_{28}$	$n - C_{15}H_{32}$
Temperature, $^{\circ}C$	230	220	210
Conversion, %	14.6	10.6	9.3
Yield of $i-C_mH_{2m+2}$, %	13.2	8.2	2.8
	2-M-Oc 42.6	2-M-Do 15.0	2-M-Te 14.6
	3-M-Oc 38.0	3-M-Do 22.3	3-M-Te 18.8
	4-M-Oc 19.4	4-M-Do 18.0	4-M-Te 15.4
		5-M-Do 22.8	5-M-Te 15.5
		6-M-Do 21.9	6-M-Te 18.0
			7-M-Te 17.7

Hydrocracking on Pt/HZSM-5 is purely ionic, i.e., no hydro-
genolysis on Pt-sites takes place. This can be concluded
from the absence of methane and ethane. Typical carbon num-
ber distributions of the cracked products from n-tetrade-
cane and n-pentadecane are depicted in Fig. 2. For comparison
the corresponding distributions on a Y-type zeolite with
a pure primary cracking selectivity are given.

n-C$_{14}$H$_{30}$; X$_{Cr.}$ = 6 °/.   n-C$_{15}$H$_{32}$; X$_{Cr.}$ = 12 °/.

△ Pt/CaY
○ Pt/HZSM-5

mol / 100 mol cracked

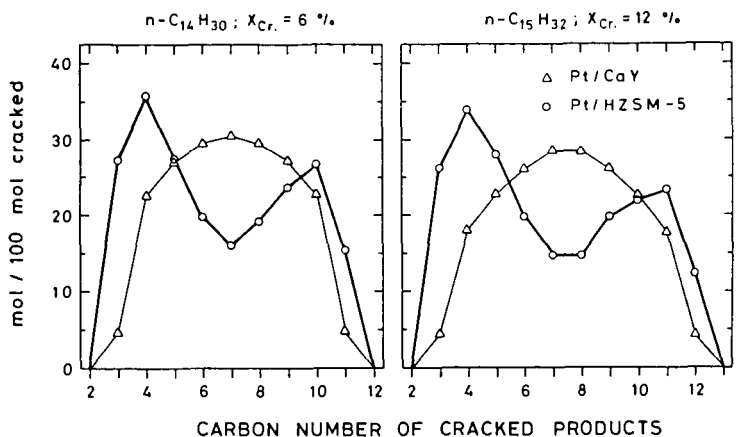CARBON NUMBER OF CRACKED PRODUCTS

Fig. 2: Carbon Number Distributions in Hydrocracking
        of n-Tetradecane and n-Pentadecane

The curves for Pt/HZSM-5 are not fully symmetrical which
is indicative of some secondary cracking. It is evident
that the cracking selectivity on Pt/HZSM-5 deviates con-
siderably from the one on faujasites. In particular, more
C_3 and C_4 as well as C_{m-3} and C_{m-4} (m = carbon number of
feed) are formed on ZSM-5. Moreover, the distribution curves
for the medium-pore zeolite exhibit distinct minima.

The cracked products on Pt/HZSM-5 consist of n-alkanes and
methyl isomers. Detailed isomer distributions will be given
in the paper. A reaction network for shape-selective rearran-
gements and β-scissions in the pores of ZSM-5 will be deve-
loped.

References

(1) P.A. Jacobs, J.A. Martens, J. Weitkamp, and H.K. Beyer,
    Farad. Discuss. Chem. Soc. 72, 353 (1982)

(2) R.J. Argauer and G.R. Landolt, US Patent No. 3 702 886
    (1972)

(3) J. Weitkamp, Ind. Eng. Chem., Prod. Res. Devel.,
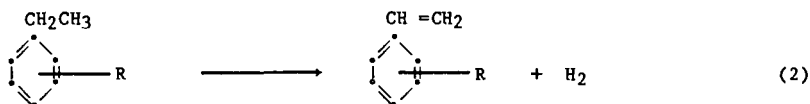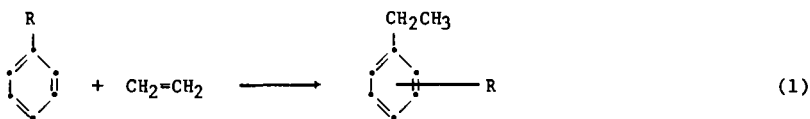   in press

Para-Methylstyrene – A New Monomer and Polymer for Industry

Warren W. Kaeding, L. Brewster Young and A. G. Prapas

Mobil Chemical Co., P. O. Box 1028, Princeton, N.J.   08540

INTRODUCTION.   The present large volume styrene industry began during World War II as part of the effort to produce synthetic rubber to replace supplies of natural rubber which were suddenly cut off from sources in Asia (1,2).   A rapid growth in polymer technology eventually followed.   A considerable number and variety of new monomers were synthesized, purified and polymerized to establish the principles and products of the large volume styrenics plastics industry as we know it today.

VINYLTOLUENE.   When toluene was substituted for benzene in the alkylation step, ethyltoluene was produced, Equation 1 (R=CH₃).   The corresponding vinyltoluene was obtained by a subsequent catalytic dehydrogenation, Equation 2, in a manner analogous to the process for producing styrene (3).   By contrast with styrene, however, a mixture of three isomers was formed.   Different polymer

$$
\text{R} \quad + \quad CH_2=CH_2 \quad \longrightarrow \quad CH_2CH_3 \; \text{---R} \tag{1}
$$

$$
CH_2CH_3 \; \text{---R} \quad \longrightarrow \quad CH=CH_2 \; \text{---R} \quad + \quad H_2 \tag{2}
$$

properties of these individual isomers and various mixtures were observed giving rise to more complex separation and purification steps.   The vinyltoluene of commerce which eventually emerged from this work is composed of approximately 35% para and 65% meta isomers determined primarily by the ratio produced during alkylation with an HCl-AlCl₃ catalyst and practical isomer separation limitations (4).

Styrene is the simplest vinyl aromatic with the fewest production and purification problems.   Polymer properties of styrene were also favored by comparison with the vinyltoluene mixtures which could be efficiently produced with the catalysts and processes available.   As a result, styrene has become the dominant vinyl aromatic monomer and polymer in the marketplace.

ZEOLITE CATALYTS.   During the past three decades, interest and knowledge of the structure and catalytic properties of the naturally occurring zeolites has grown (5,6).   More recently, this effort has expanded dramatically with the development of techniques for manufacture of many of these materials and especially with the discovery of unique, new synthetic zeolites not found in nature which have demonstrated desirable catalytic properties (7).

Zeolite catalysts are crystals composed of silicon and aluminum oxides which contain pores and channels of precise and uniform dimensions.   Chemical reactions occur primarily within the pores at catalytic sites, often acidic protons, present on the internal framework structure.   The dimensions of Mobil ZSM-5 class zeolite pores are sufficient to admit certain substituted benzene derivatives.

However, analogues with bulky side-chains or polycyclic rings can not diffuse in or out of the pores to undergo a chemical reaction or be produced within the pores. Zeolite catalysts have shape selective properties by virtue of the limited space within the pores (7).

Toluene can be alkylated with ethylene to produce ethyltoluene over (unmodified) HZSM-5 catalyst containing acidic sites, Equation 1 (8). The starting materials and products can diffuse in and out of the pores. The composition of products observed, however, differs significantly from that found with an HCl-AlCl3 catalyst. The amount of ortho isomer was reduced by an order of magnitude, Table 1. An examination of the relative minimum dimensions of the ethyltoluene isomers, Table 2, indicates that the para isomer is smallest (9). The small difference between the ortho and meta isomers is also significant. We believe that the product mix observed was a result of the precise dimensions of the zeolite catalyst pores. A subtle distinction was made between the meta and ortho isomers based on size, favoring the smaller isomer, either by rate of formation and/or rate of diffusion out of the pore (10).

PARA-SELECTIVITY. To magnify this effect, methods have been developed for reducing the effective pore and channel dimensions as originally synthesized by modification of the catalyst with physical treatments and chemical reagents. Para-selective alkylation catalysts were produced. A dramatic difference was observed for the alkylation reaction. Ninety-seven percent of the ethyltoluene product produced was the smallest para isomer. The largest ortho isomer was virtually eliminated. The rates of diffusion between the para and ortho/meta isomers were increased by three orders of magnitude with modified para-selective catalysts (10).

The use of a modified zeolite catalyst offers several advantages for production of ethyltoluene by comparison with the HCl-AlCl3 catalyst. The undesired ortho isomer, which is produced, and must be separated and recycled is virtually eliminated. Production of di- and polyethylated toluene is inhibited because of the confined space within the pores. In addition, all of the problems of corrosion, disposal and separation encountered with the use of AlCl3 are eliminated.

POLY-PARA-METHYLSTYRENE. Samples of 99+% p-methylstyrene were prepared in the laboratory. However, we have selected a 97% para-, 3% meta-methylstyrene mixture, designated PMS, for initial polymerization studies. A comparison of typical monomer properties of PMS with styrene and commercial vinyltoluene is shown in Table 3. In broad terms, PMS is similar to styrene in its polymerization behavior. PMS polymers, with a variety of molecular weights and melt flow properties, have been prepared. Analogous copolymers were also made by substituting PMS for styrene. A study of polymer properties reveals some differences as well as similarities with polystyrene, Table 4.

A potentially important advantage of poly-PMS is its lower density relative to styrene which translates to a 4% reduction in weight required to fabricate a desired product. Poly-PMS has a glass transition temperature of 113°C, 11°C higher than polystyrene, Table 4. In addition to providing an extra margin of safety for higher temperature use and storage, decreases in molding cycle times, better mold fill properties and higher melt strengths have been observed.

A potential application where poly-PMS can give a significant improvement compared with polystyrene is in the area of flame retardancy (FR) or ignition resistance. PMS-based impact resins require lower loadings of FR reagents to meet the desired ratings.

Polystyrene is very difficult to crosslink by radiation without destroying its properties. As a result, applications using this property have not been developed. The methyl group of poly-PMS, however, provides susceptible positions for crosslinking at commercially viable levels of electron beam radiation. This

converts a thermoplastic to a thermoset resin, significantly improving its grease resistance and flammability behavior.

SUMMARY. Styrene has enjoyed a special position among vinylaromatic monomers because of its lack of isomers and consequent ease and simplicity of production. Our discovery of novel technology to produce p-ethyltoluene has enabled us to manufacture a substituted vinyl aromatic monomer selectively. Since much benzene is produced from toluene, the direct use of toluene for PMS eliminates the first process step for styrene. Quantities of PMS from a semi-commercial plant are now available for the critical cost/performance test in the marketplace to eventually determine its place in the polymer industry.

REFERENCES
1. Baruch Committee Report, "The Rubber Situation", House Document No. 836, U.S. Printing Office, Sept. 12, 1942; p. 28.
2. Boundy, R.H.; Stoesser, S.M. In "Styrene – Its Polymers, Copolyers, and Derivatives"; Reinhold: New York, 1952; p. 11.
3. Boundy, R.H.; Boyer, R.F. In "Styrene – Its Polymers, Copolymers, and Derivatives"; Reinhold: New York, 1952.
4. Coulter, K.E.; Kehde, H.; Hiscock, B. F. "High Polymers"; Leonard, E.C., Ed.; Wiley-Interscience: New York, 1971; Vol. 24, pp. 548-549.
5. Weisz, P.B.; Frilette, V.J. J. Phys. Chem. 1960, 64 382.
6. Plank, C.J.; Rosinsky, E.J.; Hawthorne, W.P. Ind. Eng. Chem. Prod. Res. Dev. 1964, 3 165.
7. (a) Meisel, S.L.; McCullough, J.P.; Lechthaler, C.H.; Weisz, P.B. CHEMTECH 1976, 6 86; (b) Meisel, S.L. Philos. Trans. R. Soc. London 1981, A300 157; (c) Csicsery, S. M. "Zeolite Chemistry and Catalysis"; ACS Monograph No. 171, Rabo, J.A.; Ed.; American Chemical Society: Washington, D.C., 1976; (d) Weisz, P.B. Pure Appl. Chem. 1980, 52 2091.
8. Kaeding, W.W.; Young, L.B.; Prapas, A.G. CHEMTECH 1982 12 556.
9. (a) Kaeding, W.W.; Chu, C.; Young, L.B.; Weinstein, B.; Butter, S.A. J. Catal. 1981, 67 159; (b) Kaeding, W.W.; Chu, C.; Young, L.B.; Butter, S.A. J. Catal. 1981, 69 392.
10. Chen, N.Y.; Kaeding, W. W.; Dwyer, F.G. J. Am. Chem. Soc. 1979, 101 6783.

Table 1. Alkylation of Toluene with Ethylene
         Composition of Typical Product Streams

Compound, wt%	HCl-AlCl₃ [a]	ZSM-5 Class Zeolite	
		Unmodified	Modified
Light gas and Benzene	0.2	1.0	0.9
Toluene [b]	48.3	74.4	86.2
Ethylbenzene and Xylenes	1.2	1.2	0.5
p-Ethyltoluene	11.9	7.0	11.9
m-Ethyltoluene	19.3	14.7	0.4
o-Ethyltoluene	3.8	.3	0
Aromatic $C_{10}+$	14.4	1.4	0.1
Tar	0.9	0	0
Total	100.0	100.0	100.0
Ethyltoluene Isomers, %			
Para	34.0	31.8	96.7
Meta	55.1	66.8	3.3
Ortho	10.9	1.4	0

(a) Ref. 4
(b) Excess toluene is used to prevent polyalkylation and resultant build-up of
    $C_{10}+$ and tars.

Table 2. Minimum Dimensions of Alkyl Aromatics [a]

Hydrocarbon	Minimum Cross Section Å
Benzene	7.0
Toluene	7.0
Ethylbenzene	7.0
o-Xylene	7.6
m-Xylene	7.6
p-Xylene	7.0
o-Ethyltoluene	7.7
m-Ethyltoluene	7.6
p-Ethyltoluene	7.0

(a) From Fischer-Hirschfelder-Taylor hard sphere molecular
    models.

161

Table 3. Typical Monomer Properties

	PMS	Styrene	Vinyltoluene
Purity (wt% vinyl)	99.7	99.7	99.2
Isomer Distribution			
Para	97	--	33
Meta	3	--	66.7
Ortho	--	--	0.3
Refractive Index (nD25)	1.5408	1.5440	1.5395
Density, $g \cdot cm^{-3}$ (25°C)	0.892	0.902	0.893
Viscosity, cps (25°C)	0.79	0.72	0.78
Surface Tension, $dynes \cdot cm^{-1}$ (25°C)	34	32	31
Boiling Point (°C @ 760 mmHg)	170	145	168
Freezing Point (°C)	-34	-31	-77
Volume Contraction on Polymerization			
(% Calculated @ 25°C)	12	14	12
Heat of Polymerization			
($Kcal \; mole^{-1}$)	15-17	17	15-17

Table 4. Properties of Typical Polymers

Properties	Poly PMS [a]	Polystyrene
Specific gravity, gm/ml	1.01	1.05
Melt flow rate (condition G)	2.5	2.5
Thermal		
Glass transition temp. (°C)	113	102
Vicat Softening (°C)	116	109
Heat distortion temp. (°C)	95	89
Mechanical		
Tensile strength at break (psi x 10^{-3})	7.0	7.6
Elongation (%)	3.0	3.0
Tensile modulus (psi x 10^{-5})	3.2	3.6
Flexural strength (psi x 10^{-5})	12	13
Hardness (Rockwell M)	82	74
Izod impact (ft.lbs./in.)	0.3	0.3

(a) 97% para, 3% meta isomers

162

CO/H_2 CHEMISTRY IN A CHANGING ENVIRONMENT

Roy L. Pruett
Exxon Research and Engineering Company
Corporate Research Laboratories
P. O. Box 45,
Linden, NJ   07036

The catalytic chemistry of CO/H_2 has been the subject of concentrated research during the past 10 years, and especially during the past 3. This effort has been based on several assumptions, which include two that are key: (a) the cost of petroleum and petroleum-derived chemical raw materials (e.g., ethylene) will continue to escalate at a rapid pace; (b) the partial oxidation of coal to CO/H_2 for both fuel and chemical purposes will become economically competitive.

In keeping with this activity, a large number of potential products have been synthesized from CO/H_2. These vary from the simplest molecules, such as methanol, methane and ethylene, to much more complicated molecules, such as vinyl acetate, durene, long-chain α-olefins, etc.

At the present time, there have been significant changes in the projected timing for some CO/H_2 applications. These are caused by: (a) decreased demand for crude, due to conservation efforts and the accompanying oversupply and price stabilization; (b) increased emphasis on natural gas and natural gas liquids as sources for methanol and other basic commodity chemicals, especially in certain parts of the world rich in these resources.

The result of the changing environment has been a decrease in development efforts toward chemicals and fuels, except for those areas in which special situations exist. This presentation will include discussions of a number of processes which have been experimentally demonstrated, a number which are proceeding toward commercialization, some recently publicized results in key areas, and a discussion of how the changing environment has altered the outlook on CO/H_2 chemistry.

Synthesis Gas Conversion With a Transition Metal-Zeolite Catalyst

H. W. Pennline, V. U. S. Rao, R. J. Gormley, and R. R. Schehl

U. S. Department of Energy
Pittsburgh Energy Technology Center
P. O. Box 10940
Pittsburgh, PA   15236

INTRODUCTION

Recently, much interest has been generated in the synthesis of hydrocarbon
fuels from low ratio hydrogen-to-carbon monoxide mixtures using indirect
liquefaction catalysts. Studies have shown that a low H_2:CO ratio synthesis
gas is produced by the more efficient, second generation gasifiers (1). One
of the objectives of the catalyst research program of the U. S. Department of
Energy/Pittsburgh Energy Technology Center is to investigate various indirect
liquefaction catalyst systems that are capable of using low ratio synthesis
gas mixtures.

Of particular interest are catalysts that exhibit shape-selective properties.
With the advent of the Mobil methanol-to-gasoline process, ZSM-5 and other
medium pore zeolite systems have been investigated (2,3,4). Work at PETC has
involved the direct conversion of low ratio hydrogen-to-carbon monoxide synthesis
gas to liquid fuels via transition metal-zeolite combinations. In past experi-
mentation, cobalt and iron, either promoted or unpromoted, have been investigated
in tubular microreactors or in bench-scale mixed reactors. Due to the interesting
preliminary results obtained with a Co-Th-ZSM-5 catalyst, a process variable
study with this catalyst system was undertaken.

EXPERIMENTAL

The catalyst was prepared by physically mixing the transition metal-promoter
coprecipitate with the zeolite. Cobalt-thoria in a ratio of about 10/1 was
coprecipitated from a solution of the nitrates of these metals with sodium
carbonate, washed, dried, and sieved through 200 mesh. The ammonium form of
ZSM-5 was fabricated according to information in the patent literature (5).
The dried NH_4-ZSM-5 with a silica/alumina ratio of 30/1 was then sieved
through 200 mesh, mixed with the dried coprecipitate, and rolled overnight for
intimate mixing. Initially this mixture was pelleted for testing. However,
due to the frangibility of the pellets, further testing was conducted with
catalyst that was extruded with Catapal SB alumina and dried. The structural
integrity of the extrudates was greatly enhanced by the alumina binder.
Microreactor tests of the pelleted versus the extruded catalyst indicated that
the addition of the alumina binder did not significantly affect the catalyst
behavior. Extrudates were 1/8-inch-diameter cylinders with random lengths of
approximately 1/8-inch, and the final catalyst composition was 12.5 percent
cobalt, 1.2 percent thoria, 10-15 percent alumina, and the remainder ZSM-5.

The studies were carried out in a mixed reactor system as described by Berty (6).
The catalyst extrudates were loaded into a 2-inch-diameter basket and supported
by a stainless steel screen. Impeller speed was 1240 rpm. An outer furnace
heated the reactor, while excellent bed temperature control was obtained by a
modification that involved the installation of a coil in the reactor head
through which air could flow for faster heat removal.

The schematic of the system is shown in Figure 1. Synthesis gas is stored in large gas holders at ambient conditions. The gas is then boosted to high pressures after going through a silica gel trap for dehumidification and an activated carbon trap to remove sulfur impurities. The high-pressured gas is stored in a bank of aluminum cylinders rather than carbon steel cylinders to prevent carbonyl formation. Before entering the system, the gas is again flowed through an activated carbon trap. The flow is metered and controlled by a mass flow meter, and hydrogen can be blended with the $1H_2:1CO$ synthesis gas via a similar apparatus. Products exit the reactor via a downward sloping heated line (200°C) and enter a hot trap (200°C) where heavy hydrocarbons, if produced, are condensed. Lighter products are condensed in water-cooled or air-cooled traps. The product gas is metered by a wet test meter and can be directed to an on-line gas chromatograph that can analyze hydrocarbons up to C_8.

The catalyst was brought to synthesis conditions in an identical manner for each test. Initially the reactor was pressurized to 300 psig with hydrogen. The activation procedure began by flowing hydrogen at 1000 hr^{-1} space velocity over the catalyst while rapidly heating to 200°C. After maintaining this temperature level for two hours, the catalyst was heated to 350°C for twenty-one hours under the hydrogen flow. It has been reported in the literature that a 350°C reduction greatly enhances the hydrogen adsorption capacity of a cobalt catalyst (7). Afterwards, the catalyst temperature was reduced to 250°C and then the pressure was decreased to 100 psig. At these conditions the synthesis gas flow rate was incrementally increased over an hour until the design space velocity for the test was reached. Care was taken at this critical point so that temperature runaway did not occur. After this induction step, the pressure was increased to operating conditions, and afterwards the temperature was increased (10°C/hr) to synthesis conditions. Trap drainings, flow, and gas analyses were performed on a 24-hour basis for a material balance determination. All tests in this study used a $1H_2:1CO$ feed gas.

The gaseous and liquid products were characterized by various techniques. Product gas exiting the system was analyzed for hydrocarbons up to C_8 by gas chromatography. Liquid hydrocarbon samples, after a physical separation from the aqueous phase, were characterized by simulated distillation ASTM D-2887, fluorescent indicator adsorption ASTM D-1319, and bromine number ASTM D-1159. The aqueous fraction was analyzed by mass spectroscopy, and the water content was determined by the Karl Fischer reagent technique.

RESULTS AND DISCUSSION

To determine if deactivation would be a problem in the study, one of the first experiments in the process variable scan was a life test conducted at 280°C, 300 psig, and 1000 hr^{-1} space velocity of $1H_2:1CO$ synthesis gas. Data listed in Table 1 for test 1-39 at different times on stream indicate that catalyst deactivation is significant. The initial high (H_2+CO) conversion of 83.8 percent decreases after 417 hours on stream to 56.6 percent. The hydrocarbon product distribution also shifts to a lighter fraction with time, as noted by the increase in percent CH_4 (23.4 to 42.4) and by the decrease in C_5+ weight percent (61.0 to 38.5), which corresponds to the decreasing liquid product yield. The functionality of the liquid oil was constant throughout the test, with a high olefin (76) and low paraffin (20) and aromatic (4) percentages. Aqueous analyses indicated that +99 percent of this fraction was water. It

165

was concluded from this test that deactivation was a key factor, and subsequently all comparisons would be done after the same time on stream using a different catalyst charge for each test.

Test 1-42 was conducted to elucidate the role of the zeolite function of the bifunctional catalyst at the lower temperature of 280°C. Coprecipitated cobalt and thorium were added in the same proportion as the ZSM-5 based catalyst to calcined Catapal SB gamma alumina, and the mixture was then extruded with uncalcined alumina. When this test is compared to 1-39, the conversion versus time curves are almost identical, indicating that the Fischer-Tropsch component, Co-Th, is responsible for the synthesis activity of the catalyst and also is the functional component deactivating with time. However, the hydrocarbon distribution is different in each case, with the alumina based cobalt-thorium yielding a heavier product than the ZSM-5 based catalyst. This is evidenced in Table 1 by the greater wax fraction in the hydrocarbons with the alumina based catalyst (10.3 percent versus 1.8 percent) and less of the liquid oil fraction boiling in the gasoline range, as determined by simulated distillation (68 percent versus 89 percent).

The functionality of the liquid product oils indicates that more olefins are produced with the ZSM-5 based catalyst than with the alumina based catalyst. Proton NMR studies of the oils indicate that the ZSM-5 based catalyst produces a high degree of branching, whereas the alumina based catalyst product is linear. Also, β-olefins with negligible α-olefins are formed with the ZSM-5 based catalyst, whereas the opposite occurs with the alumina based catalyst.

The effect of reaction temperature was observed in four separate tests at 260°, 280°, 300°, and 320°C at process conditions of 300 psig and 4000 hr^{-1} space velocity. Results are listed in Table 1. With an increase in temperature, the hydrocarbon distribution shifts to a lighter product, as indicated by the increasing CH_4 fraction, the decreasing C_5+ fraction, and the increasing fraction boiling in the gasoline-range. Also interesting is the functionality of the product oil. With a decrease in reaction temperature from 280°C, the olefin/paraffin ratio decreases and approaches a paraffinic product, which is characteristic of cobalt catalysts, thus indicating that at the lower temperature ($\leq$ 260°C), the zeolite function does not significantly influence the reaction mechanism. The test at 300°C yielded an oil fraction not too different functionally from the 280°C test. However, at 320°C, a significant amount of aromatics was formed (46%), which can be attributed to the acid-catalyzed reactions within the zeolite framework at the higher temperature. No hydrocarbons above a carbon number of 12 were formed.

Unfortunately, at the elevated temperatures, the rate of deactivation is quite significant, as seen in Figure 2. As expected, initial conversions are greater at the higher temperatures, but the rate of deactivation is also greater at the higher reaction temperatures. Accelerated carbon or coke formation at the higher temperature could explain the rapid deactivation.

The effect of the promoter thorium can be determined by comparing test 1-57 (12.5% Co-ZSM-5) and test 1-41 (12.5% Co-1.2% ThO_2-ZSM-5), which are at the same process conditions. The thorium increases the activity of the cobalt-ZSM-5, as evidenced by the conversion data. Liquid products are more olefinic with the promoted catalyst. Also, the thorium shifts the product to a heavier hydrocarbon distribution, as noted by the decrease in the methane fraction, the increase in the C_5+ fraction, and the increase in the wax fraction.

The effects of different methods of catalyst pretreatment, which included calcination in air of only the zeolite component before mixing and extrusion, calcination in air of the total extruded catalyst, and chemically treating the zeolite before mixing and extrusion, were investigated. After the standard activation procedure and at process conditions of 4000 hr^{-1} space velocity, 300 psig, and 280°C, the activities of all catalysts tested, as characterized by conversion, were identical. A catalyst air-calcined at 350°C exhibited similar results to an uncalcined catalyst activated in hydrogen at 350°C, and no major differences existed between the calcination of only the zeolite component as compared to calcination of the total catalyst.

Three tests with Co-Th-ZSM-5 were conducted at identical process conditions, with the only difference being the calcination temperatures of the respective catalysts: 538°C (test 2-6), 450°C (test 2-2), and no calcination (test 1-41). The simulated distillation results in Table 1 indicate that a lighter gasoline range liquid product is formed after the two higher temperature calcinations, although the conversions and liquid oil yields for all three tests are very similar. The aromatic fraction in the liquid oil increases (2, 7, and 10 percent) with the increasing temperature of calcination. Calcination evidently increases the strength of the acid sites in the zeolite component, and this leads to a greater aromatic formation.

In another comparison, the ZSM-5 component was exchanged with HCl (test 1-54) rather than the usual NH_4Cl exchange (test 1-41) with the purpose of increasing the strength of the acid sites. The uncalcined zeolites were then individually mixed with equal amounts of cobalt – thorium and extruded. Each catalyst was tested in a Berty reactor as in the previous preparative work: a space velocity of 4000 hr^{-1} with $1H_2$:1CO synthesis gas, 280°C, and 300 psig. Results indicate the activity of both catalysts was the same with time on stream. However, the product selectivity for the two catalysts was different. The product from the HCl-exchanged catalyst was much lighter than that from the NH_4Cl-exchanged catalyst, as seen by the difference in gasoline-range hydrocarbons (89 versus 70 percent). Although the functionality of the liquid product is still high in olefin content for both catalysts, the aromatic content from the HCl-exchanged catalyst was higher (11 percent) than that from the NH_4Cl-exchanged catalyst (2 percent).

SUMMARY

From this study with the promoted transition metal-zeolite combination, several conclusions can be made. At medium temperature and with a low H_2:CO ratio synthesis gas, the cobalt-thorium-ZSM-5 synthesizes a highly branched olefinic product. Deactivation at these conditions can be attributed to the Fischer-Tropsch component of the catalyst. As the higher optimum temperature for the catalytic activity of the zeolite component is approached, a high fraction of aromatics is formed in the liquid product. The effect of the addition of the promoter thorium to the transition metal-zeolite catalyst is to increase olefin production and to increase the amount of liquid hydrocarbon formation. A pretreatment step (calcination or chemical), which does not alter the synthesis activity of the catalyst, activates the acid sites of the zeolite component and thus increases production of aromatics.

DISCLAIMER

Reference in this report to any specific commercial product, process, or service is to facilitate understanding and does not necessarily imply its endorsement or favoring by the United States Department of Energy.

REFERENCES

1. Hildebrand, R. E., and Joseph. L. M., 1979. Presented at the Methanol Symposium, 13th Middle-Atlantic ACS Meeting.

2. Chang, C. D., Lang, W. H., and Silvestri, A. J., 1979. J. Catal. 56:268.

3. Caesar, P. D., Brennan, J. A. Garwood, W. E., and Ciric, J., 1979. J. Catal. 56:274.

4. Rao, V. U. S., Gormley, R. J., Pennline, H. W., Schneider, L. C., and Obermyer, R., 1980. ACS Div. Fuel Chem., Prepr. 25:119.

5.   Argauer, R. J., and Landolt, G. R., 1972. U. S. Patent 3,702,886.

6. Berty, J. M., 1974. Chem. Eng. Prog., 70:68.

7. Kibby, C. L., Pannell, R. B., and Kobylinski, T. P., 1980. Presented at 7th Canadian Symposium on Catalysis, Alberta, Canada.

TABLE 1. Process Conditions and Synthesis Results

| CFSTR Test No.	1-39	1-39	1-39	1-42	2-10	1-41	1-44	1-43	1-57	2-6	2-2	1-54
Hours on Stream	33	201	417	33	37	40	32	33	37	36	36	38
Space Velocity, hr^{-1}	1000	1000	1000	1000	4000	4000	4000	4000	4000	4000	4000	4000
Temperature, °C	280	280	280	280	260	280	300	320	280	280	280	280
(H_2+CO) Conversion	83.8	67.9	56.6	80.5	25.9	61.4	66.7	54.8	55.4	64.4	66.7	63.7
H_2 Conversion	93.3	87.1	76.0	91.7	33.9	77.9	82.3	68.8	72.9	82.5	84.8	82.3
Hydrocarbon Distribution, wt%												
CH_4	23.4	34.5	42.4	22.5	17.6	18.1	38.8	65.5	26.5	20.0	18.5	21.2
C_2H_6+C_2H_4	3.9	5.4	6.1	4.1	2.4	3.1	5.7	9.7	4.0	3.9	3.2	3.1
C_3H_8+C_3H_6	5.9	6.4	7.8	5.9	5.1	5.2	5.2	5.2	7.4	4.9	4.0	3.7
C_4H_{10}+C_4H_8	4.0	3.8	5.2	4.6	4.6	6.0	6.9	5.1	7.7	3.7	3.6	6.5
C_5+	61.0	49.6	38.5	52.6	54.7	62.9	43.3	14.5	54.4	66.4	70.0	65.4
Wax	1.8	0.3	0	10.3	15.6	4.8	0.1	0	0	1.1	0.8	0
Liquid Oil Product Composition, wt%												
Aromatics	4	2	2	2	3	2	4	46	4	10	7	11
Olefins	76	83	80	43	36	82	74	25	29	72	76	68
Saturates	20	15	18	55	61	16	22	29	67	18	17	21
Liquid in Gasoline Range (BP < 204°C), wt%	89	85	90	68	58	70	91	95	85	85	85	89
Liquid Yield, gm oil/gm cat-hr	0.13	0.08	0.05	0.09	0.13	0.39	0.27	0.07	0.27	0.41	0.42	0.38
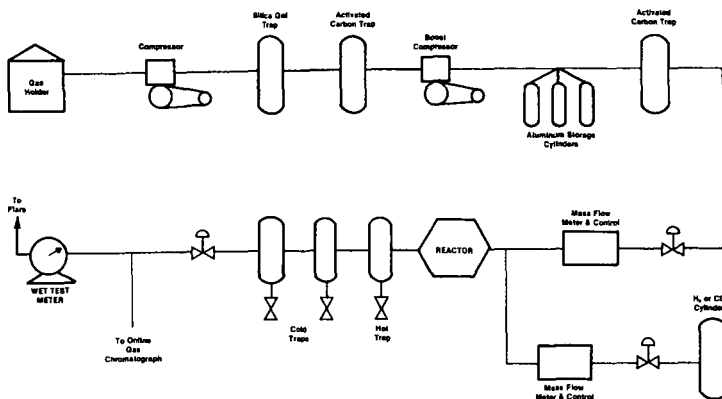
FIGURE 1.   SCHEMATIC OF REACTOR SYSTEM
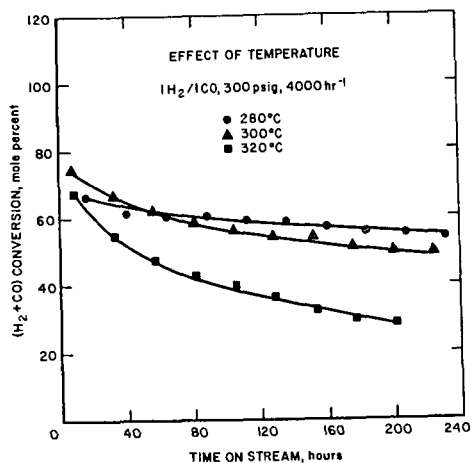
FIGURE 2.   EFFECT OF REACTION TEMPERATURE
ON CONVERSION WITH TIME

THE ROLE OF THE SURFACE OXYMETHYLENE SPECIES IN SYNFUEL CATALYSIS

R. S. Sapienza and W. A. Slegeir

Energy Technology Programs
Department of Energy & Environment
Brookhaven National Laboratory
Upton, New York 11973

Even with the recent interest in synthesis gas chemistry, the mechanisms of the various reactions and the role the catalyst plays has yet to be unequivocally established. A review of the research work carried out to elucidate the reaction mechanisms does not yield consistent conclusions in spite of the great efforts of many investigators and the use of many different scientific tools. A comparison of reaction results does not make it probable to assume basically different reaction mechanisms for different catalysts. The subtle differences noted should show greater potential for interpretation but present theories fall short of providing a unified picture capable of explaining or predicting catalyst behavior.

Although seemingly unrelated, all catalyzed hydrogenations of carbon monoxide have underlying similarities which suggest that a common reaction intermediate may be involved. A surface oxymethylene (oxygen-coordinated formaldehyde) may be the key intermediate in these reactions and may represent a link in their chemistries.
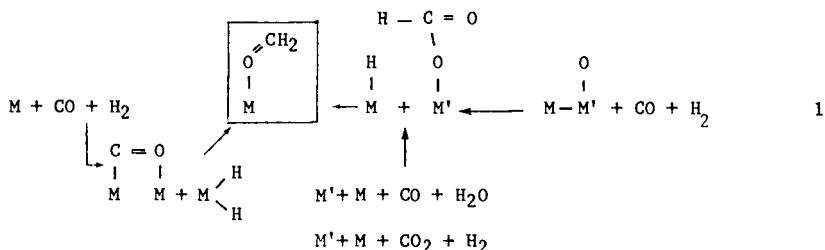
We have previously proposed[1] that the metal catalyzed reactions of synthesis gas proceed via chemisorbed carbon monoxide reacting with hydrogen to yield an
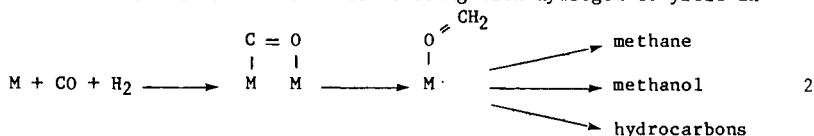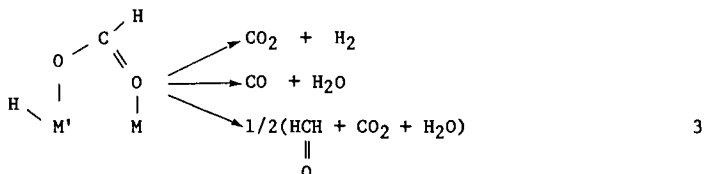

oxygen coordinated species. This oxymethylene intermediate can be hydrogenated to methane or can undergo chain growth by reaction with similar species, thus generating straight chain products in an analogous manner to other proposed theories, and would account for the presence of oxygenated products. One can envision this bonding scheme as allowing mobility of "an oxide surface carbene". Bond strengths of metal oxides and the oxidation-reduction cycle of the metal surface are critical factors in determining product character and distribution (Figure 1).

This mechanism which integrates features of the carbide and carbenol inter-
mediate theories[2] has been successful in developing a new series of highly
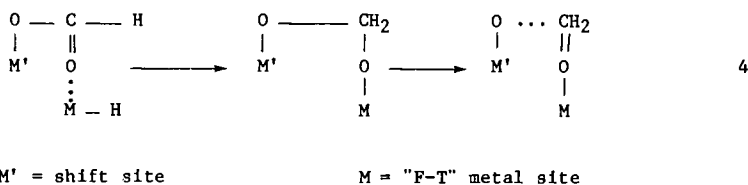active Fischer-Tropsch (F-T) catalysts.

The reversibility between reduced and various oxidized states of the catalyst
is an essential feature for catalyst activity in the Kolbel-Engelhardt (K-E)
synthesis.[3]Active catalysis demands some sites which promote water-gas shift
activity and other sites which generate F-T intermediates. It seemed probable to us
that the interaction of the water-gas shift intermediates with F-T active metal
sites could explain experimental observations.

Spectroscopic studies of zinc oxide, magnesia, alumina, and iron-chromia cata-
lysts suggest that the water-gas shift reaction proceeds through surface metal for-
mate species.[4]Other work on the decomposition of metal formates is also
revealing. Their decomposition is thought to need vacant sites to occur and is
enhanced by the presence of foreign metal ions.[5]A bicoordinated structure can be
visualized which reacts by one of three pathways.

$$
\begin{array}{c}
H \\
\diagup \\
O \xrightarrow{} C \\
 \diagdown\!\diagdown \\
 O \\
H | \\
\diagdown | \\
 M' M
\end{array}
\quad
\begin{array}{l}
\longrightarrow CO_2 \;+\; H_2 \\[4pt]
\longrightarrow CO \;+\; H_2O \\[4pt]
\longrightarrow 1/2(HCH + CO_2 + H_2O) \\
 \| \\
 O
\end{array}
\qquad 3
$$

In such decompositions, most interest in the literature has focussed upon the
dehydrogenation and dehydration reactions but the minor reaction which leads to the
formation of formaldehyde became the center of our attention. Although little data
on this byproduct and other organics are available and little is known about the
mechanism involved, appreciable amounts (~10%) of formaldehyde are formed in formic
acid decompositions catalyzed by thoria, alumina, and zinc oxide.[6]

Mechanistic studies at Brookhaven National Laboratory (BNL) indicate that the
water-gas shift formate intermediate may be the important transfer agent in the
Kolbel-Engelhardt synthesis, generating the surface oxymethylene intermediate on a
separate "F-T" metal site.[7]

$$
\begin{array}{c}
O \!-\! C \!-\! H \\
| \| \\
M' O \\
\vdots \\
M \!-\! H
\end{array}
\;\longrightarrow\;
\begin{array}{c}
O \!-\!\!-\!\!-\! CH_2 \\
| | \\
M' O \\
 | \\
 M
\end{array}
\;\longrightarrow\;
\begin{array}{c}
O \cdots CH_2 \\
| \| \\
M' O \\
 | \\
 M
\end{array}
\qquad 4
$$

M' = shift site   M = "F-T" metal site

As described for the F-T reaction the metal site will determine the eventual
product character and distribution (Table 1) and may explain the promoting effects
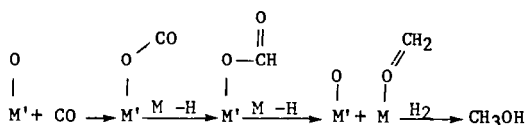of alkali metals in F-T catalysis, i.e., enhanced formate formation.

Table 1
The Use of Various Metals for the Hydrogenation of Zinc Formate

M	t_{CH_3OH}	$t_{C_xH_y}$
Cu/ZnO	11.7	trace
Pt/Al$_2$O$_3$	11.5	trace
Pd/Al$_2$O$_3$	22.6	0.1
Ni/SiO$_2$	trace	8.9
Co/SiO$_2$	0.1	14.8
Fe/Al$_2$O$_3$	trace	2.4

water as solvent, 500 psi, H$_2$, 245°C, t = mole prod/mol M'

The link between metal and metal oxide catalyzed reaction of carbon monoxide are also tied to the formate transfer reaction. (In general metal oxide syngas reactions proceed via similar reaction path with methanol as the main product.)
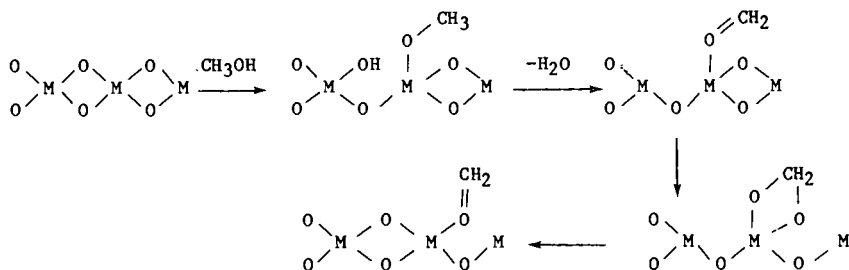
The formaldehyde-formate relationship leads to a plausible mechanism for the formation of methanol from synthesis gas. In fact, the high yield of formaldehyde ($\sim$25%) from the decomposition of zinc formate was actually considered as a commercial synthetic preparation, but was never realized. However, the reduction of the surface formaldehyde (oxymethylene) so produced was likely the cornerstone of the earliest methanol synthesis.

$$
\begin{array}{c}
& & & O & & & & \\
& & \nearrow^{CO} & \parallel & & & CH_2 & \\
O & O & O-CH & O & O & \nearrow\!\!\!/ & & \\
| & | & | & | & | & & & \quad\quad 5\\
M'+ CO \longrightarrow M' \xrightarrow{M\ -H} M' \xrightarrow{M\ -H} M' + M \xrightarrow{H_2} CH_3OH &
\end{array}
$$

As can be seen from this hypothesis, each of the metal centers in a methanol catalyst will have a particular function. One metal can be thought of as a formate center, the other as a hydrogenating center.This description of the role of formate has been used at BNL to design new K-E and methanol catalysts.

Finally, the oxymethylene species may also be involved in the initial hydrocarbons formed from methanol over non-reducible oxide catalysts. This would include products derived in the isosynthesis[2]as well as the zeolite controlled methanol conversions.[8]In both chemistries the formation of a carbenoid species from methanol seems likely. This species may be an oxymethylene formed on an acid site. As mentioned earlier, the oxide surface would allow mobility of the carbene (eq.6) and reaction wih itself or other methanol molecules would be expected to yield ethylene and dimethyl ether respectively. Carbene addition to the double bond of formed olefins can also occur. This explanation is consistent with recent deuterated water observations in the conversion of methanol to ethylene[9] and is in accord with the mechanistic findings of Chang.[8]

$$O\diagdown M \diagup O \diagdown M \diagup O \diagdown M \quad \xrightarrow{\ CH_3OH\ } \quad O\diagdown M \diagup \overset{OH}{} \diagdown M \diagup O \diagdown M \quad \xrightarrow{\ -H_2O\ } \quad O\diagdown M \diagup \overset{O=CH_2}{} \diagdown M \diagup O \diagdown M$$

(oxymethylene intermediate reaction scheme)

In summary, we have proposed that a common intermediate may be involved in many synthesis gas and related conversions. This oxymethylene moiety can be derived directly from carbon monoxide and hydrogen over a metal catalyst or indirectly from a formate intermediate in reaction involving steam or on metal oxide surfaces. We believe that the oxymethylene species symbolizes the link between these chemistries and the potential route to developing new synthesis gas catalyst systems.

References

1. R. S. Sapienza, M. J. Sansone, L. D. Spaulding, and J. F. Lynch, "Fundamental Research in Homogeneous Catalysis", Vol. 3, M. Tsutsui, Ed., Plenum, p. 129, 1979.

2. H. H. Storch, N. Golumbic, and R. B. Anderson, "The Fischer-Tropsch and Related Synthesis", Wiley, New York, 1951.

3. H. Kolbel and F. Engelhardt, Erdol u. Kohle 3, 529 (1950).

4. a) e.g., Y. Amenomiya and G. Pleizier, J. Catal. 76, 345 (1982).
    b) W. A. Slegeir, R. S. Sapienza, and B. Easterling, "Catalytic Activation of Carbon Monoxide", ACS Symposium Series No. 152, P.C. Ford, et., Washington, 1981.

5. a) P. Mars, J. J. F. Schotten, and P. Zwietering, Adv. in Cat., Vo. 14, 35 (1964).
    b) G. M. Shaborwa, Doklady Akad Nauk SSR 133, 1375 (1960).
    c) R. E. Eischens and W. A. Plisken, "Actes Du Deuxieme Congre's Intern. de Catalyse, Paris, 1960, pp. 789, Ed. Technip, Paris (1961).

6. a) P. Sabatier "Catalysis in Organic Chemistry" translated by E.E. Reid, Van Nostrand, NY 1923.
    b) K. Hofman and H. Schibsted, Chem. Ber. 51, pp. 1389, 1398 (1918).

7. W. A. Slegeir, Final Report, BNL-51423, October 1980.

8. a) C. D. Chang and A. J. Silvestri, J. Catal. 47, 249 (1977).
    b) C. D. Chang, J. Catal. 74, 203 (1982).

9. T. Mole and J. A. Whiteside, J. Catal. 75, 284 (1982).

Figure 1.   The oxide mechanism.[1]
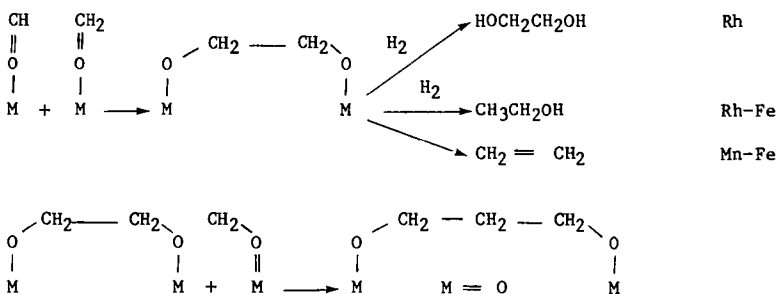
INTERMEDIATES TO ETHYLENE GLYCOL:
CARBONYLATION OF FORMALDEHYDE CATALYZED BY NAFION®
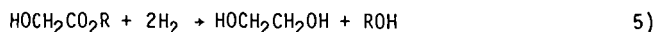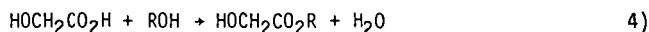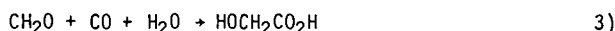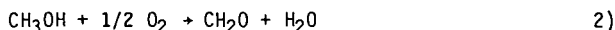SOLID PERFLUOROSULFONIC ACID RESIN

Dan E. Hendriksen

Corporate Research-Science Laboratories
Exxon Research and Engineering Company
P.O. Box 45
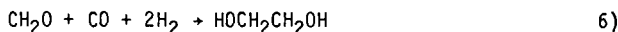Linden, New Jersey 07036

INTRODUCTION

Carbon monoxide and hydrogen can be converted to ethylene glycol by a variety of direct and indirect routes. This work explores an indirect route proceeding through the acid-catalyzed carbonylation of formaldehyde, using a novel strong acid catalyst, Nafion solid perfluorosulfonic acid resin. The glycolic acid product of this carbonylation may be esterified and then hydrogenated to yield ethylene glycol. Ethylene is presently the feedstock for ethylene glycol production; the ethylene is partially oxidized to ethylene oxide,[1a] which is then hydrolyzed to yield ethylene glycol.
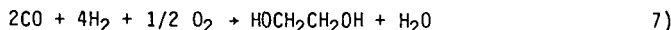
In this work, the following sequence of reactions is envisioned.

$$CO + 2H_2 \rightarrow CH_3OH \qquad\qquad 1)$$

$$CH_3OH + 1/2\ O_2 \rightarrow CH_2O + H_2O \qquad\qquad 2)$$

$$CH_2O + CO + H_2O \rightarrow HOCH_2CO_2H \qquad\qquad 3)$$

$$HOCH_2CO_2H + ROH \rightarrow HOCH_2CO_2R + H_2O \qquad\qquad 4)$$

$$HOCH_2CO_2R + 2H_2 \rightarrow HOCH_2CH_2OH + ROH \qquad\qquad 5)$$

Equations 3, 4, and 5 may be combined to yield equation 6,

$$CH_2O + CO + 2H_2 \rightarrow HOCH_2CH_2OH \qquad\qquad 6)$$

and the sum of equations 1 - 5 is equation 7.

$$2CO + 4H_2 + 1/2\ O_2 \rightarrow HOCH_2CH_2OH + H_2O \qquad\qquad 7)$$

In this sequence, equations 1 and 2 are the conventional processes for methanol[1b] and formaldehyde[1c] production, respectively. Both are high volume chemicals whose production technology is well-developed. The remaining transformation desired, starting with formaldehyde, is shown as equation 6. This is accomplished through the carbonylation of formaldehyde to yield glycolic acid, as shown in equation 3, followed by the esterification of this acid, equation 4, and the hydrogenolysis of the ester to ethylene glycol, equation 5.

The overall reaction from carbon monoxide and hydrogen, equation 7, is instructive since it reveals that this process essentially couples two reactions, the direct synthesis of ethylene glycol from CO/H_2, equation 8,

$$2CO + 3H_2 \rightarrow HOCH_2CH_2OH \qquad \qquad 8)$$

and the burning of hydrogen, equation 9.

$$H_2 + 1/2\ O_2 \rightarrow H_2O \qquad \qquad 9)$$

While conversion to ethylene glycol is severely limited by the unfavorable thermo-dynamics of the direct synthesis, equation 8, the coupling of this reaction with the highly exothermic equation 9 results in a sequence in which the high-energy intermediate formaldehyde may be quantitatively converted to ethylene glycol with no thermodynamic constraints.

It is well known that strong acids catalyze the carbonylation of formal-dehyde to yield glycolic acid. Solid acid catalysts for this reaction have been explored to some extent, but there is only a single example in the patent litera-ture of catalysis by Nafion®. In this case, the carbonylation of formaldehyde was carried out in acetic acid solvent to yield acetylglycolic acid.[2] The present work significantly extends the reaction chemistry accessible with this novel acid catalyst.

RESULTS AND DISCUSSION

"Nafion-H" Resin.[a] There are several properties of DuPont's "Nafion-H" perfluorosulfonic acid resin which make it an ideal candidate for the strong acid-catalyzed carbonylation of formaldehyde. First, it is a superacid; i.e., stronger in intrinsic acidity than 100% sulfuric acid. The resin is a copolymer of tetra-fluorethylene and perfluoro-3, 6-dioxa-4-methyl-7-octensulfonic acid, resulting in a structure:

$$
\begin{array}{l}
-(CF_2\text{-}CF_2)_n - CF_2 - CF - \\
\qquad\qquad\qquad\qquad\quad | \\
\qquad\qquad\qquad\qquad\quad O \\
\qquad\qquad\qquad\qquad\quad | \\
\qquad\qquad\qquad\qquad\quad CF_2 \\
\qquad\qquad\qquad\qquad\quad | \\
\qquad\qquad\qquad\qquad\quad CF - CF_3 \\
\qquad\qquad\qquad\qquad\quad | \\
\qquad\qquad\qquad\qquad\quad O \\
\qquad\qquad\qquad\qquad\quad | \\
\qquad\qquad\qquad\qquad\quad CF_2 \\
\qquad\qquad\qquad\qquad\quad | \\
\qquad\qquad\qquad\qquad\quad CF_2 \\
\qquad\qquad\qquad\qquad\quad | \\
\qquad\qquad\qquad\qquad\quad SO_3H
\end{array}
$$

---
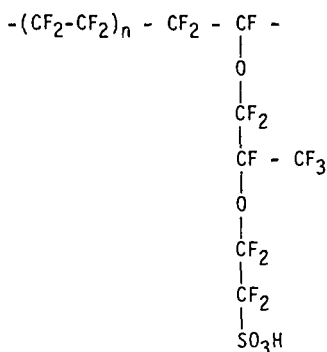
[a] "Nafion-H" is a convenient notation to indicate the acid form of this ion exchange resin. "Nafion" is a registered trademark of DuPont.

By analogy, one might expect the resin to be nearly as acidic as trifluoromethane sulfonic acid, CF_3SO_3H. DuPont claims that its acidity is of the same order as $AlCl_3 \cdot HCl$. Second, the resin is thermally very stable. DuPont states that there should be no problem with deterioration below 175°, and their safety data show significant decomposition only above 270°. Others have found the material to be stable and useful to at least 220°.[3] Third, the resin is swelled by polar organic solvents, allowing reactants to diffuse into the resin granules. This makes the interior acid sites available, as well as the acid sites on the catalyst surface. Furthermore, the resin is chemically inert, being deactivated only by ion exchange with e.g., Fe^{3+}. Such deactivated catalysts are readily regenerated by the same technique used to prepare the acid form of the resin. The resin can be prepared in a range of equivalent weights from 1000 to 1800 to fit specific needs, and offers all the classic advantages of a solid catalyst in the ease of separation of products.

The choice of a solvent to use with Nafion-H is nontrivial. As stated, polar organic solvents are desired because they swell the resin. Acetic acid is useful but is not inert in the reactions studied here. Water and alcohols are found to decrease the activity of the catalyst when present in excess. Ethers such as glyme or diglyme were found not to be inert under reaction conditions, while THF is known to be polymerized over Nafion-H at room temperature.[4] However, p-dioxane was found to yield no GC-observable decomposition products when heated at 150° for 3 hours over the Nafion-H resin, and was used in most of the experiments reported here.

Carbonylation in the Presence of Water. With water present in the dioxane solvent, glycolic acid is presumably the product of formaldehyde carbonylation, as in equation 3. The most extensive series of experiments was done using these reactants. The series of experiments shown in Table I illustrates several aspects of this reaction. First, the reaction occurs readily under these conditions, giving routine yields of ca. 70% at 150°. The first two experiments may be compared to see that the reaction remains incomplete even after 3 hours at 130°, indicating a substantial temperature effect in this range. The series was run primarily to test the durability of the Nafion-H catalyst during these five reactions. The same Nafion-H catalyst was used in each of these reactions, and was only rinsed with dioxane and sucked dry on a filter between reactions. The yield of glycolic acid does indeed stay constant at 150°, with only a slight unexplained dip in the fourth reaction, indicating that the Nafion-H did maintain its catalytic activity through all the reactions. A different measure of this catalytic activity is the equivalent weight of the resin before and after the series. The initial equivalent weight was 1282 g/ equivalent, and afterwards was 1315 g/equivalent, a decrease in available acidity of less than three percent. This could conceivably be accounted for by washout of monomer during the first reaction.

A number of reactions were run in order to determine the effect of carbon monoxide pressure on the yield of glycolic acid in this system. The results are shown in Table II. With the other reaction conditions constant, the yield did increase from 50% to 80% upon increasing the pressure from 1500 psi to 4500 psi. While this does indicate that increasing the pressure of CO results in higher yields, the data should not be interpreted as showing that high pressures are required for high yields. The equipment used here was a rocking autoclave, and more efficient stirring may well enhance the efficiency of the reaction.

One reaction was done with a mixture of hydrogen and carbon monoxide to verify that the presence of hydrogen would have no effect on the yield. This run is also shown in Table II. The yield, 73%, is slightly higher than in comparable runs without hydrogen, but no significance is attached to this. In the presence

of this Nafion-H acid catalyst the hydrogen is expected to act only as a diluent, requiring proportionately higher total pressures to achieve the same carbon monoxide partial pressure as in the absence of the hydrogen.

The effect of water on the yield of glycolic acid in this reaction system was also explored. These data are shown in Table III-1. The amount of formaldehyde in these runs was reduced so that the initial mole ratio of water to Nafion-H could be varied and held approximately constant during a run, without being affected by the reaction. This molar ratio of water to Nafion-H was expected to change the effective acidity of the Nafion-H, which would in turn affect the yield in a given time. The reaction with the most water present, a 20:1 ratio of H_2O to H^+, did not result in complete conversion of the formalde-hyde. Decreasing the ratio results in an optimum yield at a 5:1 ratio of water to acid. Decreasing the ratio still further to 2:1 and even 1:1 surprisingly results in a constant yield of about 50% glycolic acid (analyzed as methyl glycolate after conversion to the ester). Such yields in the presence of only half as much water as formaldehyde raise the question of whether glycolic acid is truly the reaction product, or whether dehydrated forms of glycolic acid such as the cyclic dimer glycolide, Figure 1a, or oligomers, Figure 1b, might not be the actual products.
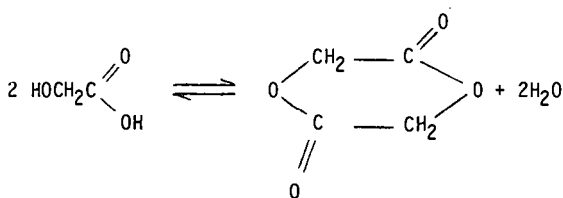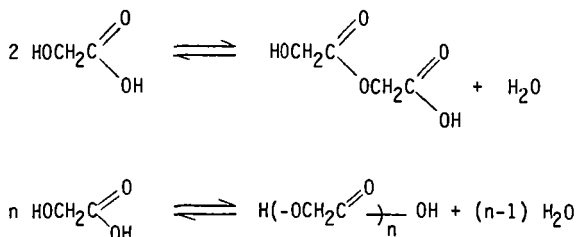

FIGURE 1a. Formation of Glycolide

FIGURE 1b. Formation of Glycolic Acid Oligomers

An indication that these dehydrated forms of glycolic acid are the actual products under these reaction conditions was gained from a semi-quantitative GC analysis of these reaction solutions for water. This analysis showed that all the water ini-tially added to the reaction solution was still present in solution at the end of the reaction, and consequently could not be combined as glycolic acid. A reaction with no water added was included in an earlier series, shown in Table III-2. These three reactions also indicate that there is an optimum water to acid ratio, but a yield of even 25% with no water added is somewhat surprising. All these data demonstrate that too much water in the reaction solution reduces formaldehyde

conversion and concomitantly glycolic acid yield, but the results at the lower levels of water are less definitive.

The preceding data show that in these reactions the conversion of formaldehyde is complete, or nearly so, while the yield of glycolic acid is always substantially less than quantitative. There are obviously by-products in this reaction. This subject has not been extensively investigated, but some comments on the suspected by-products and their mode of formation can be made.

The most likely side reaction is the acid-catalyzed reaction of formaldehyde with itself, instead of the desired acid-catalyzed reaction with carbon monoxide. One such reaction is the formation of methyl formate from formaldehyde,[6a] equation 10,
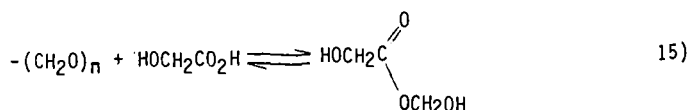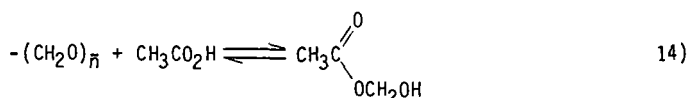
$$2 \ CH_2O \rightarrow HCO_2CH_3 \hspace{3cm} 10)$$

but no evidence has been found to support this. Another possibility is the acid-catalyzed condensation of formaldehyde to polyhydroxy aldehydes, equation 11.

$$(n + 1) \ CH_2O \rightarrow H-[CH(OH)]_n-CHO \hspace{2.5cm} 11)$$
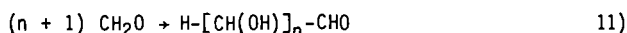
This reaction would be similar in stoichiometry to the formose reaction,[5] the base catalyzed condensation of formaldehyde to sugars and a mixture of polyhydroxy aldehydes. The solutions after reaction were varying shades of brown, and the Nafion-H sometimes turned a dark brown or even black, especially when the reaction contained little water or was exposed to high temperatures. This is reminiscent of the acid-catalyzed carbonization of sugars, equation 12.

$$H-[CH(OH)]_n-CHO \rightarrow (n + 1)C + (n + 1) \ H_2O \hspace{2cm} 12)$$
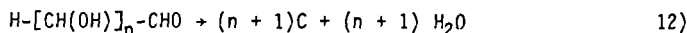
If these ideas about the nature of the byproducts are correct, then one approach to suppress the condensation of the formaldehyde would be to chemically separate the formaldehyde monomers with a solvent or an added component. The Nafion-H, as a strong acid, rapidly catalyzes polymerization of formaldehyde to polyoxymethylene (paraformaldehyde), and catalyzes the corresponding depolymerization at higher temperatures as well.[6a] Therefore, a reversible chemical interaction is needed to separate the formaldehyde monomers while permitting the carbonylation to proceed. Examples of such interactions to form unstable adducts are reaction with water, equation 13, to form methylene glycol;[6b] with acetic acid, equation 14), to form the unstable methylene glycol ester;[6c] and analogously with glycolic acid, equation 15.

$$-(CH_2O)_{\overline{n}} + H_2O \rightleftharpoons HOCH_2OH \hspace{3cm} 13)$$

$$-(CH_2O)_{\overline{n}} + CH_3CO_2H \rightleftharpoons CH_3C\overset{O}{\underset{OCH_2OH}{\diagup\diagdown}} \hspace{2.5cm} 14)$$

$$-(CH_2O)_n + HOCH_2CO_2H \rightleftharpoons HOCH_2C\overset{O}{\underset{OCH_2OH}{\diagup\diagdown}} \hspace{2cm} 15)$$

Other investigators have disclosed the use of acetic acid as a solvent to yield acetylglycolic acid, equation 16, using a Nafion-H catalyst.[2] In the sulfuric

$$CH_3CO_2H + CH_2O + CO \rightarrow CH_3CO_2CH_2CO_2H \quad 16)$$
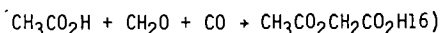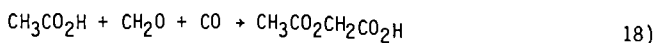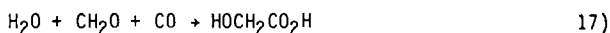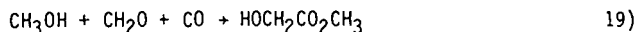
acid catalyzed reaction, glycolic acid has been disclosed as a useful solvent for enhancing yields.[7] However, data obtained in this study and shown in Tables IV-1 and IV-2 indicate that an equimolar amount of acetic acid has no effect in this reaction. In the absence of water the acetic acid actually decreases the yield. Glycolic acid, whether added wet or dehydrated, also decreases the yield of glycolic acid from formaldehyde. The reason for this decrease in yield is not readily apparent.

This Nafion-H catalyzed carbonylation of formaldehyde in dioxane/water has a number of aspects which make it an attractive intermediate reaction in a process for ethylene glycol preparation. A summary of these favorable aspects is as follows:

1. The Nafion-H solid acid catalyst is easily separated from the reaction products, a classic advantage of heterogeneous catalysts.

2. As demonstrated by others, solid acid resins similar to Nafion-H appear to be virtually non-corrosive.[2]

3. The catalyst is thermally stable, has shown no loss of activity with use, and is easily regenerable if necessary, e.g., due to contamination with other cations. Polar solvents swell the catalyst, which allows utilization of interior acid sites.

4. The acid catalyst retains its activity in the presence of substantial amounts of water; therefore, dry formaldehyde (as trioxane or paraformaldehyde) is not required.

5. The reaction is not affected by hydrogen, which acts only as a diluent for the carbon monoxide. The catalyst has no activity for the undesired reduction of formaldehyde to methanol. Consequently, synthesis gas could be used without separation or the carbon monoxide could be concentrated before use, and the separated hydrogen subsequently used for hydrogenolysis of the glycolic acid ester.

6. The reaction proceeds under reasonable conditions of temperature and pressure.

7. The glycolic acid product is stable to further reaction.

8. The dioxane solvent appears inert under reaction conditions.

Carbonylation in Ester Solvents. The acid-catalyzed carbonylation of formaldehyde has been carried out with water as discussed above, equation 17, with acetic acid, equation 18, and with methanol,[8],[9] equation 19.

$$H_2O + CH_2O + CO \rightarrow HOCH_2CO_2H \qquad\qquad 17)$$

$$CH_3CO_2H + CH_2O + CO \rightarrow CH_3CO_2CH_2CO_2H \qquad\qquad 18)$$

$$CH_3OH + CH_2O + CO \rightarrow HOCH_2CO_2CH_3 \qquad \qquad 19)$$

The reaction with acetic acid as solvent is reported to be efficient and specific, but the acetylglycolic acid product must be hydrolyzed and then esterified before it can be hydrogenated to ethylene glycol. The reaction with methanol as solvent would be ideal if it yielded only the methyl ester. However, substantial yields of alkoxy acids and their esters are also invariably produced in the presence of alcohols. These may be hydrogenated to glycol ethers, useful as solvents, but cannot serve as intermediates to ethylene glycol.

The reaction using an ester as solvent, e.g. methyl acetate in equation 20, appears not to have been reported before.

$$CH_3CO_2CH_3 + CH_2O + CO \rightarrow CH_3CO_2CH_2CO_2CH_3 \qquad \qquad 20)$$
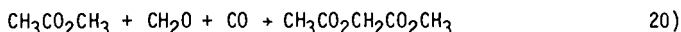
The product of the reaction with an ester, in this case methyl acetylglycolate, can be transesterified, e.g. with methanol as in equation 21 to yield methyl glycolate and regenerate methyl acetate.

$$CH_3CO_2CH_2CO_2CH_3 + CH_3OH \rightarrow CH_3CO_2CH_3 + HOCH_2CO_2CH_3 \qquad \qquad 21)$$
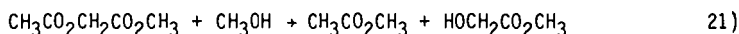
The methyl acetate can then be separated and the methyl glycolate hydrogenated to ethylene glycol.

Some formaldehyde carbonylations using methyl acetate as solvent are shown in Table V-1. It may be seen from the first reaction that the yield of methyl acetylglycolate, intermediate to ethylene glycol, is over 60%, but there is also some production of methyl methoxyacetate, 15% in this case. In the analysis of the reaction products from this run it was noted that some acetic acid was formed, presumably from the methyl acetate. The second reaction demonstrates that adding a small amount of acetic acid at the beginning of the reaction does not affect the yields of the two products. Addition of methanol at the beginning of the reaction has a profound effect, however, as shown in the third reaction. This may be because the formaldehyde is converted to methylal, $(MeO)_2CH_2$, by the added methanol. All the formaldehyde not accounted for in the products was recovered as methylal. Addition of water at the beginning of the reaction also decreases the yield of methyl acetylglycolate, and results in the formation of some free acids, notably methoxyacetic acid.

Methyl formate was also tested as an ester solvent, with typical results shown as the first reaction in Table V-2. The main reaction product expected here is methyl formylglycolate, $HCO_2CH_2CO_2CH_3$, but methyl glycolate, possibly derived from the former product by decarbonylation, is also found. Methyl methoxyacetate is formed in even greater yield than with methyl acetate as solvent.

A unique aspect of the reactions using methyl formate as solvent is that no CO pressure needs to be applied, as the second reaction in Table V-2 confirms. The methyl formate presumably acts as a source of CO, and the overall reaction in equation 22 results.

$$HCO_2CH_3 + CH_2O \rightarrow HOCH_2CO_2CH_3 \qquad \qquad 22)$$

182
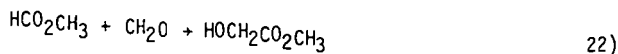
This reaction has been investigated by others using different strong acids.

The carbonylation of formaldehyde using Nafion-H resin does proceed in ester solvents, but not with complete selectivity to intermediates to ethylene glycol. The reaction might nevertheless be interesting as a means of coproducing ethylene glycol and glycol ethers.

Reactions of Methylal. In the preceding work using ester solvents the focus was on intermediates to ethylene glycol, avoiding the alkoxy esters or acids which can be produced as byproducts. These alkoxy esters or acids do have value, however, since they can be hydrogenated to glycol ethers, which are articles of commerce and are useful as solvents. Consequently, some reactions were run to determine if methylal could be carbonylated to methyl methoxyacetate efficiently and selectively over Nafion-H resin, as in equation 23.

$$CH_3OCH_2OCH_3 + CO \rightarrow CH_3OCH_2CO_2CH_3 \qquad 23)$$
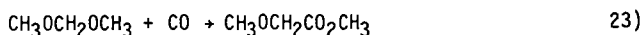
The results are shown in Table VI. The first reaction was carried out in dioxane solvent and resulted in only modest yields of both methyl methoxyacetate and methyl glycolate. Using a mixed methanol/dioxane (50:50) solvent resulted in no reaction at all. When methyl acetate was used as the solvent though, a good yield of both methyl methoxyacetate and methyl acetyl glycolate resulted; the former was not produced selectively.

There could be some question over whether methyl glycolate is inert to further reaction in this catalyst system, or if it can be methylated by the Nafion-H to form methyl methoxyacetate. One reaction was run in order to test this possibility. Methyl glycolate was reacted in a mixed methanol/dioxane solvent (10/40 by volume) over the Nafion-H resin using standard reaction conditions. No methyl methoxyacetate was found in the reaction solution, and the methyl glycolate was recovered quantitatively.
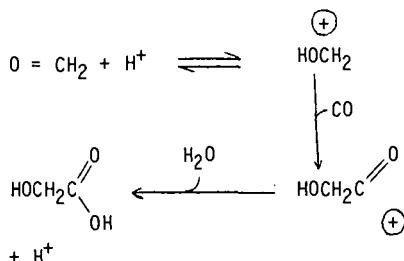
These results indicate that methylal can be carbonylated efficiently to methyl methoxyacetate, especially in ester solvents, but the reaction is not selective and results in substantial amounts of intermediates to ethylene glycol as well.

Aspects of the Mechanism. The acid-catalyzed reaction of formaldehyde with carbon monoxide belongs to the class known as Koch reactions.[10] The Koch reaction usually refers to the reaction of an olefin with carbon monoxide, as exemplified by the reaction of isobutene with CO and water, equation 24, to product pivalic acid.

$$\begin{array}{c} CH_3 \\ \diagdown \\ \diagup C = CH_2 + CO + H_2O \xrightarrow{H^+} (CH_3)_3CCO_2H \\ CH_3 \end{array} \qquad 24)$$
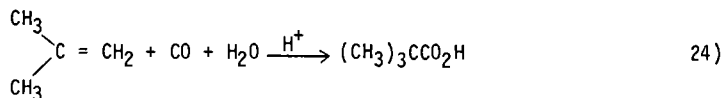
The first step in a Koch reaction is formation of a carbonium ion from the substrate and the acid catalyst. The carbonium ion then adds carbon monoxide to form a more stable acylium ion. This finally reacts with water to form the

free acid, or with an alcohol to form an ester. The reaction with formaldehyde
is:

$$O = CH_2 + H^+ \rightleftharpoons \overset{\oplus}{HOCH_2}$$

$$HOCH_2 \overset{CO}{\downarrow}$$

$$HOCH_2C\overset{O}{\underset{OH}{\diagup}} \xleftarrow{\quad H_2O \quad} \underset{\oplus}{HOCH_2C}\overset{O}{\diagup}$$

$$+ H^+$$

The ease with which the Koch reaction takes place depends on how easily the sub-
strate is protonated. Protonation of formaldehyde requires a strong acid; some
data on the proton affinity of formaldehyde have been obtained.[11]

EXPERIMENTAL

        Materials: Glycolic acid was obtained as wet crystals (Aldrich) or 70%
aqueous solution (Pfaltz & Bauer). It was analyzed by titration with 0.1 M NaOH
using a phenolphthalein indicator. The "Nafion" 501 perfluorosulfonic acid resin
was obtained as a sample from the Plastic Products Division of DuPont. This
material consists of granules nominally 0.2 to 0.5 mm in diameter, and has an
equivalent weight of about 1200. It was received as the potassium sulfonate and
was converted to the acid form and analyzed essentially as recommended by
DuPont. Conversion to the acid form is achieved by soaking the resin about five
times in 4 M HCl, allowing time for exchange and with superficial washing with
distilled water between HCl treatments. This is followed by washing with
distilled water until the washings show a neutral pH, after which the material is
dried in a vacuum oven overnight at about 110°. The Nafion-H was stored in sealed
jars or in a desiccator as it can absorb appreciable amounts of water from the
air. Analysis of the acid form was carried out by soaking the resin in water with
an excess of sodium chloride, and titrating the liberated HCl with 0.1 M NaOH.
Dioxane was dried by refluxing over calcium hydride followed by distillation. All
other materials were reagent grade and used as received.

        Reactions: The reactions with carbon monoxide were carried out in a
300 cc rocking autoclave equipped with a glass liner, which contained 50 cc of
reaction solution over the Nafion-H. Carbon monoxide was introduced before
heating. The starting time of the reaction was taken as the time the autoclave
reached temperature (after approximately 30 minutes) and the autoclave was allowed
to cool and rock overnight after the heat was turned off at the end of the reac-
tion time. Formaldehyde was added as trioxane, the cyclic trimer; 8g, or ~6
mequiv Nafion-H was used in each run, and ~50 ml of p-dioxane was used as solvent.

        Analysis of Reaction Products: Analysis of the products was by gas
chromatography using peak area integration and a hexadecane internal standard.
Since glycolic acid gave poor sensitivity and reproducibility, this product was
analyzed as methyl glycolate by refluxing the entire reaction solution, including
the Nafion-H, with an excess of methanol before GC analysis. A semi-quantitative
estimate of the unreacted formaldehyde could be made through analysis of the
methylal resulting from reaction of methanol with the formaldehyde. These
analyses used a 6' x 1/8" Carbowax 20 M column, programming from 80° to 225° at

2°/min. A blank run, substituting a known amount of glycolic acid for formaldehyde, verified the utility of this analysis for glycolic acid. The reaction (mole ratios: glycolic acid, 10: water, 3.5: Nafion-H, 1; 150°, 3h, P_{CO} = 2500 psi)· resulted in analysis for 96% of the added glycolic acid. This result also indicates that the glycolic acid, once formed, is inert to further reaction under these conditions. This is in contrast to a catalyst system in which further carbonylation to malonic acid followed by decarboxylation to acetic acid proved to be a major problem.[12]

Preparations:

(1) Methyl glycolate, $HOCH_2CO_2CH_3$, (MG), was prepared by thermal reaction between dehydrated glycolic acid and excess methanol at 210° for 10 hours in a rocking autoclave.[13] The glycolic acid was dehydrated in a rotary evaporator by raising the temperature slowly to 180°.[13] Methyl glycolate was distilled under vacuum (22 mm, 61°) b.p. 150°, lit. 151.1°.[14a]

(2) Acetylglycolic acid, $CH_3CO_2CH_2CO_2H$, was prepared by heating dehydrated glycolic acid with excess acetic acid 10h at 200°. The product was recrystallized from ether/toluene. m.p. 63-65°; lit. 66-68°.[14b]

(3) Methyl acetylglycolate, $CH_3CO_2CH_2CO_2CH_3$, (MAG), was prepared by reaction of methyl glycolate with acetyl chloride in methyl acetate solvent. The product was distilled under vacuum; b.p. 82-83° at 22 mm.

(4) Methyl methoxyacetate, $CH_3OCH_2CO_2CH_3$, (MMAc), was prepared by refluxing commercially obtained methoxyacetic acid with an excess of methanol over Nafion-H and distilling the product; b.p. 128°, lit 131°.[14c]

ACKNOWLEDGMENTS

TABLE I

CARBONYLATION OF FORMALDEHYDE TO GLYCOLIC ACID
DURABILITY TEST USING THE SAME NAFION-H CATALYST[a]

Temperature	Time	P_{CO}	Unreacted Formaldehyde	Yield Glycolic Acid
130	3 h	2600	29%	38%
150	3 h	2700	5%	63%
150	5 h	2600	4%	68%
150	5 h	2700	6%	56%
150	5 h	2700	4%	69%

[a]Mole ratios: H_2O, 10: CH_2O, 10: H^+, 1.

TABLE II

CARBONYLATION OF FORMALDEHYDE TO GLYCOLIC ACID.
DEPENDENCE OF YIELD ON CARBON MONOXIDE
PRESSURE, AND A REACTION IN THE PRESENCE OF HYDROGEN[a]

P_{CO} (psig)	Yield Glycolic Acid	Time
1500	48%	5 h
2500	61%	5 h
4600	79%	3 h
3000[b]	73%	3 h

[a]Mole ratios: H_2O, 10: CH_2O, 10: H^+, 1; Temperature 150+°C.

[b]The gas used was 4000 psi of 25:75 H_2:CO.

TABLE III

CARBONYLATION OF FORMALDEHYDE TO GLYCOLIC ACID.
DEPENDENCE OF YIELD ON H_2O/H^+ RATIO[a]

	MOLE RATIOS			
	H_2O :	CH_2O :	H^+	Yield Glycolic Acid
1.	20	2	1	36%[b]
	10	2	1	44%
	5	2	1	57%
	2	2	1	49%
	1	2	1	48%
2.	20	10	1	61%
	10	10	1	72%
	0	10	1	25%

[a]Time, 3h; P_{CO}, 2500 psi; Temperature 150+°C

[b]Incomplete conversion

TABLE IV-1

EFFECT OF ADDED ACETIC ACID[a]

MOLE RATIOS							Yield
AcOH	:	H_2O	:	CH_2O	:	H^+	Glycolic Acid
--		10		10		1	72%
10		--		10		1	40%
10		10		10		1	71%

[a]Time, 3h; Temperature, 150+°C; P_{CO}, 2500 psi

- -

TABLE IV-2

EFFECT OF ADDED GLYCOLIC ACID

Time	P_{CO}	Initial $HOCH_2CO_2H$	:	H_2O	:	CH_2O	:	H^+	Yield Glycolic Acid[a]
2 h	2500	11		4		12		1	40%
3 h	4000	12		(-8)[b]		10		1	13%

[a]Yield = (total yield - amount added)/moles CH_2O; Temperature, 150+°C

[b]The initial added glycolic acid was 66% dehydrated.

187

TABLE V-1

CARBONYLATION OF FORMALDEHYDE IN METHYL ACETATE[a]

$$CH_3CO_2Me + CH_2O + CO \rightarrow$$

$$CH_3CO_2CH_2CO_2Me \text{ (MAG) and } MeOCH_2CO_2Me \text{ (MMAc)}$$
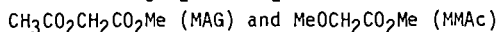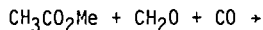
Added Component	Added Comp/CH_2O	%YIELDS		Notes
		MAG	MMAc	
--	--	61	15	b
Acetic Acid	1	63	13	
Methanol	2	18	23	c
Water	1	31	18	d

[a]Time, 3h; Temperature, 150°; P_{CO}, 2500 psi; Mole ratios: CH_2O, 10: H^+, 1.

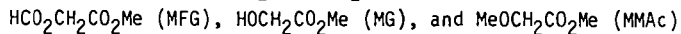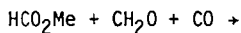[b]Acetic acid found in reaction products.

[c]Methylal yield was 58%.

[d]Also substantial yields of methyl glycolate (18%) and methoxyacetic acid, $CH_3OCH_2CO_2H$. Time = 0.5 h.

- -

TABLE V-2

CARBONYLATION OF FORMALDEHYDE IN METHYL FORMATE

$$HCO_2Me + CH_2O + CO \rightarrow$$

$$HCO_2CH_2CO_2Me \text{ (MFG), } HOCH_2CO_2Me \text{ (MG), and } MeOCH_2CO_2Me \text{ (MMAc)}$$

% YIELDS			
MFG	MG	MMAc	Notes
11	11	31	a
5	17	21	b

[a]Temperature, 150°, P_{CO}, 2500 psi; Time 3h.

[b]No CO added, ΔP = +200 psi; Temperature, 150°; Time, 5h.

TABLE VI

CARBONYLATION OF METHYLAL TO
$MeOCH_2CO_2Me$ (MMAc), $HOCH_2CO_2Me$ (MG), and $CH_3CO_2CH_2CO_2Me$ (MAG)[a]

Solvent	% YIELDS		
	MMAc	MG	MAG
dioxane	20	17	not a product
methanol/dioxane, 50:50	0	0	not a product
methyl acetate	49	trace	39

[a]Time, 3h; Temperature 150°; P_{CO}, 2500 psi; Mole ratios: $(MeO)_2CH_2$, 10: H^+, 1.

REFERENCES

(1) Thomas, C. L., Catalytic Processes and Proven Catalysts. Academic Press, New York, 1970. a) p. 205; b) p. 149; c) p. 208.

(2) Preparation of Hydroxy-carboxylic Acids and Their Derivatives. G. B. Patent 1,499,245 to D. R. Nielsen, January 25, 1978; Assignee PPG Industries, Inc., U.S. Application 570,691, filed April 23, 1975.

(3) Pineri, M., Private communication, July 1979.

(4) Poly(tetramethylene ether) Glycol. U.S. Patent 4,120,903 to G. Pruckmayr and R. Weir, October 17, 1978; Assignee DuPont.

(5) Shigemasa, et al., J. Catalysis 58, 296 (1979), and references therein.

(6) Walker, J. F., Formaldehyde. 3rd edition, R. E. Krieger Publishing Company, Huntington, New York, 1975. a) p. 253; b) p. 55; c) p. 345.

(7) Process for the Preparation of Glycolic Acid. U.S. Patent 2,153,064 to A. T. Larson, April 4, 1939; Assignee E. I. DuPont.

(8) Process for the Preparation of Alkyl Glycolates. U.S. Patent 2,211,625 to D. J. Loder, August 13, 1940; Assignee DuPont.

(9) Alkoxy Acid or Ester Preparation. U.S. Patent 3,948,977 to S. Suzuki, April 6, 1976; Assignee Chevron Research Company.

(10) Falbe, J., Carbon Monoxide in Organic Synthesis. Springer-Verlag, New York, 1970. p. 123.

(11) Hopkinson, A. C., Holbrook, N. K., Yates, K. and Csizmadia, I. G., J. Chem. Phys., 49, 3596 (1968).

(12) Catalytic Applications of Oxidative Addition of Alkyl Halides to Transition Metal Complexes. S. J. Lapporte and V. P. Kurkov in Organotransition-Metal Chemistry, Y. Ishii and M. Tsutsui, Eds., 1975, p. 199, Plenum Press, New York.

(13) Process for the Production of Ethylene Glycol. U.S. Patent 4,087,470 to S. Suzuki, May 2, 1978; Assignee Chevron Research Company.

(14) CRC Handbook of Chemistry and Physics, 49th edition. a) p. C-94; b) p. C-93; c) p. C-96.

STRUCTURE AND REACTIVITY OF
RHODIUM COMPLEX HYDROFORMYLATION CATALYSTS

Alexis A. Oswald, Dan E. Hendriksen, Rodney V. Kastrup
Joseph S. Merola, Edmund J. Mozeleski and John C. Reisch*

Exxon Research and Engineering Co., P. O. Box 45, Linden, NJ 07036
and Exxon Chemical Co.,* P. O. Box 241, Baton Rouge, LA 70821

INTRODUCTION

In the present work, the reactivity and selectivity of various t-phosphine rhodium complex hydroformylation catalysts are correlated with their structures. Such a study is of particular interest at this time because there has been a rapid commercial development in this area during the last 10 years and because the structure of the catalyst complexes can now be well characterized by nuclear magnetic resonance spectroscopy (NMR) under simulated hydroformylation conditions.

Known triphenylphosphine rhodium carbonyl hydride and novel, more stable alkyldiphenylphosphine rhodium carbonyl hydride complexes were particularly investigated in this study. The catalyst behavior of various alkyldiphenylphosphine rhodium carbonyl hydrides was studied as a function of substitution and branching of the alkyl groups. As a result of this work rhodium complexes of alkyldiphenylphosphine were recognized as potentially highly attractive catalyst candidates of increased stability for continuous hydroformylation.

It should be recalled that the triphenylphosphine rhodium carbonyl hydride (Ph_3P complex) catalyst system was discovered by Professor Wilkinson and coworkers in the late 1960's as a low pressure, low temperature catalyst for the selective hydroformylation of 1-olefins to produce n-aldehydes (1). Pruett and Smith at Union Carbide Corp., and the Wilkinson group at Imperial College found in the same period that the selectivity of Wilkinson's catalyst to n-aldehydes was greatly increased by the addition of excess Ph_3P ligand, especially at low CO partial pressures(2). The discovery of these effects resulted in the commercial development by Union Carbide and Davy McKee of a low pressure propylene hydroformylation process based on a catalyst system containing the tris-phosphine complex and excess triphenylphosphine ligand (3,4,5).

The commercial rhodium hydroformylation process operates at about 100°C. The gaseous propylene, H_2 and CO reactants are continuously introduced into a well stirred solution of the catalyst while a vapor mixture of unreacted reactants and products is being flashed off (Figure 1). The ratio of normal versus iso-butyraldehyde products in such an operation is high, in excess of ten. For an effective removal of high boiling aldehyde products in such a process, increased reaction temperatures are obviously advantageous.
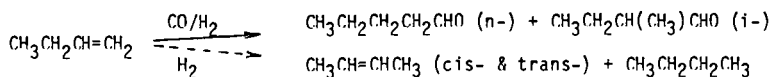
We have previously reported on our work relating to the mechanisms of triphenylphosphine rhodium complex catalyzed hydroformylations (6,7,8). We postulated that, in selective 1-n-olefin hydroformylation to n-aldehydes, the tris-(triphenylphosphine) rhodium carbonyl hydride complex is the stable precursor of the reactive trans-bis phosphine species. This postulate is based on correlating the data on equilibria among various Ph_3P-Rh complexes with hydroformylation rates and selectivities.

The structures of the various Ph_3P-Rh complexes and their equilibria were determined via NMR in the presence of varying amounts of excess Ph_3P and under different CO partial pressures. Studies of hydroformylation catalysis were carried out mainly using 1-butene as a reactant for the selective production of n-valeraldehyde at temperatures in excess of 100°C.

In the present work, the catalytic and structural studies were extended to various tris-(alkyldiphenylphosphine) rhodium carbonyl hydride complexes and related catalysts (Ph_2PR complexes). The previously described experimental methods were used

(6). Although the use of these catalysts was found to require higher temperatures than that of the Ph_3P complex catalysts, high selectivities toward valeraldehydes, particularly the n-isomer, could be maintained coupled with an increase in catalyst stability. Details of the work are described in Exxon patents (9). In this presentation, correlations of catalyst structure and activity are emphasized.

Using 1-butene instead of propylene in this laboratory allowed an additional insight into the reaction mechanism since isomerization side reactions producing 2-butenes could be also readily studied:

$$CH_3CH_2CH=CH_2 \xrightleftharpoons[H_2]{CO/H_2} \quad \begin{array}{l} CH_3CH_2CH_2CH_2CHO \ (n-) + CH_3CH_2CH(CH_3)CHO \ (i-) \\ CH_3CH=CHCH_3 \ (cis- \ \& \ trans-) + CH_3CH_2CH_2CH_3 \end{array}$$

In contrast to the voluminous, prior patent literature, the present batch hydroformylation studies included not only the determination of the normal to iso (n/i) ratio of the aldehyde products but the paraffin hydrogenation and internal olefin isomerization by-products as well. A limited study of continuous hydroformylation, via a continuous product flash-off operation, was also made.

RESULTS AND DISCUSSION

In contrast to Ph_3P complexes, Ph_2PR complexes were generally not considered for hydroformylation catalysis. For example, propyldiphenylphosphine, a Ph_3P degradation product during continuous propylene hydroformylation, was mainly regarded as a catalyst modifier rather than as a catalyst ligand on its own (10-12). In the present work, the structure and catalytic activity of Ph_2PR complexes was studied in detail and compared with those of the corresponding Ph_3P complexes.

Most of the Ph_2PR studies to be discussed were carried out with $Ph_2PCH_2CH_2C(CH_3)_3$ and $Ph_2PCH_2CH_2Si(CH_3)_3$ because they readily provided crystalline rhodium carbonyl hydride complexes. When an excess of these ligands was reacted with ethanolic solutions of rhodium dicarbonyl acetyl acetonate and then with hydrogen at ambient temperature, the corresponding tris-phosphine complexes were formed as pure crystalline precipitates. The following overall reaction took place

$$3 \ Ph_2PR + Acac \ Rh(CO)_2 + H_2 \longrightarrow (Ph_2PR)_3Rh(CO)H + AcacH + CO$$
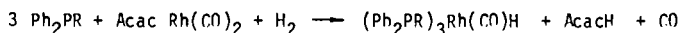
The same reaction occurred when other alkyldiphenylphosphines were used. However, most of the products separated as oils.

Most of the alkyldiphenyl phosphine reactants used were prepared in our laboratory. The preferred displacement approach to these compounds involved the reaction of lithium diphenylphosphide with the appropriate alkyl chlorides in tetrahydrofuran, e.g.

$$Ph_2PLi + ClCH_2CH_2C(CH_3)_3 \longrightarrow Ph_2PCH_2CH_2C(CH_3)_3$$
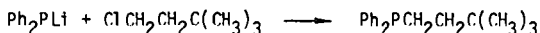
The addition approach utilized the free radical chain addition of diphenyl phosphine to the corresponding olefins. The additions were inititated by irradiation with broad spectrum ultraviolet light and preferably employed activated olefinic reactants at a reaction temperature of about 15°, e.g.

$$Ph_2PH + CH_2=CHSi(CH_3)_3 \longrightarrow Ph_2PCH_2CH_2Si(CH_3)_3$$

On changing the structure of the alkyl group of the Ph_2PR ligands, major changes in catalyst activity were observed, primarily due to steric crowding. Steric crowding affected the structure and stability of the Ph_2PR complexes formed. The structure of the catalyst complexes, in turn, determined reactivity and selectivity.

All the findings including hydrocarbon by-product formation, could be corre-

lated with changing equilibria between the catalyst complexes present in hydrofor-
mylation systems and with the steric and electronic effects of ligands on such equili-
bria. These equilibria and the critical reaction steps are shown by the outline of an
overall mechanistic scheme in Figure 2.

According to the figure, coordinatively saturated alkyldiarylphosphine
rhodium complexes of varying carbonylation degrees are the main components of such
hydroformylation catalyst systems. Upon reversible dissociation, these unreactive
complexes generate coordinatively unsaturated species which react with the olefin and
in turn, with CO and H_2 to provide the normal and iso aldehyde products, with the re-
generation of the catalyst.

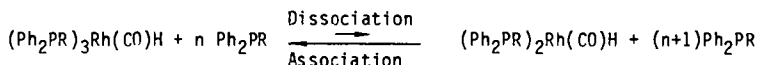### 1. Studies of Catalyst Complex Structures and Equilibria by NMR

In comparative NMR studies, first the structure and stability of Ph_2PR and
Ph_3P complexes were compared. Differences in the behavior of specific Ph_2PR ligands
were also studied to ascertain electronic and steric influences of substituting the R
alkyl groups.

Ligand exchange studies of the tris-Ph_3P complex using sterically non-crowded
Ph_2PR reactants generally showed substantial reaction:

$$(Ph_3P)_3Rh(CO)H \ + \ 3 \ Ph_2PR \ \longrightarrow \ (Ph_2PR)_3Rh(CO)H + 3 \ Ph_3P$$
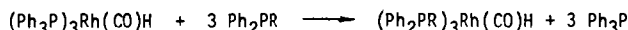
The more basic Ph_2PR ligand formed a more stable complex than Ph_3P. In the above re-
action, the ratio of complexed $Ph_2PCH_2CH_2C(CH_3)_3$ to complexed Ph_3P in the -60 to + 35°
temperature range was about 3.

Ligand exchange between complexed and free phosphine ligands also occurred,
in a reversible manner, when there was only one phosphine present. Such an exchange
took place via coordinatively unsaturated trans-bis-phosphine rhodium carbonyl hydride
intermediates:

$$(Ph_2PR)_3Rh(CO)H + n \ Ph_2PR \ \xrightleftharpoons[\text{Association}]{\text{Dissociation}} \ (Ph_2PR)_2Rh(CO)H + (n+1)Ph_2PR$$

Since the equilibria strongly favor the coordinatively saturated tris-phosphine com-
plexes, only the NMR spectra of these species could be detected. However, the rate of
ligand dissociation could be determined by line shape analyses of the signals.

The qualitative aspects of the comparative ^{31}P NMR ligand exchange studies of
the $Ph_2PCH_2CH_2C(CH_3)_3$, Ph_3P and $Ph_2PCH_2CH_2Si(CH_3)_3$ complex systems are indicated by the
[31]P spectra in Figures 3a and b. At -60°C, the typical doublet signal of the tris-
phosphine complexes plus singlet signals of the free phosphines were observed for all
three systems. However, the doublet signal of the Ph_2PR type complexes remained sharp
at 35° while the Ph_3P complex exhibited a broad doublet. Similarly, the Ph_2PR complex
still showed a very broad doublet at 60° where the doublet of the Ph_3P complex had
already collapsed. Further increases in the ligand exchange rates, resulted in a
single composite signals for the Ph_3P and Ph_2PR systems at 90° and 120°, respectively.

Clearly higher temperatures in the Ph_2PR complex systems were necessary to
reach ligand exchange rates comparable to that of the Ph_3P complex. Since the increase
in ligand exchange rate parallels that of complex dissociation to yield coordinatively
unsaturated species, these data indicate that in the Ph_2PR complex systems a comparable
generation of such reactive species occurs at higher temperatures. This suggests that
to achieve comparable hydroformylation rates, higher temperatures are needed when com-
plexes of Ph_2PR are used in place of Ph_3P. On the other hand, at the higher tempera-
tures, the Ph_2PR complexes are more stable than the Ph_3P complex.

In view of recent suggestions, of a potential CO dissociation from the tris-
Ph_3P complex to generate hydride species leading to n-aldehyde products (13, 14),
ligand exchange was also studied by ^{13}C NMR. For these studies, [13]CO enriched tris-
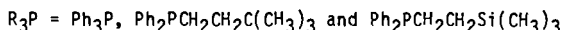
phosphine complexes were used. Such complexes could be readily derived by reacting the corresponding tetrakis-phosphine rhodium hydride complexes with ^{13}CO at atmospheric pressure. For example, the following sequence of reactions was carried out with $Ph_2PCH_2CH_2C(CH_3)_3$ and $Ph_2PCH_2CH_2Si(CH_3)_3$:

$$4\ Ph_2PR + RhCl_3 \xrightarrow{\ NaBH_4\ } (Ph_2PR)_4RhH \xrightarrow{\ ^{13}CO\ } (Ph_2PR)_3Rh(^{13}CO)H$$
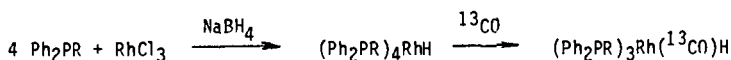
The first reaction to form the tetrakis-phosphine rhodium hydride was carried out in 10 minutes in refluxing ethanol solution in a manner reported for the Ph_3P derivative (15). The resulting crystalline hydride could be reacted with ^{13}CO at room temperature either in toluene solution or ethanol suspension.

Variable temperature ^{13}C NMR studies of tris-phosphine monocarbonyl hydride complexes are illustrated by Figure 4. The spectra indicate that at -30°, the Ph_3P complex has the expected structure. The double quartet signals of the complexed ^{13}CO show coupling to one rhodium and three phosphine ligands. At increased temperatures up to 110°C, this signal of the Ph_3P complex collapsed into doublets. That was the consequence of the exchange of the phosphine ligands. Rhodium coupling remained since no ^{13}CO dissociation occurred. However, free ^{13}CO could be detected in this system at 140°C when free triphenyl phosphine ligand was used as the solvent (P/Rh = 260).
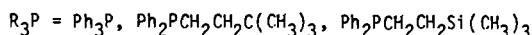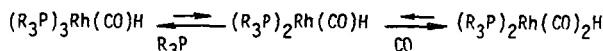
The ^{13}CO NMR studies show that the CO ligand of these tris-phosphine monocarbonyl hydride complexes is very strongly bound. During hydroformylation, carbonyl free phosphine rhodium hydride complexes are not present, except under non-equilibrium CO starvation conditions. The main reaction in these systems is always phosphine rather than CO dissociation. Proton NMR studies of the hydride region of tetrakis-phosphine rhodium hydrides were known(16). The dissociation in d-toluene solutions of three tetrakis-phosphine rhodium hydrides was studied by ^{31}P NMR ligand exchange methods in the presence of excess phosphine ligands in the present work.

$$(R_3P)_4RhH + 5R_3P \rightleftharpoons (R_3P)_3RhH + 6\ R_3P$$

$$R_3P = Ph_3P,\ Ph_2PCH_2CH_2C(CH_3)_3\ and\ Ph_2PCH_2CH_2Si(CH_3)_3$$

In general, it was found that significant ligand exchange of these hydrides occurred at much lower temperatures than those observed for the corresponding carbonyl hydrides. The doublet signal of the tetrakis-triphenylphosphine rhodium hydride collapsed at -30° while the corresponding Ph_2PR complexes gave broad singlet signals for complexed ^{31}P at about + 20°. Thus it was found Ph_2PR ligands are more strongly complexed than Ph_3P in carbonyl free rhodium hydrides as well.

The increase in hydrogenation and isomerization side reactions during 1-butene hydroformylation under CO starvation conditions can be explained by the formation of carbonyl free rhodium hydride complexes. Tetrakis-triphenylphosphine rhodium hydride is a known hydrogenation catalyst (16). In the present work, it was found to be an effective 1-butene isomerization catalyst even at 0°. Its low temperature catalytic activity is attributed to its facile dissociation to provide the corresponding highly reactive tris-phosphine rhodium hydride.

At increased CO partial pressure, tris-phosphine rhodium carbonyl hydrides are converted to the corresponding trans-bis-phosphine dicarbonyl hydrides via the following equilibrium reactions:

$$(R_3P)_3Rh(CO)H \underset{R_3P}{\rightleftharpoons} (R_3P)_2Rh(CO)H \underset{CO}{\rightleftharpoons} (R_3P)_2Rh(CO)_2H$$

$$R_3P = Ph_3P,\ Ph_2PCH_2CH_2C(CH_3)_3,\ Ph_2PCH_2CH_2Si(CH_3)_3$$

Complexes of Ph_3P and Ph_2PR type ligands showed similar equilibria between mono- and dicarbonyl hydride complexes.

Increased concentrations of excess phosphine ligand effectively reduced the amount of dicarbonyl hydride formed. This is illustrated by Figure 5. The figure shows that, in the absence of a significant excess of the Ph_2PR type ligand, conversion to the dicarbonyl hydride is essentially complete under about 200 kPa pressure of 1 to 1 H_2/CO. However, at a five-fold excess of Ph_2PR (P/Rh ratio of 15/1) the ratio of dicarbonyl to monocarbonyl complex is only about 1 to 3.

In the case of bis-phosphine dicarbonyl hydride complexes, the relative dissociation rates of phosphine and carbonyl ligands were also studied by NMR:

$$CO + (Ph_3P)_2Rh(CO)H \rightleftharpoons (Ph_3P)_2Rh(CO)_2H \rightleftharpoons Ph_3PRh(CO)_2H + Ph_3P$$
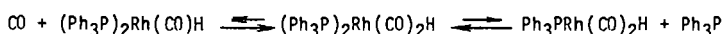
A 1% solution of the bis-Ph_3P complex plus excess Ph_3P to provide a P/Rh ratio of 9 were used for the study. This solution was prepared under 400kpa $H_2/^{13}CO$ pressure, from the tetrakis-Ph_3P complex which was largely converted to the desired bis-phosphine rhodium dicarbonyl hydride. Variable temperature NMR studies indicated reversible CO and phosphine ligand dissociation.

As it is shown by Figure 6, the ^{13}C NMR spectrum of the resulting solution showed the expected double triplet for the complexed ^{13}CO ligand as well as the singlet signal of free ^{13}CO. At + 35°, the fine structure of the complexed CO disappeared. Also, the signals of complexed and free ^{13}CO considerably broadened as a consequence of CO exchange. At 90°C, only one, broad ^{13}CO signal was obtained due to further increased ligand exchange rates.

Similar variable temperature ^{31}P NMR studies showed reversible phosphine ligand dissociation. However, a free versus bound Ph_3P ratio much below the expected value was found at low temperature. This suggests the presence of unidentified rhodium complex species undergoing rapid ligand exchange.

When 1-olefins are hydroformylated under conditions where the dicarbonyl hydride predominates in the above type of system, the n/i ratio of aldehyde products is greatly decreased but still remains above two. It is believed that most of the remaining preference of such catalyst systems for producing n-aldehydes is due to ^{13}CO dissociation to provide the trans-bis-phosphine monocarbonyl hydride intermediate of linear hydroformylation.

The electronic effects on the properties of tris-Ph_2PR rhodium carbonyl hydride catalyst complexes were studied by substituting groups of varying electrophilicity on the β-carbons of the alkyl groups of their ligands. The basicities of some of these ligands of general formula $Ph_2PCH_2CH_2R'$ and their ^{31}P NMR parameters of their complexes are shown by Table I.

The data of the table indicate that by appropriate electronegative β-substituents the proton basicity of aqueous alkyldiphenylphosphines was reduced to the level of triphenylphosphine. However, no apparent correlation could be observed between the inverse basicity values, ΔHNP's, and the NMR parameters. Most of the $Ph_2PCH_2CH_2R'$ complexes showed little change of their chemical shift and coupling constant values. Also, all the $Ph_2PCH_2CH_2R$ ligands displaced Ph_3P from its complex. Thus the observed basicity was not a major factor in the NMR data.

In view of the above study, the difference between the sterically non-hindered alkyldiarylphosphine and triphenylphosphine complexes is apparently attributed to minor differences in their π-backbonding ability and steric hindrance.

Steric hindrance was found to have a major effect on the structure of the complexes formed when α- and β- branched alkyldiphenylphosphine ligands were used. These effects were first studied by determing the degree of Ph_3P ligand displacement with such Ph_2PR ligands as indicated by the following simplified scheme

$$(Ph_3P)_3Rh(CO)H + 6 Ph_3PR \rightleftharpoons (Ph_2PR)_3Rh(CO)H + 3Ph_3P + 3Ph_2PR$$
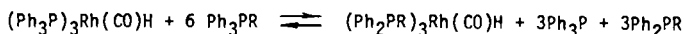
In the case of the monomethyl branched ligands, such as isobutyl-, secondary butyl- and cyclohexyl- diphenylphosphines, partial displacement occurred. The ratio of bound Ph_2PR to Ph_3P was about 3 to 2. However, β, β- and α,α-dimethyl branched ligands such

as neopentyl- and t-butyl-diphenyl phosphines were not able to displace any of the Ph_3P.

Displacement of Ph_3P by the above sterically hindered phosphine ligands could be enhanced under about 400 kpa H_2/CO pressure. This pressure results in the formation of major amounts of the bis-triphenylphosphine rhodium dicarbonyl hydride complex. The latter, in turn, was found to be more subject to displacement by the sterically demanding phosphine ligands:

$$(Ph_3P)_2Rh(CO)_2H + 6Ph_2PR + Ph_3P \rightleftharpoons (Ph_2PR)_2Rh(CO)_2H + 4Ph_2PR + 3Ph_3P$$

Thus, at equilibrium the mixtures containing monosubstituted ligands showed the displacement of about 80% of the Ph_3P from the dicarbonyl complex. However, there was still no noticable displacement by the neopentyl and t-butyl derivatives.

The above inhibition of ligand displacement is clearly due to steric effects. Electronic effects would result in increased ligand displacement since these branched alkyldiphenylphosphine ligands have higher basicities than their straight chain isomers.

Another effect of steric crowding is on the dissociation rate of the complexes formed. This is illustrated by the example of triphenylphosphine plus isobutyl-diphenylphosphine rhodium complex catalyst system in Figure 7. The -30°C spectrum of this system shows that both ligands participate in the complex formation to form four different tris-phosphine complexes. However, no distinct phosphorus signals of these complexes can be observed at ambient temperature. Only a broad phosphorus signal is observed in the complex region. This indicates a high ligand exchange rate at a relatively low temperature. This is clearly the consequence of increased phosphine dissociation due to steric decompression:

$$[Ph_2PCH_2CH(CH_3)_2]_3Rh(CO)H \rightarrow [Ph_2PCH_2CH(CH_3)_2]_2Rh(CO)H + Ph_2PCH_2CH(CH_3)_2$$
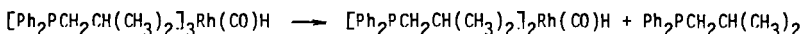
The increased dissociation rate to provide reactive coordinatively unsaturated complex species results in increased catalytic activity. However, steric crowding also results in a reduced ratio of monocarbonyl hydride versus dicarbonyl hydride complexes, i.e. reduced n/i ratio of products.

2. Hydroformylation Process Studies

The main aim of the present 1-butene hydroformylation studies was to determine the effect of the structure of phosphine-rhodium complex catalysts on activity, selectivity and stability. The well known Ph_3P complex catalyst system which we studied previously(6) was a catalyst primarily used for comparison in this work. As a $Ph_2PCH_2CH_2R'$ type alkyldiarylphosphine ligand, 2-trimethylsilylethyldiphenylphosphine (SEP), was studied in detail.

In the following at first, the Ph_3P and SEP based rhodium complex hydroformylation catalyst systems will be compared at different temperatures and excess phosphine concentrations. Thereafter, the detailed structural effects of various Ph_2PR ligands will be discussed with emphasis on steric crowding. The catalytic results will be correlated with the structural findings of the NMR studies.

The effect of temperature on the Ph_3P and SEP complex catalyst systems is shown in Table II. Most of the batch experiments were carried out at a one molal phosphine ligand concentration to maintain the selectivity and stability of the catalyst at increased temperatures. The results show that, at comparable temperatures, the triarylphosphine complex is always more active than the alkyldiarylphosphine complex. However, the activity and selectivity of the latter is better maintained particularly at higher temperatures.

At the relatively low temperature of 110°, a lower n/i aldehyde product ratio is obtained with the SEP complex. However, there is no significant difference between

the higher n/i values of the two systems at 145°. In the 135 to 160° range, the use of
the SEP complex leads to a higher total (n+i) aldehyde selectivity. This is mainly due
to the reduced butene-1 to butene-2 isomerization side reactions in the presence of the
more basic SEP ligand. The top temperature of 160° has generally less adverse effect
on the selectivity of the SEP complex system.

The effect of increasing concentrations of the SEP and Ph_3P ligands at 145°
is shown in Table III. This increase in both systems resulted in a decreased activity
but increased n/i aldehyde selectivity. At high ligand concentrations, the n/i values
depended on the phosphine concentration rather than on the P/Rh ratio. When these
phosphines were used as the only solvents, the n/i ratios reached maximum values but
the selectivities to total aldehyde products decreased.

The SEP and Ph_2P rhodium complex catalyst systems were also compared in
continuous 1-butene hydroformylation, operating via product flash-off (PFO) from the
reaction mixture (Figure 1). The reaction conditions and data obtained are shown by
Table IV.

In the first three experiments, the SEP system was operated at 120° while the
Ph_3P system was running at 100°. Most importantly the results indicate that the
increased temperature of the SEP-Rh system is highly advantageous for achieving higher
butene conversions without increasing the stripping gas rate. At the lower temperature
of the Ph_3P-Rh system, a higher conversion operation was not feasible under these con-
ditions because of the limited product flash-off capability due to vapor liquid
equilibria. It is noted that the selectivities of the two systems are similar.

In the other three experiments, the stability of the SEP and Ph_2P based
rhodium catalyst systems was compared in a six day continuous PFO operation at 145°C.
The butene conversion achieved with the SEP system showed less than 10% change. The
conversion in the case of the Ph_3P system dropped from 82 to 65% during the test
period. About 1/2% per day of the Ph_3P ligand was converted to butyldiphenylphosphine
via ortho-metalation(10). No similar degradation of the SEP ligand was observed. In
addition, as shown by the table, the selectivity of the SEP complex system was somewhat
higher and did not change significantly when a mixture of 1- and 2-butenes was used in
place of the pure 1-butene feed. (The 2-butene is apparently of very low reactivity
under these conditions).

In more detailed PFO process studies of the SEP-Rh catalyst system at 120°,
complete maintenance for 30 days of both hydroformylation activity and selectivity was
established. In these studies, the n/i ratios of the valeraldehyde products were
correlated with the excess phosphine ligand concentration and CO partial pressure. As
was expected on the basis of the NMR studies of catalyst structures, the n/i ratio was
directly dependent on the [SEP] and inversely dependent on the pCO.

The catalytic properties of a high number of alkyldiphenylphosphine rhodium
complexes were studied in batch experiments. Comparative results obtained with
complexes of ligands of the formula $Ph_2PCH_2CH_2R'$ and Ph_3P are shown by Table V.

The results show that, at the 1M phosphine concentrations, all the
$Ph_2PCH_2CH_2R'$ complexes are highly selective catalysts for hydroformylation at 145°.
They provide aldehyde products having n/i ratios in the 8.9-18.9 range. In general,
their product linearity is similar to that of the Ph_3P system (n/i = 11.2). The total
aldehyde selectivity of the Ph_2PR complex catalyst is higher. Their n + i aldehyde
selectivity is in the 86.9 to 91.8% range while the corresponding n + i value of the
Ph_3P system is 81.2. However, as expected on the basis of the NMR ligand dissociation
rates, the Ph_3P system is more than twice as active.

The activity and selectivity of all these catalysts is highly dependent on
the excess phosphine ligand concentration. When the phosphine ligand concentration was
dropped to 0.14 M, the reaction rate usually increased about fourfold and the n/i ratio
of the aldehyde products decreased to about a half of the previous value. Of course,
these effects are expected on the basis of the catalytic mechanisms suggested by the
NMR studies.

No definite correlation could be found between the basicity of the
$Ph_2PCH_2CH_2R'$ ligands and the catalytic properties of their rhodium complexes. Overall

the differences among these complexes were smaller than the difference between them as a group and the Ph$_3$P complex. The Ph$_3$P ligand stands out by virtue of its increased π-backbonding ability which weakens the CO coordination to the rhodium. Also, Ph$_3$P is a sterically more demanding ligand than Ph$_2$PCH$_2$CH$_2$R' ligands. Both properties increase the reactivity of the Ph$_3$P-Rh complex catalyst system.

The effect on catalysis of the steric crowding of alkyldiphenyl phosphine ligands by methyl substitution on the α- or β-carbon atoms of their alkyl group was also studied. The comparative experiments were carried out using two different ligand concentrations at 145°. The results are shown by Table VI.

Compared to straight chain and γ-methyl substituted alkyldiphenylphosphines, the α- and β-methyl substituted derivatives led to increased hydroformylation rates but reduced selectivities. The rate increasing effect was observed at the higher phosphine ligand concentration of 1M. The selectivities were decreased in terms of lower n/i ratios of aldehyde products and increased isomerization side-reactions to 2-butenes. The isomerization was particularly increased at the low ligand concentration of 0.14 M. At an extreme, this resulted in a reduced reaction rate since 2-butenes are much less reactive than 1-butene. The effect of steric crowding was further increased when the α, α- and β, β-dimethyl substituted alkyldiphenylphosphines were used in place of the monomethyl substituted ligands.

The increased reactivity of branched alkyldiphenylphosphine rhodium complexes is attributed to the accelerated dissociation via steric decompression of tris-phosphine rhodium carbonyl hydride complexes to provide reactive species. The reduced n/i ratio of the products is due to the increase of rhodium dicarbonyl hydride catalyst complexes. The increased isomerization to 2-butenes is apparently a consequence of the reversibility of reactions forming the secondary butyl rhodium complex intermediate.

CONCLUSIONS

The present correlation of the structure of t-phosphine rhodium carbonyl hydride complexes with high temperature hydroformylation catalysis data leads to the extension of our previously proposed rhodium hydroformylation mechanisms to alkyldiphenylphosphine ligand based catalysts. In view of their increased stability, alkyldiphenylphosphines are now recognized as rhodium complex catalyst ligands potentially superior to the commercially widely used triphenylphosphine.

Alkyldiphenylphosphines form remarkably stable tris-phosphine rhodium carbonyl hydride complexes of the formula (Ph$_2$PCH$_2$CH$_2$R')$_3$Rh(CO)H. These act as a preferred reversible reservoir for the generation of the highly reactive, coordinatively unsaturated trans-bis-phosphine carbonyl hydride intermediates of 1-n-olefin hydroformylation to provide mostly n-aldehyde products. In accord with the complex equilibria found among variously carbonylated rhodium complex catalyst precursors, the stability and selectivity of such catalyst systems directly depends on the excess phosphine ligand concentration. It is inversely related to the partial pressure of the CO reactant. Changes in the R' group of such ligands did not result in any profound change of the catalytic properties of their rhodium complexes although they caused wide variations in their proton basicities.

In contrast branched alkyldiphenylphosphines having β- or α- alkyl substituents e.g.

$$Ph_2PCH_2CH(CH_3)_2 \quad Ph_2PCH(CH_3)CH_2CH_3 \quad Ph_2PCH_2C(CH_3)_3 \quad Ph_2PC(CH_3)_3$$
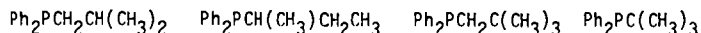
form rhodium carbonyl hydride complexes of widely differing stabilities. These complexes in turn exhibit a broad range of catalyst behavior. Tris-phosphine rhodium carbonyl hydride complexes of these ligands are thermally unstable due to steric crowding. This facilitates the generation of reactive species. Under CO pressure, complexes of these ligands are largely converted to bis-phosphine rhodium dicarbonyl hydride, (Ph$_2$PR)$_2$Rh(CO)$_2$H, intermediates of nonselective hydroformylation.

Thus profound electronic differences between sterically noncrowded alkyldiphenylphosphine and triphenylphosphine rhodium carbonyl hydride complexes resulted in two types of catalyst systems having distinct properties. In contrast, small changes in the electronic character of alkyldiphenylphosphine complexes did not cause significant changes in catalysis. However, small changes in the steric requirements of α- and β- branched alkyldiarylphosphines produced tremendous changes in the catalytic behavior of their rhodium complexes. Moderate steric crowding of such complexes may result in highly desired catalyst properties. However, such steric effects on catalysis are difficult to predict.

ACKNOWLEDGEMENTS

LITERATURE CITED

1. Osborn, J. A., Jardine, F. H., Young, J. F. and Wilkinson, G., J. Chem. Soc. A, 1966, 171.
2. Pruett, R. L. and Smith, J. A., Org. Chem. 1969, 34, 327; U. S. Patent 3,527,809; Evans, D., Osborn, J. A. and Wilkinson G., J. Chem. Soc. A, 1968, 3133.
3. Brewester, E. A. V. and Pruett, R. L., U. S. Patent 4,247,486; Bryant, D. R. and Billig, E., U.S. Patent 4,277,627 (both assigned to Union Carbide Corp.).
4. Chem. Eng. Dec. 5, 1977, 110.
5. New Syntheses with Carbon Monoxide, Editor: Falbe, J., Springer Verlag, Berlin-Heidelberg-New York, 1980, Chapter 1 on "Hydroformylation, Oxo Synthesis Roelen Reaction" by Cornils, B.
6. Oswald, A. A., Hendriksen, D. E., Kastrup, R. V. and Merola, J. S., Preprints, Div. Pet. Chem., Inc., Am. Chem. Soc. Natl. Meeting, Las Vegas, Nev., Spring 1982, 27 (2) 292. Advances in Synthesis Gas Chemistry Symposium, Presentation on "Rhodium Hydroformylation Mechanisms."
7. Advances in Chemistry, Editors: Alyea, E. C.; Meek, D. W., American Chemical Society, 1982, 196, 78, Chapter on ^{31}P NMR Studies of Equilibria and Ligand Exchange in Triphenylphosphine Rhodium Complex and Related Chelated Bis-Phosphine Rhodium Complex Hydroformylation Catalysts" by Kastrup, R. V., Merola, J. S., Oswald, A. A.
8. ACS Symposium Series Editors: Quin, L. D., Verkade, J. G., 1981, 171, 503, Chapter on ^{31}P NMR Studies of Catalytic Intermediates in Triphenylphosphine Rhodium Complex Catalyzed Hydroformylations," Oswald, A. A., Kastrup, R. V., Merola, J. S., Mozeleski, E. J.
9. Oswald, A. A., Jermansen, T. G., Westner, A. A., Huang, I-D., Patent Cooperation Treaty (PCT) International Patent Publication No. WO/80/01690, August 21, 1980, British Patent Application 8,223,961, February 21, 1983, and U. S. Patent 4,298,541 (assigned to Exxon Research and Engineering Co.)
10. Gregorio, G., Montrasi, G., Tampieri, M., Cavalieri d'Oro, P., Pagani, G., Andreetta, A., Chim. Ind. (Milan) 1980, 62 (5), 389.
11. Paul, J. L., Pieper, L. W. and Wade, E. L., U.S. Patent 4,151,209 (to Celanese Corp.).
12. Morrell, D. G. and Sherman, P. D., U.S. Patent 4,260,828 (to Union Carbide Corp.).
13. Hughes, O. R. and Young, D. A., J. Am. Chem. Soc. 1981, 103, 6636.
14. Unruh, J. D. and Christenson, J. R., J. Mol. Cat. 1982, 14, 19.
15. Levison, J. J., and Robinson, S. D., J. Chem. Soc. A, 1970, 2947.
16. Dewhurst, K. C., Keim, W. and Reilly, C. A., Inorg. Chem. 1968, 1, 546; Dewhurst, K. C., U. S. Patent 3,480,659 (assigned to Shell Oil Co.).
17. Streuli, C. A., Anal. Chem. 1960, 32, 985.

Figure 1

SCHEME OF CONTINUOUS HYDROFORMYLATION UNIT WITH CONTINUOUS PRODUCT FLASH-OFF

UNREACTED H_2, CO, OLEFIN
LOW BOILING BY-PRODUCTS

SEPARATOR

H_2
CO
OLEFIN

COOLER

FEED PREHEATER

ALDEHYDE PRODUCT + HIGH BOILING BY-PRODUCTS

CATALYST SOLUTION

PFO REACTOR
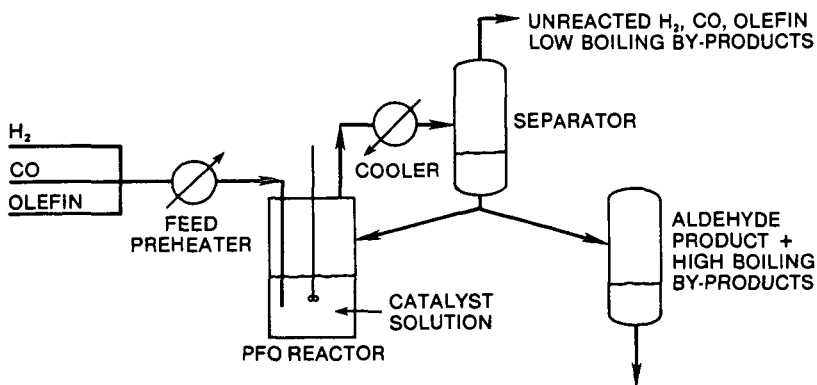
Figure 2

CATALYTIC INTERMEDIATES IN PHOSPHINE RHODIUM COMPLEX CATALYZED HYDROFORMYLATION OF 1-BUTENE

Non-reactive Complexes	$(R_3P)_2Rh(CO)_2H$	$(R_3P)_3Rh(CO)H$	$(R_3P)_4RhH$
	T ⇌ R_3P CO ⇌ T	T ⇌ R_3P CO ⇌ T	T ⇌
Reactive Complexes	$(R_3P)Rh(CO)_2H$	$(R_3P)_2Rh(CO)H$	$(R_3P)_3RhH$
	Non-selective ↓ C_4^-	Selective ↓ C_4^-	Side Reaction ↓ C_4^-
Product Intermediates	$(R_3P)Rh(CO)_2H$ | $CH_3CHCH_2CH_3$	$(R_3P)_2Rh(CO)H$ | $CH_2CH_2CH_2CH_3$	$(R_3P)_3Rh$ | $CH_2CH_2CH_2CH_3$
	↓ CO	↓ CO	↓ H_2
Products	CH_3CH_2CHCHO | CH_3	$CH_3CH_2CH_2CH_2CHO$	$CH_3CH_2CH_2CH_3$ + $CH_3CH = CHCH_3$

FIGURE 3
³¹P NMR STUDY OF LIGAND EXCHANGE AT VARIOUS TEMPERATURES
(Ph₃PR)₃Rh(CO)H + 6 Ph₂PR ⇌ (Ph₂PR)₅ Rh(CO)H + 7 Ph₃PR
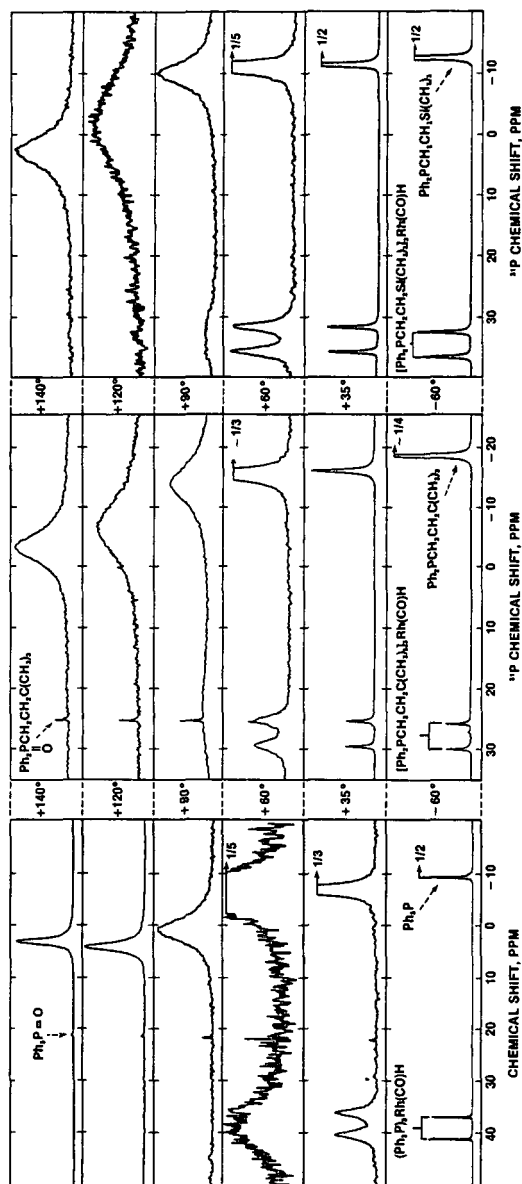
Figure 4

EFFECT OF TEMPERATURE ON ¹³CO NMR SPECTRUM: P/Rh = 9
CO + (Ph₃P)₃RhH ⇌ (Ph₃P)₃Rh(CO)H ⇌ (Ph₃P)₃Rh(CO)H + Ph₃P

+110°
+90°
35°: Under N₂   +35°
−30°

¹³C CHEMICAL SHIFT, PPM
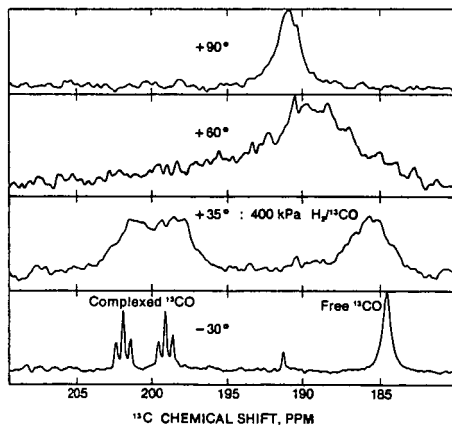
Figure 5

EFFECT OF EXCESS PHOSPHINE UNDER 200 kPa H₂/CO AT 0°
(Ph₃PR)₂Rh(CO)₂H + nPh₂PR ⇌ (Ph₃PR)₃Rh(CO)H + (n-1)Ph₂PR + CO
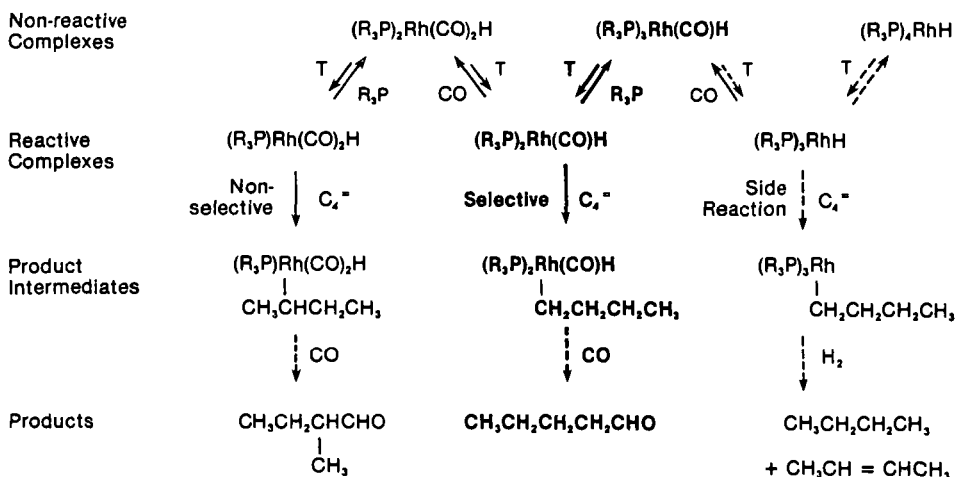

[Ph₂PCH₂CH₂Si(CH₃)₃]₃Rh(CO)H   12 Ph₂PCH₂CH₂Si(CH₃)₃   n = 12
n = 6
n = 3
[Ph₂PCH₂CH₂Si(CH₃)₃]₂Rh(CO)₂H   n = 0.3

³¹P CHEMICAL SHIFT

Figure 6

EFFECT OF TEMPERATURE ON ¹³CO NMR SPECTRUM: P/Rh = 9
CO + (Ph₃P)₂Rh(CO)H ⇌ (Ph₃P)₂Rh(CO)₂H ⇌ Ph₃PRh(CO)₂H + Ph₃P

+90°
+60°
+35° : 400 kPa H₂/¹³CO
Complexed ¹³CO   Free ¹³CO   −30°

¹³C CHEMICAL SHIFT, PPM
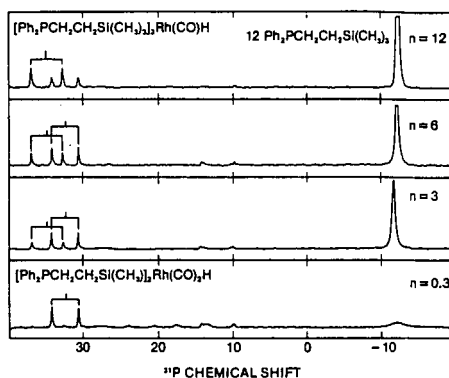
Figure 7

EFFECT OF MODERATE STERIC HINDRANCE
ON LIGAND DISPLACEMENT AND EXCHANGE

(Ph₃P)₃Rh(CO)H + 6Ph₂PR ⟶ (Ph₂PR)₃Rh(CO)H ● 3Ph₂PR + 3 Ph₃P
(Ph₃P)₂(Ph₂PR)Rh(CO)H ---- Ph₃P(Ph₂PR)₂Rh(CO)H
35°   Ph₃P   Ph₂PR
Ph₂PR ≡ Ph₂PCH₂CH(CH₃)₂
−30°   Ph₃P

³¹P CHEMICAL SHIFT, PPM
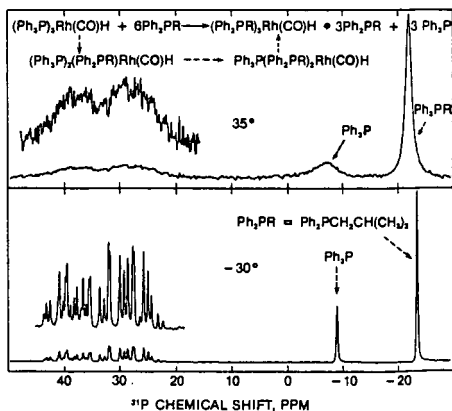
Table I

Δ HNP'S of $Ph_2PCH_2CH_2R$ LIGANDS AND ^{31}P NMR PARAMETERS[a]
OF THEIR $(Ph_2PCH_2CH_2R')_3Rh(CO)H$ COMPLEXES

Phosphine Ligand			Phosphine Complex	
Structure	Inverse Basicity,[b] ΔHNP	Chem. Shift ppm	Chem. Shift α,ppm	Coupling Constant J_{P-Rh},cps
$Ph_2PCH_2CH_2Si(CH_3)_3$	385	-12.2	34.6	150
$Ph_2PCH_2CH_2C(CH_3)_3$	412	-16.8	27.5	152
$Ph_2PCH_2CH_2CH_2CH_2CH_2CH_3$	392	-16.8	27.5	151
$Ph_2PCH_2CH_2Ph$	416	-16.6	27.6	153
$Ph_2PCH_2CH_2-N\langle\rangle$ O	450	-23.0	21.6	151
$Ph_2PCH_2CH_2CO_2CH_3$	455	-17.7	27.9	151
$Ph_2PCH_2CH_2SO_2CH_3$	543	-18.6	27.3	151
Ph_3P	510	-7.5	38.3	155

[a] At 35° in toluene solvent, relative to 1M phosphoric acid.
[b] Basicity determinations were carried out according to the modified method of Streuli(17) using perchloric acid as a titrant and pure nitromethane as a solvent. Half neutralization potentials (HNP's) were determined relative to the value of diphenyl guanidine.

Table II

EFFECT OF TEMPERATURE ON THE HYDROFORMYLATION OF 1-BUTENE WITH
TRIS-PHOSPHINE RHODIUM CARBONYL HYDRIDE CATALYSTS USING TRIPHENYLPHOSPHINE
(TPP) AND 2-TRIMETHYLSILYL-ETHYLDIPHENYLPHOSPHINE (SEP) AS LIGANDS

Reactions at 2500 kPa of 5/1H$_2$/CO with 20g 1-Butene Plus 80g Mixture of 1 M Phosphine
Ligand Plus 2-Ethylhexyl Acetate Using AcacRh(CO)$_2$ as Catalyst Precursor

Seq. No.	Ligand	Temp. °C	Rh Conc. mM	H$_2$/CO Feed	H$_2$/CO Consumption Dependent Factors (at 50% Conversion)				Aldehyde Linearity		Product Parameters					
					Ratio Final	Rate Constant k min^{-1} Normalized at 1 M Rh	Found	Reaction Time min	n/i Ratio	$\frac{100n}{n+i}$ %	Aldehyde Selectivity % Total n+i	n	i	By-Products Selectivity % 2-Butenes	Butane
1	SEP	110	4.00	52/48	4.9	8	0.032	22	7.6	88.4	93.9	83.0	10.9	4.3	1.8
2		125	1.00	52/48	4.6	26	0.026	27	8.2	89.1	94.1	83.8	10.3	4.0	1.9
3		135	1.00	53/47	5.1	46	0.046	15	9.8	90.8	90.2	81.9	8.3	5.9	3.9
4		145	1.00	54/46	6.9	73	0.073	10	11.4	91.9	89.2	82.1	7.2	6.8	3.9
5		160	0.50	56/44	6.9	130	0.065	11	11.3	91.9	82.8	76.1	6.7	10.8	6.4
6		170	0.25	56/44	5.2	160	0.040	17	8.9	89.9	78.7	70.8	7.9	13.8	7.5
7	TPP	90	3.00	52/48	5.0	11	0.033	22	12.3	92.5	89.6	82.8	6.8	7.7	2.7
8		110	0.50	52/48	5.1	34	0.017	40	12.9	92.8	91.3	84.8	6.5	5.7	3.0
9		125	0.50	52/48	4.7	116	0.058	12	11.9	92.3	89.1	82.2	6.9	7.9	3.1
10		135	0.50	54/46	6.4	156	0.078	9	12.8	92.7	84.2	78.1	6.1	10.7	5.1
11		145	0.25	54/46	5.7	200	0.050	14	11.2	91.8	81.2	74.6	6.6	13.3	5.5
12		160	0.25	56/44	5.6	256	0.064	11	7.6	88.4	78.9	69.7	9.2	15.8	5.3

Table III

EFFECT OF TRIPHENYLPHOSPHINE AND 2-TRIMETHYLSILYL-ETHYLDIPHENYLPHOSPHINE LIGAND CONCENTRATION ON THE RHODIUM HYDROFORMYLATION OF 1-BUTENE

Reactions at 145° at 2500 kPa of 5/1 H_2CO Initial Reactant (53/47 or 54/46 H_2/CO Feed) and 20g 1-Butene Plus 80g Mixture of Phosphine Ligand Plus 2-Ethylhexyl Acetate, Using AcacRh(CO)₂ as Catalyst Precursor [SEP Ligand: $Ph_2PCH_2CH_2Si(CH_3)_3$]

Seq. No.	Li-gand, L	Catalyst System Parameters			L/Rh Ratio	H_2/CO Consumption Dependent Factors (50% Conversion)				Product Parameters						By-Product Selectivity, %	
		L Concentration		Rh Conc. mM		H_2/CO Ratio Final	Rate Constant k min⁻¹		Re-action Time min	Aldehyde Linearity		Aldehyde Selectivity, %					
		M in Mixture at Start	Wt.% in Solvent				Normal-ized at 1 M Rh	Found		n/1 Ratio	100n/n+1 %	Total n+1	n	1		2-Bu-tenes	Bu-tane
1	TPP	0.14	4.7	0.05	2822	5.8	800	0.040	18	4.0	80.2	83.0	66.6	16.4		13.4	3.6
2		0.56	18.5	0.50	280	5.3	640	0.340	2	4.4	81.5	81.8	66.7	15.1		13.0	5.2
3				0.25	2240	5.1	320	0.080	9	7.6	88.4	82.3	73.6	9.7		11.7	5.1
4				2.00	200	4.9	285	0.570	1.5	7.2	87.0	80.0	70.3	9.7		14.0	5.9
5		1.00	32.9	0.25	4000	5.7	200	0.050	14	11.2	91.8	81.2	74.6	6.6		13.3	5.5
6				2.00	500	5.2	220	0.440	2	11.1	91.7	82.1	75.3	6.8		12.7	5.3
7		2.20	72.1	0.25	4400	5.9	92	0.023	32	21.7	95.6	80.0	76.5	3.5		14.3	5.7
8				2.00	1100	5.2	90	0.180	4	21.5	95.0	81.0	77.4	3.6		13.5	5.5
9		3.00	100.0	2.00	1500	3.6	48	0.096	9	31.0	96.9	73.3	71.0	2.3		19.6	7.1
10	SEP	0.14	5.0	0.10	1400	5.0	180	0.036	19	4.6	82.2	90.7	74.6	16.1		6.5	2.8
11				0.50	280	5.4	200	0.100	4	5.1	83.5	86.2	72.0	14.2		7.6	6.2
12		0.56	20.0	0.25	2240	5.5	132	0.033	21	8.0	88.8	89.6	79.6	10.0		7.0	3.4
13				2.00	200	6.0	105	0.210	3.5	9.9	90.9	86.1	78.2	7.9		8.2	5.7
14		1.00	35.9	0.50	2000	6.9	68	0.034	20	12.2	92.4	87.5	80.9	6.6		8.3	4.2
15				2.00	500	5.9	70	0.140	5	11.7	92.1	86.4	79.6	6.8		7.4	6.2
16		2.20	78.7	1.00	2200	5.1	38	0.038	18	14.6	93.6	86.9	81.3	5.6		8.7	4.4
17				2.00	1100	5.6	35	0.070	9	15.1	93.8	84.0	78.8	5.2		9.1	6.9
18		2.80	100.0	2.00	1400	5.6	25	0.050	15	20.1	95.2	82.8	78.9	3.9		9.1	8.0

204

Table IV

CONTINUOUS HYDROFORMYLATION OF 1-BUTENE IN THE PRODUCT FLASH-OFF MODE WITH SEP-Rh AND Ph_3P-Rh COMPLEX CATALYST SYSTEMS

	TPP	SEP	SEP	SEP	SEP	TPP
● Temperature, °C	100	120	120	140	140	140
Pressure, kPa	800	1050	1050	1275	1275	1275
P_{H_2}, kPa	565	675	760	724	775	724
P_{CO}, kPa	69	90	83	138	149	138
● Rhodium Conc., mM	2.50	2.50	4.44	4.44	4.44	4.44
● Phosphine Conc., mM	310	600	360	1000	1000	1000
1-Butene Feed, mole/hr/L	4.0	4.0	4.0	2.8*	2.8	2.8
Aldehyde Product, mole/hr/L	1.0	1.0	1.5	1.6	1.6	2.3
● Conversion per Pass, %	26	26	38	56	60	82
				52**	55**	65**
● n+i Selectivity %	92	92	91	90	90	84
n/i ratio	21	22	21	35	32	29
Hydrocarbon Selectivity,%	7	7	7	8	9	14
● Stripping Gas, mole/hr/L	35	25	38	24	24	21

*Plus 3 mole/hr/L 2-butenes **After 6 days operation

Table V

HYDROFORMYLATION OF 1-BUTENE WITH VARIOUS TRIS-PHOSPHINE RHODIUM CARBONYL HYDRIDE CATALYSTS

Reactions at 145° at 2500 kPa of 5/1 H_2/CO (54/46) Feed and 20g 1-Butene Plus 80g Mixture of 1M Phosphine Plus 2-Ethylhexyl Acetate Using AcacRh(CO)$_2$ as a Catalyst Precursor

Ligand No.	Ligand Structure	Rh Conc. mM	Ligand Conc. M/Kg	Final H_2/CO Ratio	Rate Constant k, min⁻¹ Calcd. 1MRh	Found	Reaction Time min.	Linearity n/1 Ratio	$\frac{n \times 100}{n+1}$ %	Selectivities, Mole % Aldehydes n+1	n	1	By-Products 2-Butenes	Butane
1	Ph$_2$PCH$_2$CH$_2$Si(CH$_3$)$_3$	1.0 / 0.1	1 / 0.14	6.2 / 5.1	86 / 363	0.043 / 0.036	16 / 19	8.9 / 4.6	89.9 / 82.2	87.1 / 90.7	78.3 / 74.6	8.8 / 16.1	7.7 / 6.5	5.2 / 2.8
2	Ph$_2$PCH$_2$CH$_2$C(CH$_3$)$_3$	0.5 / 0.1	1 / 0.14	5.5 / 5.4	100 / 490	0.050 / 0.049	14 / 14	9.8 / 4.4	90.7 / 81.6	88.6 / 90.4	80.4 / 73.7	8.2 / 16.7	7.9 / 6.9	3.5 / 2.7
3	Ph$_2$P(CH$_2$)$_5$CH$_3$	0.5 / 0.5	1 / 0.14	5.3 / 5.9	96 / 282	0.048 / 0.141	14 / 5	8.8 / 4.3	89.8 / 81.0	89.7 / 88.9	80.6 / 72.0	9.2 / 16.9	6.7 / 6.9	3.6 / 4.2
4	Ph$_2$PCH$_2$CH$_2$⟨phenyl⟩	0.5 / 0.25	1 / 0.14	5.2 / 4.9	90 / 552	0.045 / 0.138	16 / 5	10.7 / 5.5	91.5 / 84.6	90.9 / 90.2	83.1 / 76.3	7.8 / 13.9	6.4 / 6.2	2.7 / 3.6
5	Ph$_2$PCH$_2$CH$_2$-N⟨O⟩	0.5 / 0.5	1 / 0.14	4.5 / 4.9	92 / 288	0.046 / 0.144	15 / 5	9.3 / 5.4	90.3 / 84.3	91.8 / 90.6	82.9 / 76.3	8.9 / 11.3	5.6 / 4.6	2.6 / 4.8
6	Ph$_2$PCH$_2$CH$_2$SO$_2$C$_2$H$_5$	0.5 / 0.25	1. / 0.14	5.2 / 5.8	26 / 64	0.013 / 0.016	52 / 44	18.9 / 5.7	95.0 / 85.2	88.1 / 86.8	83.7 / 73.9	4.4 / 12.9	8.1 / 9.3	3.8 / 3.9
7	Ph$_3$P	0.25 / 0.05	1. / 0.14	5.7 / 5.8	200 / 800	0.050 / 0.040	14 / 18	11.2 / 4.0	91.8 / 80.2	81.2 / 83.0	74.6 / 66.6	6.6 / 16.4	13.3 / 13.4	5.5 / 3.6

Table VI

EFFECT OF THE BRANCHING OF ALKYL DIPHENYL PHOSPHINE LIGANDS ON THE RATE AND SELECTIVITY OF RHODIUM HYDROFORMYLATION

Reactions at 2500 kPa, with 5 to 1 H_2/CO and 20g 1-Butene Plus 80g Mixture of Alkyl Diphenyl Phosphine Ligand and 2-Ethylhexyl Acetate Solvent, Using $AcacRh(CO)_2$ as Catalyst precursor at 145°C

	Catalyst System Parameters				H_2/CO Consumption Dependent Factors (50 % Conv.)		Rate Constant k min^{-1}			Aldehyde Linearity		Selectivities, Mole %				
	Ph_2PR	Ligand	Rh		H_2/CO	H_2/CO	Normal-		Re-action				Aldehydes		By-Products	
Seq. No.	Structure of -R Group	Conc. M	Conc. mM	L/Rh Ratio	Ratio Feed	Ratio Final	ized at 1 M Rh	Found	Time min	n/i Ratio	$\frac{100n}{n+1}$ %	Total	n-	i-	2-Butenes	Butane
1	$-CH_2CH_2CH_2CH_3$	1.0	0.25	4000	53/47	5.2	120	0.030	23	9.6	90.5	88.7	80.3	8.4	7.8	3.5
2		0.14	0.010	1400	53/47	5.5	530	0.053	13	4.2	80.8	89.1	72.0	17.1	7.8	3.1
3	$-CH_2CH_2C(CH_3)_3$	1.0	0.50	2000	53/47	5.5	100	0.050*	14*	9.8	90.7	88.6	80.4	8.2	7.9	3.5
4		0.14	0.10	1400	53/47	5.3	490	0.049	14	4.4	81.6	90.4	73.7	16.7	6.9	2.7
5	$-CH_2C(CH_3)_3$	1.0	0.10	10000	54/46	4.9	250	0.025	27	2.6	72.5	62.9	45.6	17.3	34.7	2.4
6		0.14	0.25	560	54/46	5.0	284	0.071*	23*	1.7	63.4	52.7	33.4	19.3	44.5	2.8
7	$-CH_2CH(CH_3)_2$	1.0	0.25	4000	54/46	6.5	232	0.058	12	4.4	81.6	86.8	70.8	16.0	9.6	3.6
8		0.14	0.10	1400	54/46	6.0	580	0.058	12	3.3	76.9	76.5	58.8	17.7	21.0	2.5
9	$-CHCH_2CH_3$ CH_3	1.0	0.20	2800	53/47	5.4	220	0.044	16	3.4	77.2	86.5	66.8	19.7	10.5	3.0
10		0.14	0.05	2800	53/47	5.3	460	0.023	30	3.2	76.2	69.3	52.8	16.5	28.1	2.6
11	⬡ (h)	1.00	0.20	5000	53/47	5.3	40	0.008*	92*	3.6	78.2	87.5	68.4	19.1	9.4	3.1
12		0.14	0.10	1400	53/47	5.5	370	0.037*	20*	3.2	76.2	75.4	57.5	17.9	22.0	2.6
13	⬠ (h)	1.0	0.20	5000	53/47	5.4	190	0.038	18	5.4	84.5	88.1	74.4	13.7	8.4	3.5
14		0.14	0.05	2800	53/47	5.5	500	0.025	27	3.4	77.1	8.2	63.4	18.8	15.0	2.8

*The rate of reaction was decreasing with time. The initial rate is listed.

206

THE PREDICTION OF THE QUALITY OF COKE BY THE USE OF V^r-G DIAGRAMS

Peng Chen

Department of Fuels Engineering, University of Utah, Salt Lake City, UT 84112

Permanent address: Central Coal Mine Research Institute, Hepingli, Beijing,
                    People's Republic of China

All properties of coal are more or less related to the coalification meta-
morphism. However, caking properties (plasticity) also affect the coke strength.
Upon heating, coal undergoes chemical changes, giving rise to the evolution of gas
and condensible vapors and leaving behind a solid residue consisting almost entirely
of carbon. In the temperature range 350-500° C, depending on the rank of the coal,
coking coal softens, becomes plastic, and coalesces into a coherent mass which
swells and then forms a solid porous structure. In this series of transformation,
two important temperature zones can be distinguished. The first is that in which
the coal is plastic and the second is that at higher temperature in which the
resolidified material contracts. A strong contraction and resolidification, which
is likely to occur with coals of high volatility and plasticity, produces many
fissures in the coke, leading to lower mechanical strength. Coke strength is,
therefore, closely associated with agglomeration of particles, pore size and its
distribution, strength of cell wall and development of fissures. It is assumed
that the coke strength may be expressed statistically as a function of these two
parameters.

Many methods to predict the strength of coke have been proposed. These methods
are as follows:

(1) $\overline{R^\sigma}_{max}$--Log α_{max} diagrams put forward by Miyazu.[1] Here, $\overline{R^\sigma}_{max}$ is the mean
maximum percent reflectance of vitrinite. α_{max} is the maximum percent fluidity
measured by the Gieseler plastometer.

(2) V^r--b diagrams, put forward by Simonis.[2] Here, V^r is the percent by
weight volatile matter on a dry, ash-free basis, and b is the total dilatation of
the coal, measured by the Audibert-Arnu dilatometer.

(3) X--Y diagrams have been used in the Soviet Union.[3] Here, X is the
final drop of the expansion-pressure curve which is function of V. Y is the
thickness of the plastic layer of the Sapozhnikov test, which reflects the quantity
of the plastic mass.

(4) S.I.--C.B.I. diagrams were used by Shapiro[4]. S.I. and C.B.I. are the
abbreviations of Strength Index and Composition Balance Index. These values are
obtained from petrographic analysis.

(5) V^r--G diagrams has been put forward by the Central Coal Mine Research
Institute[5]. G is the caking index of coal, which is the modification of Roga
Index.[6]

Experimental

More than 400 samples of bituminous coals were selected from the main coal
fields of China. Among these, 177 samples of 2 tons each were taken from bitumin-
ous coal mines and seams representing different ages of coal formation and periods
of metamorphism. Examinations were made according to the requirements for coking
tests on a semi-industrial scale using a washer, a 200kg coke oven, different sizes
of automatic screens, a micum drum, etc. The raw coal was cleaned by a jig washer,

85% of the coal charged into the coke oven was less than 3mm in size and had a moisture content of 10%. The test coke-oven was constructed of aluminum and magnesium blocks. The carbonizing chamber has a width of 450mm. The coke strength was determined by the ISO/R 556-1967(E) test. The M40 index, crushing strength of coke; the M10 index, abrasive strength of coke; the F10 index, the yield of coke powder of less than 10mm, and the Q60 index,block coke of larger than 60mm after the drop-shatter test, were determined.

The proximate analysis, ultimate analysis, petrographic analysis and tests of caking and coking properties were determined. Most of the test methods adopted are similar in principle to the corresponding methods specified in the International Standards issued by ISO.

Results

Statistical analysis on the coalification metamorphism-- Volatile matter and mean maximum reflectance of coal have been most commonly used as parameters to describe the coalification metamorphism.[7,8] There is a good correlation between these two indices as shown in Table 1. Although the volatile matter index is made on whole coal and reflectance solely on vitrinite, which is generally about 50-80% in coking coal, there is still a good correlation. Ultimate analysis, such as carbon content, hydrogen content, and atomic H/C and O/C ratios have also been used (Table 2).

Table 1. Correlation Between V^r and $\overline{R^o}$ max

Source	Regression Equation	Correlation Coefficient
U.S.A.	$\overline{R^o}$ max = 2.476 — 0.0402xV^r	-0.944
Canada & Australia	$\overline{R^o}$ max = 2.519 — 0.0465xV^r	-0.884
China	$\overline{R^o}$ max = 2.12 — 0.0357xV^r	-0.917

Table 2. Correlation between C^r , H^r , O^r and V^r
(Samples 390)

Regression Equation	Correlation Coefficient
V^r = 247.76—2.52xC^r	-0.86
V^r = 15.28xH^r—49.57	0.90
V^r = 10.7+2.64xO^r	0.79
C^r = 108.28—4.15xH^r	-0.72
C^r = 94.32—1.11xO^r	-0.98

Statistical analysis of the caking properties--Although caking properties of coal are not always proportional to the coking power, they plan an essential role during carbonization in determining the strength of the coke.[9] Each test index has its own features. Most of them, such as Roga index (RI), Caking index (G), Gray-King index (GK), Crucible Swelling index Number (CSN), etc., reflect the overall result of the process which converts coal from the solid state into the plastic state and then resolidifies it into a solid coherent body with a porous structure. Some of them reflect the temperature range of the plastic state while others reflect the fluidity of the plastic mass. The

correlation of these indices, therefore, is sometimes good and sometimes poor. The correlation coefficients between indices of cohesiveness of coal are summarized in Table 3.

Table 3. Correlation Coefficients between Indices of Cohesiveness of Coal

	G	R.I.	C.S.N.	G.K.	Y	b	Log α max
G	1.00	0.98	0.78	0.94	0.83	0.73	0.86
R.I.	0.98	1.00	0.77	0.91	0.80	0.69	0.87
C.S.N.	0.78	0.77	1.00	0.80	0.63	0.58	0.37
G.K.	0.94	0.91	0.80	1.00	0.86	0.83	0.88
Y	0.83	0.80	0.63	0.86	1.00	0.92	0.66
b	0.73	0.70	0.58	0.83	0.92	1.00	0.76
Log αmax	0.86	0.87	0.37	0.88	0.66	0.76	1.00

Relationship between components and properties of coal and coke strength--
Among the 177 samples used in the coke-oven tests, 29 samples could not go through the tumbler test. After deducting the samples of charges containing >15% ash, there remained 134 coal samples. Organic components, coalification metamorphism and caking properties are internal variables characteristic of the coal used. In addition, the coke produced also depends on external variables such as the particle size of coal, the bulk density of the charge, the heating rate, the coking tempera-ture, the coking time and the structure of the coke oven. In the present study, these external variables are constant. It was, therefore, possible to use a few parameters referring to the internal variable of coal coking to reflect the relation between the property of coal and coke strength.

Trend surface analysis can be used to solve this problem. It has been carried out for 134 coal samples. The results are listed in Table 4. The F-test demon-strated the following:

(1) The second order equation, square trend-surface equation, is distinctly better than the linear equation, and

(2) The cubic equation does not have a significant difference as compared with the second order equation.

Table 4. Goodness of Fit for V^r--G on Coke Qualities

Fitting	Indices of Coke Qualities				
Trend Equation	M40	M10	Q60	Q40	F10
Liner	0.53	0.68	0.36	0.62	0.56
Square	0.69	0.82	0.50	0.80	0.77
Cubic	0.70	0.82	0.53	0.85	0.77

Therefore, the second order equation is used to indicate the trend surface. From Figures 1 and 2, the following information may be obtained:

(A) When a coal has a volatile matter (daf) of less than 30%, the coke strength is mainly controlled by the cohesiveness.

(B) When a coal has a volatile matter (daf) of more than 30%, the coke strength is controlled by both the cohesiveness and the degree of metamorphism of coal.

209

(C) As the volatile matter (daf) increase, the strength is more affected by the degree of metamorphism of coal.

(D) The effect of the degree of coal metamorphism is greater on the M40 index than on the M10 index. The effect of the cohesiveness is larger on M10 than on M40.

It may be seen from Figures 3 and 4, that the percentage of lump coke is mainly affected by the degree of coal metamorphism. As V^r increases, the percentage of lump coke decreases.

It may be seen from Figure 5 that the percentage of coke breeze is mainly affected by the cohesiveness of the coal. The higher the V^r, the more it is affected by the cohesiveness of coal.

If other indices reflecting the degree of coal metamorphism and the cohesiveness were used, similar relations would be obtained (Table 5). The combinations of V^r and other indices reflecting cohesiveness usually did not show any difference in goodness of fit for the M40 index. As for the M10 index, the combination of V^r--G is distinctly better than V^r--Y or V^r--Log α_{max}, or C.S.N. Thus, it is evident that

(1) Caking index G, which we have improved, is better than other indices reflecting cohesiveness of coal.

(2) Index V is better than $\overline{R^o}_{max}$. The former is based on whole coal and the latter is based on vitrinite in coal only.

Table 5. Comparison of Goodness of Fit when Fitting with Different Indices

Combination of Different Indices	Coke Strength				
	M40			M10	
	Square	Cubic		Square	Cubic
V^r vis. G	0.69	0.70		0.82	0.82
V^r vis. R. I.	0.69	0.70		0.78	0.81
V^r vis. Log α_{max}	0.67	0.69		0.66	0.72
V^r vis. Y	0.66	0.69		0.55	0.70
V^r vis. C.S.N.	0.68	0.72		0.56	0.59
V^r vis. b	0.63	0.67		0.44	0.62
$\overline{R^o}_{max}$-Log α_{max}	0.59	0.60		0.66	0.70
$\overline{R^o}_{max}$-$(\Sigma d)_{2/3}$*	0.57	0.62		0.33	0.39

* $(\Sigma d)_{2/3}$, vol. % of 2/3 semi-vitranite in coal plus fusinite and semi-fusinite, then plus mineral impurities in coal.

Taking advantage of these results, we can estimate the strength of coke using the diagram of V^r--G. We must point out that these results have been obtained from a semi-industrial scale oven and are different from the results in a conventional coke oven. In general, the coke strength is slightly lower for the smaller oven, but it is not important in selecting the blending ratios of coals.

If the value of blending coals in the V^r--G diagram does not fall in the optimum area, we can add some coals to the blending coals to move the position

in the V^r--G diagram into optimum area. In addition, we may use further treatment to enhance the ability to make better coke or to improve the economics of manufacturing coke. The methods of further treatment are shown in Figure 6. We can, for example, use preheating to improve the caking ability of these blending coals, which are low in caking ability and have a position in the V^r--G diagram low on the optimum area. The optimum area for blending has V^r values from 28% to 32% and G values from 60 to 75.

REFERENCES:

1. Miyazu, T., Okuyama, Y., Sugimura, H. and Kumagai, M., J. Fuel Soc. Japan, 1970, 49, 736.

2. Simonis, W., Gnuschka, G., and Beck, K. G., Gluckauf-Forschungshefte, 1965, No. 4, 201, 1965, No. 6, 301.

3. Lowry, H. H.: "Chemistry of Coal Utilization" Vol. 1, New York, John Wiley and Sons, Inc. (1945), pp.280-297.

4. Shapiro, N., Gray, R. J., and Eusner, G. R., Iron and Steel Division, AIME Proceedings, 1961, 20.

5. Chen, Peng: Coking Chemistry, 1979, No. 6, 1.

6. Chen, Peng: Coal Geology and Prospecting, 1976, No. 4.

7. Huntzens, F. J. and Van Krevelen, D. W." Fuel, 1954, 33, 88.

8. Keiichiro, K., Fuel, 1980, 59, 380.

9. Zimmerman, R. E.: "Evaluating and Testing the Coking Properties of Coal", Miller Freeman Publications, Inc., San Francisco (1979).

FIGURES:

1. Forecasting the M40 with the square trend surface.

2. Forecasting the M10 with the square trend surface.

3. Forecasting the Q60 with the square trend surface.

4. Forecasting the Q40 with the square trend surface.

5. Forecasting the F10 with the square trend surface.

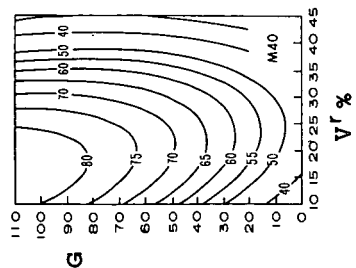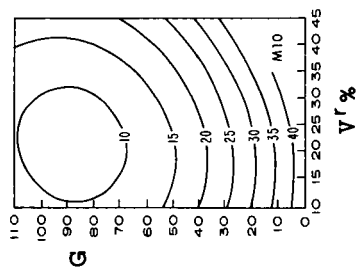6. Some methods of further treatment to improve the coke strength using V^r-G diagram.
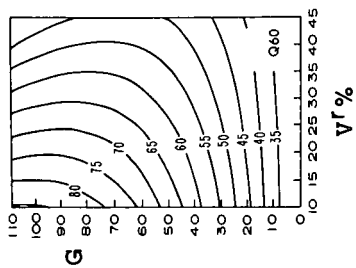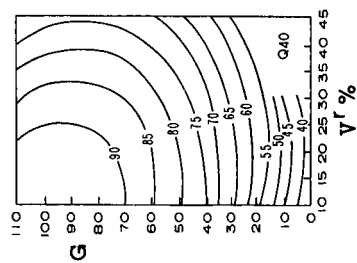
Figure 3

Figure 6

Figure 2

Figure 5

Figure 1

Figure 4